NASA TECHNICAL NOTE

NASA TN D-7411

NASA TN D-7411

FREE-FLIGHT INVESTIGATION OF THE STABILITY AND CONTROL CHARACTERISTICS OF A STOL MODEL WITH AN EXTERNALLY BLOWN JET FLAP

by

Lysle P. Parlett and Sandy J. Emerling

Langley Research Center

and

Arthur E. Phelps III

Langley Directorate,

U.S. Army Air Mobility R&D Laboratory

Hampton, Va. 23665

NATIONAL AERONAUTICS AND SPACE ADMINISTRATION • WASHINGTON, D. C. • APRIL 1974

1. Report No.	2. Government Accession No.	3. Recipient's Catalog No.
NASA TN D-7411		

4. Title and Subtitle	5. Report Date
FREE-FLIGHT INVESTIGATION OF THE STABILITY AND CONTROL CHARACTERISTICS OF A STOL MODEL WITH AN EXTERNALLY BLOWN JET FLAP	April 1974
	6. Performing Organization Code

7. Author(s)	8. Performing Organization Report No.
Lysle P. Parlett, Sandy J. Emerling, Langley Research Center; and Arthur E. Phelps III, Langley Directorate, U.S. Army Air Mobility R&D Laboratory	L-9148
	10. Work Unit No. 760-61-02-01
9. Performing Organization Name and Address: NASA Langley Research Center, Hampton, Va. 23665	11. Contract or Grant No.
	13. Type of Report and Period Covered: Technical Note
12. Sponsoring Agency Name and Address: National Aeronautics and Space Administration, Washington, D.C. 20546	14. Sponsoring Agency Code

15. Supplementary Notes

Sandy J. Emerling was a Graduate Research Scholar Assistant, George Washington University, Langley Research Center.

16. Abstract

The stability and control characteristics of a four-engine turbofan STOL transport model having an externally blown jet flap have been investigated by means of the flying-model technique in the Langley full-scale tunnel. The flight characteristics of the model were investigated under conditions of symmetric and asymmetric (one engine inoperative) thrust at lift coefficients up to 9.5 and 5.5, respectively. Static characteristics were studied by conventional power-on force tests over the flight-test angle-of-attack range including the stall. In addition to these tests, dynamic longitudinal and lateral stability calculations were performed for comparison with the flight-test results and for use in correlating the model results with STOL handling-qualities criteria.

17. Key Words (Suggested by Author(s))	18. Distribution Statement
STOL Jet flap Dynamic stability Asymmetric thrust Model flight test	Unclassified – Unlimited STAR Category 02

19. Security Classif. (of this report)	20. Security Classif. (of this page)	21. No. of Pages	22. Price*
Unclassified	Unclassified	35	$4.00

*For sale by the National Technical Information Service, Springfield, Virginia 22151

FREE-FLIGHT INVESTIGATION OF THE STABILITY AND CONTROL CHARACTERISTICS OF A STOL MODEL WITH AN EXTERNALLY BLOWN JET FLAP

By Lysle P. Parlett, Sandy J. Emerling,*
Langley Research Center

and Arthur E. Phelps III
Langley Directorate, U.S. Army Air Mobility R&D Laboratory

SUMMARY

The stability and control characteristics of a four-engine turbofan STOL transport model having an externally blown jet flap have been investigated by means of the flying-model technique in the Langley full-scale tunnel. The flight characteristics of the model were investigated under conditions of symmetric and asymmetric (one engine inoperative) thrust at lift coefficients up to 9.5 and 5.5, respectively. Static characteristics were studied by conventional power-on force tests over the flight-test angle-of-attack range including the stall. In addition to these tests, dynamic longitudinal and lateral stability calculations were performed for comparison with the flight-test results and for use in correlating the model results with STOL handling-qualities criteria.

The results of the investigation showed that in either the four-engine condition, or with one engine inoperative, longitudinal motions of the model were heavily damped over the test angle-of-attack range. The model was easy to fly up to a lift coefficient of about 4, but the longitudinal control power became marginal at higher lift coefficients because of reduced free-stream dynamic pressure. Laterally, the model was difficult to fly because of a lightly damped Dutch roll oscillation which was easily excited by the use of rudder control. Adequate damping of the oscillation could be achieved, however, by the addition of artificial stabilization about the roll and yaw axes. With one outboard engine inoperative, lateral trim could be restored by use of differential flap deflection, asymmetric leading-edge blowing, and rudder deflection. In trimmed, three-engine flight, the stability and controllability of the model were not noticeably different from what they had been during four-engine operation. The results of dynamic longitudinal and lateral stability calculations were found to be in good agreement with the flying-model results.

---

*Graduate Research Scholar Assistant, George Washington University, Langley Research Center.

INTRODUCTION

The externally blown jet flap has demonstrated a combination of high-lift capability, relative mechanical simplicity, and adaptability to current pod-mounted engine arrangements which make the concept attractive for STOL applications. Previous investigations (refs. 1 and 2) based on static-force tests have uncovered problems and developed solutions for them – notably in the areas of longitudinal trim and stability, and also in engine-out lateral trim. Dynamic characteristics have been explored by means of forced-oscillation tests (ref. 3), by free-flight tests of an early model (15 years ago) having engines representing relatively low-bypass-ratio jets operating under conditions of symmetric thrust (ref. 4), and by recent simulator studies (refs. 5 and 6) based, in part, on data from references 2 and 3.

The present investigation was undertaken to probe, by means of the free-flight-model technique, for problem areas which might have been overlooked in more conventional testing. Experience has shown the free-flight technique to be a valuable tool in exploratory investigations of new types of aircraft, particularly on VTOL and STOL configurations where large power effects and stalled, or near-stalled, conditions have to be considered. Particular emphasis was placed on engine-out conditions (one outboard engine inoperative) in which, at high lift, it is difficult to predict the development and effects of asymmetric stall, and the effects of the lateral trim devices on dynamic stability were unknown.

The model used in the investigation was a four-engine configuration with pod-mounted fan engines located close to the fuselage in a twin-engine (Siamese) nacelle. The model was very similar in general arrangement and proportions to the model of reference 2, a publication which was the culmination of a series of wind-tunnel test programs aimed at defining the aerodynamic problems, and means of solving these problems, of the STOL airplane concept utilizing an externally blown jet flap. In the present investigation the model was tested with flap deflections of 40° to 70° and was flown over a range of lift coefficients from 2.5 to 9.5 with all four engines operating. With one engine inoperative, flights were performed at lift coefficients of 4.2 and 5.5 with a mean flap deflection of 50°. Supplementary static force tests were made to determine static stability and control characteristics of the flight-test model over the flight-test angle-of-attack range including the stall. In addition to the flight and force tests, three-degree-of-freedom lateral and longitudinal stability calculations were made to determine the period and damping characteristics of the lateral and longitudinal modes of motions. The results of these calculations were correlated with the experimental model flight-test results and with current STOL handling-qualities criteria.

SYMBOLS

The longitudinal data are referred to the stability-axis system and the lateral data are referred to the body-axis system. (See fig. 1.) The origin of the axes was located to correspond to the center-of-gravity position (0.40 mean aerodynamic chord) shown in figure 2.

Measurements and calculations were made in U.S. Customary Units and are presented in both the International System of Units (SI) and U.S. Customary Units. Equivalent dimensions were determined by using the conversion factors given in reference 7.

b	wing span, m (ft)
C_D	drag coefficient, $F_D/q_\infty S$
C_L	lift coefficient, $F_L/q_\infty S$
$C_{L,trim}$	lift coefficient for conditions of pitch trim
C_l	rolling-moment coefficient, $M_X/q_\infty Sb$
C_m	pitching-moment coefficient, $M_Y/q_\infty S\bar{c}$
C_n	yawing-moment coefficient, $M_Z/q_\infty Sb$
C_Y	lateral-force coefficient, $F_Y/q_\infty S$
C_μ	engine total gross-thrust coefficient, $T/q_\infty S$
$C_{\mu,ail,L}$	left-aileron blowing-jet momentum coefficient, $R/q_\infty S$
$C_{\mu,rud}$	rudder blowing-jet momentum coefficient, $R/q_\infty S$
$C_{\mu,le}$	wing leading-edge blowing-jet momentum coefficient, $R/q_\infty S$
$C_{\mu,le,L}$	left-wing semispan leading-edge blowing-jet momentum coefficient, $R/q_\infty S$
c	local wing chord, m (ft)
$\bar{c}$	mean aerodynamic chord, m (ft)

F_A	axial force, N (lb)
F_D	drag force, N (lb)
F_L	lift force, N (lb)
F_N	normal force, N (lb)
F_Y	force along Y-axis, N (lb)
I_X	moment of inertia about X body axis, kg-m^2 (slug-ft^2)
I_{XZ}	product of inertia about X and Z body axes, kg-m^2 (slug-ft^2)
I_Y	moment of inertia about Y body axis, kg-m^2 (slug-ft^2)
I_Z	moment of inertia about Z body axis, kg-m^2 (slug-ft^2)
i_t	horizontal-tail incidence angle, positive leading edge up, deg
M_X	rolling moment, m-N (ft-lb)
M_Y	pitching moment, m-N (ft-lb)
M_Z	yawing moment, m-N (ft-lb)
P	period of oscillation, sec
ΔC_n	yawing-moment coefficient increment produced by control deflection
ΔC_l	rolling-moment coefficient increment produced by control deflection
$C_{m_{i_t}}$	rate of change of pitching-moment coefficient with respect to tail incidence, per degree
p,q,r	body-axis rolling, pitching, and yawing angular velocities, rad/sec
q_∞	free-stream dynamic pressure, $\rho V^2/2$, N/m^2 (lb/ft^2)

R	resultant force produced by boundary-layer-control jet momentum, N (lb)
S	wing area, m^2 (ft^2)
T	static thrust, N (lb)
$T_{1/2}$	time required for a mode of motion to damp to one-half amplitude, sec
V	free-stream velocity, m/sec (ft/sec)
W	weight, N (lb)
X,Y,Z	body reference axes
X_s,Y_s,Z_s	stability reference axes
x,y	wing or flap coordinates, m (ft)
α	angle of attack, deg
β	angle of sideslip, deg
γ	flight-path angle, positive for climb, deg
δ_e	elevator deflection, positive when trailing edge is down
δ_{f3}	deflection of rear element of trailing-edge flap, positive when trailing edge is down, deg
δ_j	jet deflection, positive downward, deg
ζ	ratio of damping present in oscillatory modes of motion to value required for critical damping
η	flap static turning efficiency, $\sqrt{F_A^2 + F_N^2}/T$
θ	pitch angle, positive when nose is above horizon, deg or rad
ρ	air density, kg/m^3 ($slugs/ft^3$)

ϕ bank angle, deg or rad

ψ angle of yaw, deg or rad

ω_d damped frequency of oscillatory mode, rad/sec

ω_n undamped natural frequency of oscillatory mode, rad/sec

$C_{m_\alpha} = \frac{\partial C_m}{\partial \alpha}$, per deg

$C_{l_\beta} = \frac{\partial C_l}{\partial \beta}$, per deg

$C_{n_\beta} = \frac{\partial C_n}{\partial \beta}$, per deg

$C_{Y_\beta} = \frac{\partial C_Y}{\partial \beta}$, per deg

$C_{m_q} = \frac{\partial C_m}{\partial \frac{q\bar{c}}{2V}}$ $\quad C_{n_r} = \frac{\partial C_n}{\partial \frac{rb}{2V}}$ $\quad C_{l_p} = \frac{\partial C_l}{\partial \frac{pb}{2V}}$

ΔC_{m_q} increment of artificial damping in pitch

ΔC_{n_r} increment of artificial damping in yaw

ΔC_{l_p} increment of artificial damping in roll

A dot over a symbol represents a derivative with respect to time.

MODEL AND APPARATUS

The investigation was conducted on the four-engine, high-wing jet transport model illustrated by the three-view drawing in figure 2(a). Additional dimensional characteristics of the model are given in table I. Coordinates for the wing airfoil are presented in table II. The model had the full-span Krueger leading-edge flap and the triple-slotted trailing-edge flaps shown in figures 2(a) and 2(b). Coordinates for each trailing-edge flap

element are given in table III in terms of local wing chord. The forward and middle elements of the flap system were fixed in the position shown in figure 2(b) for all tests; the rear elements, however, were pivoted to permit deflections in the range from 30° to 70°. Symmetric deflection was used, of course, to vary the lift and drag capability of the model, while asymmetric deflection was used to provide a rolling moment to help trim the rolling-moment asymmetry present with one engine inoperative. An example of such asymmetric deflection is illustrated in figure 2(c) which indicates the asymmetric deflection used in the flight tests with the left outboard engine inoperative.

Longitudinal trim and control moments were provided by an all-movable horizontal tail, on which (1) the elevator was set at a constant deflection of -50° and (2) a 17-percent leading-edge flap was installed. Lateral moments were provided by a rudder and by a conventional spoiler which could be deflected over the full semispan or, in some tests, only ahead of the outboard segment of the flaps.

Blowing systems illustrated in figure 2(d) provided boundary-layer control (BLC), when desired, for the wing leading edge, aileron (outboard trailing-edge flap segment), horizontal-tail leading edge, elevator, and rudder. In each of these systems, compressed air flowed from tubes through a row of small, closely spaced holes, then through slots to form a fairly uniform sheet along the forward surface of the airfoil or control element.

The engines used were 15.3-cm-diameter (6-in.) fans driven by compressed air and were installed at -3° incidence so that the exhaust impinged directly on the flaps. The engines were equipped with lateral exhaust deflectors for use in trimming the lateral asymmetries in engine-out tests. Figure 2(e) shows a deflector installed on an engine.

All tests were made in the 9- by 18-m (30- by 60-ft) open-throat test section of the Langley full-scale tunnel. The static-force tests were made with an internal strain-gage balance and conventional sting which entered the rear of the fuselage. Photographs of the model in force-test and flight-test conditions are presented as figures 3(a) and 3(b), respectively.

TESTS AND PROCEDURES

Static-Force Tests

In preparation for the tests, engine calibrations were made to determine gross thrust as a function of engine rotational speed in the static condition – with the model flaps off and the engine thrust deflectors off. The tests were then made by setting the engine speed to give the desired gross thrust and holding these settings constant through the ranges of angle of attack or sideslip. It has been shown in the past that the gross thrust of these engines at a constant speed is not affected significantly by forward speed for the forward speeds involved in the present tests.

Jet deflection angles and flap turning efficiency were determined from measurements of normal and axial forces made in the static-thrust condition with flaps deflected. The static thrust used in computing turning efficiency was taken directly from the engine calibrations at the appropriate rotational speed.

During the tests, six-component longitudinal and lateral force-test data were measured at several flap deflections (symmetric and asymmetric) through an angle-of-attack range of from about -5° to 35° at engine gross-thrust coefficients up to 1.1 per engine for four-engine and three-engine operation. Tests were made at various incidences of the horizontal tail, at various deflections of spoiler, rudder, ailerons, and thrust deflectors, and for various amounts of BLC blowing over aileron, rudder, and wing leading edge. The jet momentum for each of the blown surfaces was evaluated by measuring the force produced by the respective jets in the wind-off condition. Tests to determine sideslip aerodynamic stability derivatives were made at sideslip angles of -5° and 5°. Wind-on tests were made at free-stream dynamic pressures of 62.2 and 81.4 N/m^2 (1.3 and 1.7 lb/ft^2), which correspond to velocities of 10.1 and 11.6 m/sec (33 and 38 ft/sec), and Reynolds numbers of 0.31×10^6 and 0.36×10^6, respectively. These values of Reynolds numbers were approximately in the same range as those of the flight tests which varied from 0.24×10^6 to 0.56×10^6.

Free-Flight Tests

In the test setup for the free-flight tests (shown in fig. 4), the model was flown without restraint in the 9- by 18-m (30- by 60-ft) open-throat test section of the tunnel and was remotely controlled about all three axes by two human pilots. One pilot, located in an enclosure at the rear of the test section, controlled the model about its roll and yaw axes while the second pilot, stationed at one side of the test section, controlled the model in pitch. The model-thrust operator was stationed with the pitch pilot. Compressed air, electric power, and control signals were supplied to the model through a flexible trailing cable composed of electric wires and lightweight plastic tubes. This cable also incorporated a 0.32-cm (1/8-in.) steel cable (attached to the model) that passed through a pulley above the test section and was used to catch the model in the event of an uncontrollable motion or mechanical failure. The entire flight cable was kept slack during the flights by a safety-cable operator using a high-speed pneumatic winch. Further discussion of the free-flight technique, including the reasons for dividing the piloting tasks, is given in reference 8.

The control actuators were energized remotely by means of control sticks used by the pilots. Flicker-type (full-on or full-off) control was used in flying the model, and the trimming of the control surfaces was accomplished by small electric motors which were operated independently of the flicker system. The ailerons moved only downward from

their neutral position, and during flight tests were linked with the spoilers in such a manner that the deflection of a spoiler on the right wing, for instance, was always accompanied by downward deflection of the left aileron. In the engine-out condition, blowing was applied to the aileron on the engine-out wing to provide an increment of roll trim. No aileron blowing was used during four-engine operation. The rudder could be deflected simultaneously with the ailerons and spoilers, or left undeflected, at the option of the lateral pilot, and, like the ailerons, was provided with boundary-layer control only during engine-out flights. Artificial damping was applied, when desired, by deflecting the appropriate control surfaces (horizontal tail, spoiler, or rudder) by means of pneumatic servos whose output was controlled by signals from rate-sensitive gyroscopes. Strip-chart records of signals from rate gyros and control-position indicators formed a basis for evaluating the artificial damping employed during flight. Control travels used during the flight tests were $\pm 10^{\circ}$ deflection of the horizontal tail, $\pm 15^{\circ}$ deflection of the rudder, 60° deflection of the spoiler, and 17° deflection of the ailerons.

Free-flight investigations of the dynamic stability and control characteristics of the model in four-engine operation were made for symmetric flap deflections of 40°, 50°, and 60° at angles of attack from approximately 0° to 20°; thereby, a lift-coefficient range from about 2.5 to 9.5 was covered. With one outboard engine inoperative, the effects of differential (asymmetric) flap deflection and the various other lateral trim devices on dynamic stability and controllability were investigated at lift coefficients of approximately 4.2 and 5.5. The lift coefficient of 5.5 was the highest at which level flight could be obtained with the flaps set at an approach setting with a mean deflection of about 50°.

CALCULATIONS

By means of linearized equations of motion, similar to those presented in reference 9, the longitudinal and lateral directional dynamic stability characteristics of the model were calculated for comparison with the results of the free-flight tests and for use in correlating the model results with STOL handling-qualities criteria. The calculations were made by use of the mass and geometric characteristics from table I, static aerodynamic data from the present paper, and dynamic stability derivatives from reference 3. The results of the calculations are presented in terms of damping ratio, period of oscillation, and inverse time to one-half amplitude. Frequency and damping parameters from these calculations were scaled up, using dynamic scaling relationships presented in reference 10, to predict some of the handling qualities of an airplane having a 24.4-m (80-ft) wing span. The initial response of this airplane was calculated by using equations from reference 11, a rudder deflection of 15°, spoiler deflection of 60°, and horizontal-tail incidence change of 10° being assumed.

DETERMINATION OF STATIC STABILITY AND CONTROL CHARACTERISTICS OF FLIGHT-TEST MODEL

Longitudinal Characteristics

Wind-off data.- The static turning characteristics of the engine-wing-flap system are compared with those of three previous investigations (refs. 2, 12, and 13) in figure 5. These data show that the turning efficiency η for the present model was higher at a flap deflection δ_{f3} of 50° than that for previous externally blown jet-flap models, but that the jet deflection (turning angle), particularly for the 70° flap deflection, was low compared with that for the previous models. The poor turning performance at the higher flap setting for the present model may be associated with the fact that larger, higher bypass-ratio engines were simulated in the present study, and that the flap might be less effective in capturing and turning this larger diameter engine exhaust flow.

Wind-on data.- The wind-on longitudinal characteristics of the model for flap deflections of 40°, 50°, and 70° are presented in figures 6 to 8. The high lift coefficients shown in these figures are representative of those which would be required to provide safety margins for STOL operation, but the pitching-moment data show that high lift is accompanied by problems in the areas of longitudinal stability and trim. One result common to all test configurations and thrust levels was that a pitch-up occurred at angles of attack generally at or just above the stall. Data for the 40° flap deflection (fig. 6) show that before the pitch-up was encountered, the model was stable at all but the highest value of C_{μ} and had a positive pitching moment. It would be quite simple to reduce this positive moment to zero, for trim, by unloading the tail since the jet flap gives a very large diving moment with tail off. For higher flap deflections (and higher lift coefficients), figures 7 and 8 show that the tail incidence of 5° produces stability at low values of α and C_{μ}, but not enough moment for trim. Lower tail incidences (0° and -5°) provide trim, except at the highest thrust levels, but the loss of stability at these reduced incidences is an indication of tail stall. Comparison of figure 9 with figure 7 shows that boundary-layer control in the form of leading-edge blowing on the wing increases lift coefficient, but also produces more negative pitching moments which compound the trim problem. In order to help overcome the difficulties of producing trim and stability simultaneously during the flight tests, which will be discussed in a later section, the horizontal tail was equipped with leading-edge and trailing-edge blowing to prevent the tail from stalling. No force-test data are available for the tail-blowing condition, however, because of malfunctioning of the blowing system during the force-test program.

In order to give some indication of realistic flight conditions based on the model results, lift and drag data from figures 6 to 9, with appropriate corrections for pitch trim, are summarized in figures 10 and 11 in forms for convenient analysis. A fundamental assumption in the following analysis is that the model will give the same performance with

three engines operating as with four for the same total gross-thrust coefficient after it is trimmed. This assumption is supported by data and analyses presented in references 13 and 14, and in figure 12 of the present paper. The engine-out data of figure 12 are presented for lateral trimmed conditions using the trimming methods developed in this investigation. The data show little penalty on the performance of the configuration with the use of these trimming methods. If an approach condition is assumed with $\delta_{f3} = 50^{\circ}$, $C_L = 4.0$, and $\gamma = -6^{\circ}$ (solid symbol, fig. 10(b)), then the configuration is about 15° below the stall and at a speed slightly greater than 1.2 times the stall speed to afford safe stall margins. If the configuration has a thrust-weight ratio slightly in excess of 0.45 with one engine inoperative, the descent can be arrested without a change in flap setting or airspeed in the event of a wave-off, even with an engine out. If the flap deflection is then reduced to 40° (fig. 10(a)), a climb out can be made at $\gamma = 3^{\circ}$, still without increasing airspeed. These performance margins would seem to indicate a reasonable degree of safety and are approximately those of reference 14. Figure 11 shows the effect of adding leading-edge boundary-layer control. The shift of the curves to the left indicates the possibility of operating at somewhat higher lift coefficients with a given installed thrust.

Lateral Characteristics, Symmetric Thrust

The static lateral stability derivatives of the model are presented in figure 13. These data show that the model with power on is directionally stable $\left(\text{positive } C_{n_\beta}\right)$ and has the large positive-dihedral-effect $\left(\text{negative } C_{l_\beta}\right)$ characteristic of externally blown jet-flap configurations (refs. 2 and 13). The effects of engine thrust are to increase the directional stability and positive dihedral effect at high angles of attack for all flap deflections. At the deflection of 70°, however, large increases in thrust produce noticeably destabilizing effects on C_{n_β} and reductions in $-C_{l_\beta}$ at low angles of attack.

The lateral control characteristics of the model are shown in figures 14 and 15. The spoilers (fig. 14) are shown to be a powerful source of roll control, but the ailerons (shown deflected with the spoilers in fig. 15) are ineffective. Note also that only one aileron was deflected, and that in a downward direction only. This lack of effectiveness of the aileron is not surprising since the ailerons are part of the full-span flap system and were initially deflected 50°. Further deflection to 70° of the outboard part of the flap, where power would have little effect in keeping the flow attached to the flap, would not be expected to produce any significant additional lift increment.

Lateral Characteristics, Asymmetric Thrust

The lateral asymmetries of the model with one engine not operating are shown in figures 16 and 17. Figure 16(a) shows the large rolling and yawing moments which accompany the failure of one outboard engine. Figure 17(a) shows less asymmetry with an inboard engine not operating. Comparison of figure 16(a) with figure 16(c) shows that

asymmetric leading-edge boundary-layer control reduces the roll asymmetry by about half, and almost eliminates the yaw asymmetry.

Figure 18 shows lateral stability derivatives for the three-engine (left outboard engine out) condition. A comparison of these data with those for four-engine operation (fig. 13) shows little effect of engine-out operation on the lateral stability derivatives.

The effectiveness of several devices intended as means of restoring lateral trim in engine-out conditions is presented in figures 19 to 24. In the interest of expediting the investigation, these devices were installed additively and tested without the removal of previous ones. Therefore, the data plots show cumulative effects and in most cases the model is overtrimmed with an engine out. For summary figure 25, however, appropriate subtractions have been performed to show direct comparisons of the individual contribution of each of the several devices. It is important to realize that the curves of figure 25 represent increments only, and that the net moments would be obtained by adding values from figure 25 to some basic engine-out values such as those presented in figure 16(a).

One of the most obvious examples of the effectiveness of lateral trim devices is shown in figure 19 for asymmetric flap deflection and leading-edge boundary-layer control. Figure 19(a) shows that for $C_\mu = 1.22$, the model is almost completely trimmed at all angles of attack up to 15°. It is to be noted that solid symbols in figure 19(b) represent almost exactly the approach condition of the performance analysis example previously discussed in connection with figure 10(b). Figure 19, therefore, shows that lateral trim can be achieved in a realistic approach condition with little performance penalty even with one outboard engine inoperative. It is significant that the required trimming moments can be produced by a combination of differential flap deflection and boundary-layer control; so the entire effectiveness of the spoilers and rudder then remain available for lateral maneuver control.

Figure 20(a) shows that boundary-layer control over one aileron is effective in furthering roll trim to higher values of C_μ. Figure 21(a) shows that lateral thrust deflectors are also very effective, particularly in that they produce favorable yawing moments.

FLIGHT-TEST RESULTS AND DISCUSSION

The flight-test conditions covered a range of flap angles from 40° to 60° and of angles of attack from approximately 0° to 20°. The trim lift coefficients varied from 2.5 to 9.5. Variations in lift coefficient were accomplished by each of two methods: (1) by increasing flap deflection while keeping angle of attack low, or (2) by increasing angle of attack at constant flap deflection.

Longitudinal Characteristics

At the lower flap settings investigated and over a lift coefficient range up to $C_L \approx 4$, the model was fairly easy to fly in pitch. The pitch response of the model provided by 10° deflection of the horizontal tail was sluggish, but the pitch control was considered adequate for maneuvering the model within the test section and for overcoming random disturbances in the tunnel airstream. The model was dynamically stable and the pitching motions were well damped. This behavior was not unexpected since the model was statically stable (see low-α data of figs. 6 to 9) and had high values of damping in pitch (ref. 3). These high values of pitch damping together with high pitch inertia are the factors mainly responsible for the sluggish control response; but it should be noted that these factors also made the model insensitive to gust disturbances so that very little pilot effort was required to maintain steady flights for prolonged periods once a trim attitude had been established. As the lift coefficient was increased because of an increase in flap deflection (α being kept low), the demand on the horizontal tail to produce pitch trim increased with the result that the maneuver control provided by the tail was progressively reduced. The tail provided pitch trim up to a lift coefficient of about 5.5 with the wing flaps set at 60°, but any attempt to maneuver the model resulted in tail stall and the model would dive out of control. Boundary-layer control in the form of blowing over the leading edge of the horizontal tail and on the elevator delayed the tail stall, and flights were made for the 60° flap condition up to a lift coefficient of about 7.0. The longitudinal characteristics were then similar to those at lower lift coefficients except that the model response was somewhat more sluggish at higher lift, probably because of the reduced free-stream dynamic pressure.

The requirement for boundary-layer control on the horizontal tail of the model does not necessarily imply that it would be required on a full-scale airplane: at the low Reynolds numbers inherent in the model tests, stall occurs at a lower angle of attack than at full scale. In reference 12 the discussion of horizontal-tail requirements indicates that at full scale the trim capability of an unblown horizontal tail is approximately 15 percent greater than at model scale.

In order to provide some indication of the control effectiveness of the horizontal tail for pitch control, the initial angular-acceleration response in pitch has been calculated for the control deflections used in the flight tests and is presented in figure 26. These data have been scaled up to corresponding angular accelerations for an airplane having a wing span of 24.4 m (80 ft) and are compared with a boundary for satisfactory control response of STOL airplanes taken from reference 15. These data show that the pitch control response would apparently be considered "unsatisfactory" by pilots of full-scale aircraft. This result correlates with the sluggish pitch response noted in the model flight tests.

The calculations and model flight tests are in good agreement in showing deterioration of response as the angle of attack was increased. It is interesting to note, however, that the deterioration in response did not occur in direct proportion to the reduction in free-stream dynamic pressure (as shown by the lower curve); but rather, the response reduced at some lower rate because of the power effects which increased the local dynamic pressure at the tail and tended to offset the reduction in free-stream dynamic pressure as the lift coefficient was increased.

By increasing angle of attack (and thrust) at a constant flap deflection of 50°, the model was flown over an angle-of-attack range from approximately 0° to 20° and at lift coefficients up to 9.5. To help overcome the large drag values associated with conditions of high lift and high angle of attack, the additional forward thrust was provided by a compressed-air jet exhausting rearward from the tail of the model. With this jet in operation, level flight in the tunnel represented descent conditions where gravity provides a component of forward force (a description of this descent simulation is presented in ref. 8). The flights for the 50° flap condition were made without boundary-layer control on the horizontal tail since, at the high angle-of-attack conditions, the tail trim requirements were relieved. At the high angle-of-attack conditions, the damping in pitch was artificially augmented by about 15 percent $\left(\Delta C_{m_q} = -6\right)$ as a precaution against model damage in the event of a pitch-up. The most significant result noted as angle of attack was increased to 20° was that the model could be flown without too much difficulty although force-test data had shown neutral, or even negative, static stability near the stall and a pitch-up at the stall. Flight characteristics in the low angle-of-attack range were similar to those for other flap settings in that the motions were well damped and the model was fairly easy to fly in spite of sluggish response to control. As lift coefficient was increased, the response became even more sluggish because of decreased dynamic pressures, and at the highest lift coefficient flown, the control effectiveness was barely adequate to permit sustained flight.

The fact that the model could be flown up to high angles of attack under conditions of static instability is attributed to its high value of damping in pitch. Reference 16 points out that the stick-fixed maneuver point is the most rearward center-of-gravity location at which the model is dynamically longitudinally stable, and that the location of the maneuver point is a direct function of pitch damping. In order to determine the stick-fixed maneuver boundary for the present configuration, calculations were made by using measured aerodynamic data and the results are presented in figure 27. Also presented in this plot are values of C_{m_q} and C_{m_α} corresponding to the flight-test conditions, including those at the higher angles of attack where the model became statically unstable. These results show all the model flight-test points to be in the range of positive maneuver margin, where experience has shown that models can be flown in spite of static instability.

For comparison purposes, period and damping characteristics of the longitudinal short-period mode have been calculated by means of linearized three-degree-of-freedom equations of motion. The results of the calculations are presented in figure 28 and agree with those of the flight tests. The configuration is dynamically stable, with a short-period oscillation so heavily damped (aperiodic at lift coefficients over 7.5) that increasing the pitch damping by 15 percent produces very little effect. In order to determine the effect of a large change in C_{m_q}, calculations were made with the value of this derivative doubled. The results show that doubling C_{m_q} produced an appreciable change in the period and damping characteristics of the short-period mode.

In order to provide some idea of the handling qualities to be expected from a full-scale airplane in externally blown-flap operation, frequency and damping parameters calculated for the longitudinal short-period mode of the model have been scaled up, by means of the dynamic scaling relationships presented in reference 10, to corresponding parameters for an airplane having a wing span of 24.4 m (80 ft). These scaled-up parameters are presented in figure 29; the boundaries, taken from reference 17, are based on pilot opinion of the handling qualities of many current STOL transport configurations. The pilot opinion to be expected on the basis of this analysis correlates with the results of the free-flight model tests (i.e., the short-period longitudinal behavior of the full-scale airplane would probably be satisfactory through a large range of angle of attack and would be relatively unaffected by the addition of a small amount of artificial damping). The model pilot had judged the model very easy to fly longitudinally, with or without artificial damping.

It is acknowledged that factors other than the short-period longitudinal mode have a strong influence over a configuration's handling qualities. However, because of limitations inherent in the model-flight-test technique, long-period, large-amplitude motions typical of the phugoid mode cannot easily be observed, nor can their effects be evaluated completely. References 5 and 6, for instance, in presenting the results of a simulator study of an externally blown flap airplane, state that the basic damping in pitch had to be augmented for satisfactory phugoid characteristics, although the unaugmented short-period characteristics had been considered satisfactory.

For all tests with one engine inoperative, in which the major concern was lateral behavior, longitudinal stability augmentation was again employed out of consideration for safety of the model. Flights were made at lift coefficients of 4.2 and 5.5 without encountering any problems in longitudinal stability or trim. For comparable conditions of lift coefficient and artificial damping, respectively, the longitudinal stability and control with one engine inoperative were considered to be the same as with all engines operating.

Lateral Characteristics

Symmetric thrust.- The most obvious lateral characteristics of the model were a very lightly damped Dutch roll oscillation and, at the highest lift coefficients, low control

power. The model had certain aerodynamic and mass characteristics known from past experience to be heavy contributors to unsatisfactory Dutch roll behavior. Prominent among these were the large positive effective dihedral and the steep negative (nose-down) inclination of the principal axis of inertia. The Dutch roll appeared at all lift coefficients and was easily excited by the use of rudder control. For many conditions, the simultaneous deflection of spoiler and aileron produced combinations of rolling and yawing moments which closely simulated coordinated lateral control. Addition of rudder deflection would, under these conditions, produce excessive favorable yaw, and thus excite the oscillation. For many flights, therefore, the rudder was left undeflected, the spoilers and ailerons then being the only sources of lateral control.

With spoilers and ailerons providing the lateral control, at a flap deflection of 40° and a lift coefficient of 2.5 (the lowest tested) the model was flyable but required very careful piloting. Lateral behavior here was poor because at such low angles of attack (near 0°) the principal axis of inertia was inclined approximately 15° below the flight path. (It should be noted that this steep inclination of the principal axis is not necessarily associated with the general configuration, but occurs in this particular model because of the unrealistically heavy construction of the horizontal and vertical tails.) The destabilizing effect of this negative inclination is discussed in reference 18. The spoiler-aileron combination was effective enough for steady flight, and even permitted recoveries from intentional disturbances. This result is in generally good agreement with the results of lateral response calculations (presented in fig. 30) which show that for an airplane with a span of 24.4 m (80 ft), this control system would be considered generally satisfactory at lift coefficients up to about 5. When the lift coefficient was increased (by increasing flap deflection to 50°, then to 60°), the angle of attack remained low and the Dutch roll characteristics were again poor and troublesome, and, because of the reduced free-stream dynamic pressure, the spoiler-aileron combination became less effective for controlling the model. Therefore, rudder deflection was restored to the control system but did not excite the Dutch roll as strongly as it did under lower lift, higher dynamic-pressure conditions, possibly because of the reduced rudder control power or a reduction in the favorable yaw characteristics of the spoiler-aileron combination, or both.

The Dutch roll oscillation problem was removed at all lift coefficients by the addition of artificial damping about the lateral axes. The damping in roll was more than doubled $\left(\Delta C_{l_p} = -2\right)$ and the damping in yaw was increased by about one-third $\left(\Delta C_{n_r} = -0.1\right)$. With the artificial damping the model became dynamically stable and could be flown smoothly for long periods of time at any of the several lift coefficients at which flights were attempted up to $C_L = 9.5$ $(\alpha = 20^{\circ})$.

Although the lateral control generally appeared adequate in the lower lift coefficient range for maneuvering the model within the test section and for overcoming disturbances

in the tunnel airstream, there was the expected deterioration in control power with decreasing dynamic pressure and, at the highest lift coefficient flown, the control power was hardly adequate for flying the model. Figure 30 shows that at full scale the control response at high lift coefficients would be expected to be unsatisfactory.

For purposes of comparison with model-flight-test results, the lateral period and damping characteristics of the model were calculated and the results are presented in figure 31. The calculated results are shown to be in good agreement with the flight-test results in that the Dutch roll oscillation of the model is shown to be lightly damped (unstable for some conditions) but can be heavily damped by artificial stabilization.

No variations in inertia parameters were attempted during the flight tests, but the effects of such variations have been calculated and are presented in figure 32. The calculations show that halving I_Z and reducing I_{XZ} to zero (exaggerations of the effects that would have been produced by reducing the weight of the horizontal tail) would each have resulted in improved Dutch roll damping.

In order to provide some idea of the handling qualities expected from a full-scale externally blown-jet-flap airplane, frequency and damping parameters calculated for the Dutch roll mode of the model have been scaled up to corresponding parameters for an airplane having a wing span of 24.4 m (80 ft). These scaled-up parameters are presented in figure 33 along with boundaries for satisfactory damping taken from reference 17. Figure 33 predicts that the Dutch roll behavior of such an airplane without stability augmentation would receive a pilot rating of "unsatisfactory" at high values of C_L which correlates with the lateral difficulties experienced by the model pilot while flying the unaugmented model. It is interesting to note that the amount of artificial damping which stabilized the oscillation of the model, if applied to the full-scale airplane, would probably improve the Dutch roll characteristics enough so that they would receive a pilot rating of "satisfactory." It should be noted, however, that the Dutch roll characteristics are not the only factors in pilot evaluation of full-scale-airplane lateral behavior. The spiral mode, for instance, can be important but cannot be investigated in free-flight wind-tunnel tests. In addition, the type of control system and the type of stability augmentation system are important in the overall evaluation of the lateral characteristics of the full-scale airplane.

Asymmetric thrust.- Static-force tests discussed earlier in this paper have shown that the moments required for the restoration of lateral trim in a one-engine-inoperative condition are large but can be trimmed by simultaneous use of certain devices. Flight tests, all at a mean flap deflection of about 50°, were performed to evaluate the effects, if any, that these trim devices might have on the dynamic characteristics of the model. The model was flown with one outboard engine inoperative at lift coefficients of 4.2 and 5.5, the higher value being the limit set by the available thrust. The corresponding angles of attack were 2° and 6°, respectively.

A combination of the differential flap deflection shown in figure 2(c), boundary-layer blowing over the leading edge of the engine-out wing, and 30° of rudder trim (with rudder boundary-layer control) provided most of the corrective moments in each of the two configurations which were successfully flown with one outboard engine inoperative. The remainder of the required moment was supplied by aileron boundary layer blowing on the engine-out wing or, alternatively, 18° of lateral deflection of the slipstream deflectors on the operating engines. The individual contributions of each of these devices, as determined by force tests, have been presented in figure 25. Since the spoiler-aileron combination used for maneuvering was not required as part of either trim system, the lateral response to control was generally the same as it had been in the four-engine condition – that is, generally adequate for maneuvering the model within the limits of the tunnel and for overcoming random disturbances of the tunnel airstream. The flight tests, performed with the same values of artificial damping which had provided stable Dutch roll oscillation characteristics in four-engine operation, showed that the lateral dynamic characteristics were not affected by the sources of lateral trim in any trimmed condition; the lateral behavior was the same as in four-engine operation.

SUMMARY OF RESULTS

A free-flight investigation of the dynamic stability characteristics of an externally blown-jet-flap STOL transport model in high-lift configurations has yielded the following results:

1. Longitudinal motions were heavily damped over the test angle-of-attack range. The model was easy to fly up to a lift coefficient of about 4, but the longitudinal control became marginal at higher lift coefficients because of the reduced free-stream dynamic pressures.

2. Laterally, the model was difficult to fly because of a lightly damped Dutch roll oscillation which was easily excited by the use of rudder control; adequate damping of the oscillation could be achieved, however, by the addition of artificial stabilization about the roll and yaw axes.

3. In trimmed, three-engine flight the dynamic behavior of the model was not noticeably different from that for four-engine operation.

Langley Research Center,
National Aeronautics and Space Administration,
Hampton, Va., December 19, 1973.

REFERENCES

1. Parlett, Lysle P.; Freeman, Delma C., Jr.; and Smith, Charles C., Jr.: Wind-Tunnel Investigation of a Jet Transport Airplane Configuration With High Thrust-Weight Ratio and an External-Flow Jet Flap. NASA TN D-6058, 1970.

2. Parlett, Lysle P.; Greer, H. Douglas; Henderson, Robert L.; and Carter, C. Robert: Wind-Tunnel Investigation of an External-Flow Jet-Flap Transport Configuration Having Full-Span Triple-Slotted Flaps. NASA TN D-6391, 1971.

3. Grafton, Sue B.; Parlett, Lysle P.; and Smith, Charles C., Jr.: Dynamic Stability Derivatives of a Jet Transport Configuration With High Thrust-Weight Ratio and an Externally Blown Jet Flap. NASA TN D-6440, 1971.

4. Johnson, Joseph L., Jr.: Wind-Tunnel Investigation at Low Speeds of Flight Characteristics of a Sweptback-Wing Jet-Transport Airplane Model Equipped With an External-Flow Jet-Augmented Slotted Flap. NACA TN 4255, 1958.

5. Grantham, William D.; Sommer, Robert W.; and Deal, Perry L.: Simulator Study of Flight Characteristics of a Jet-Flap STOL Transport Airplane During Approach and Landing. NASA TN D-6225, 1971.

6. Grantham, William D.; Nguyen, Luat T.; Patton, James M., Jr.; Deal, Perry L.; Champine, Robert A.; and Carter, C. Robert: Fixed-Base Simulator Study of an Externally Blown Flap STOL Transport Airplane During Approach and Landing. NASA TN D-6898, 1972.

7. Mechtly, E. A.: The International System of Units – Physical Constants and Conversion Factors (Second Revision). NASA SP-7012, 1973.

8. Parlett, Lysle P.; and Kirby, Robert H.: Test Techniques Used by NASA for Investigating Dynamic Stability Characteristics of V/STOL Models. J. Aircraft, vol. 1, no. 5, Sept.-Oct. 1964, pp. 260-266.

9. Woodcock, Robert J.; and Drake, Douglas E.: Estimation of Flying Qualities of Piloted Airplanes. AFFDL-TR-65-218, U.S. Air Force, Apr. 1966. (Available from DDC as AD 483 622.)

10. Gainer, Thomas G.; and Hoffman, Sherwood: Summary of Transformation Equations and Equations of Motion Used in Free-Flight and Wind-Tunnel Data Reduction and Analysis. NASA SP-3070, 1972.

11. Gilbert, William P.; and Libbey, Charles E.: Investigation of an Automatic Spin-Prevention System for Fighter Airplanes. NASA TN D-6670, 1972.

12. Freeman, Delma C., Jr.; Parlett, Lysle P.; and Henderson, Robert L.: Wind-Tunnel Investigation of a Jet Transport Airplane Configuration With an External-Flow Jet Flap and Inboard Pod-Mounted Engines. NASA TN D-7004, 1970.

13. Parlett, Lysle P.; and Shivers, James P.: Wind-Tunnel Investigation of an STOL Aircraft Configuration Equipped With an External-Flow Jet Flap. NASA TN D-5364, 1969.

14. Parlett, Lysle P.; Fink, Marvin P.; and Freeman, Delma C., Jr. (With appendix B by Marion O. McKinney and Joseph L. Johnson, Jr.): Wind-Tunnel Investigation of a Large Jet Transport Model Equipped With an External-Flow Jet Flap. NASA TN D-4928, 1968.

15. Innis, Robert C.; Holzhauser, Curt A.; and Quigley, Hervey C.: Airworthiness Considerations for STOL Aircraft. NASA TN D-5594, 1970.

16. Johnson, Joseph L., Jr.: Low-Subsonic Flight Characteristics of a Model of a Supersonic-Airplane Configuration With a Parawing as a Landing Aid. NASA TN D-2031, 1963.

17. Anon.: V/STOL Handling-Qualities Criteria. I – Criteria and Discussion. AGARD Rep. No. 577, 1970.

18. Sternfield, Leonard: Effect of Product of Inertia on Lateral Stability. NACA TN 1193, 1947.

TABLE I.- MASS AND DIMENSIONAL CHARACTERISTICS OF MODEL

Weight, N (lb)	668	(150)
Moment of inertia:		
I_X, kg-m^2 (slug-ft^2)	16.4	(12.1)
I_Y, kg-m^2 (slug-ft^2)	32.1	(23.7)
I_Z, kg-m^2 (slug-ft^2)	43.1	(31.8)
I_{XZ}, kg-m^2 (slug-ft^2)	7.9	(5.8)
Fuselage:		
Length, m (ft)	3.05	(10.0)
Wing:		
Area, m^2 (ft^2)	1.28	(13.7)
Span, m (ft)	3.09	(10.13)
Aspect ratio	7.5	
Mean aerodynamic chord, m (ft)	0.454	(1.49)
Spanwise location of mean aerodynamic chord, m (ft)	0.623	(2.05)
Tip chord, m (ft)	0.204	(0.67)
Root chord, m (ft)	0.622	(2.04)
Sweep of quarter-chord line, deg	24	
Dihedral of quarter-chord line, deg	-3.5	
Engines:		
Spanwise location of inboard engines, m (ft)	0.314	(1.03)
Spanwise location of outboard engines, m (ft)	0.497	(1.63)
Incidence of all engine center lines, deg	-3.0	
Exit area (per engine), m^2 (ft^2)	0.0154	(0.166)
Vertical tail:		
Span, m (ft)	0.610	(2.0)
Root chord, m (ft)	0.473	(1.55)
Tip chord, m (ft)	0.321	(1.05)
Area, m^2 (ft^2)	0.242	(2.60)
Sweep of quarter-chord line, deg	35	
Horizontal tail:		
Span, m (ft)	1.52	(4.99)
Root chord, m (ft)	0.421	(1.38)
Tip chord, m (ft)	0.156	(0.51)
Area, m^2 (ft^2)	0.437	(4.71)
Sweep of quarter-chord line, deg	25	
Rudder:		
Span, m (ft)	0.558	(1.83)
Chord, inboard end, m (ft)	0.168	(0.55)
Chord, outboard end, m (ft)	0.125	(0.41)
Hinge-line location, percent chord	55	
Sweep of hinge line, deg	34	
Elevator:		
Span, m (ft)	0.537	(1.76)
Chord, inboard end, m (ft)	0.110	(0.36)
Chord, outboard end, m (ft)	0.055	(0.18)
Hinge-line location, percent chord	73	
Sweep of hinge line, deg	17	
Aileron:		
Span, m (ft)	0.378	(1.24)
Chord, inboard end, m (ft)	0.0732	(0.24)
Chord, outboard end, m (ft)	0.046	(0.15)
Spoiler:		
Span, m (ft)	1.45	(4.75)
Chord, inboard end, m (ft)	0.061	(0.20)
Chord, outboard end, m (ft)	0.024	(0.08)

TABLE II.- AIRFOIL COORDINATES FOR WING

(a) Coordinates 17.37 cm (6.84 in.) from center line

x_{upper}		y_{upper}		x_{lower}		y_{lower}	
cm	in.	cm	in.	cm	in.	cm	in.
-0.01	-0.0056	0.33	0.13	0.15	0.06	-0.28	-0.11
.08	.032	.58	.23	.36	.14	-.46	-.18
.20	.0792	.76	.30	.51	.20	-.58	-.23
.40	.1592	.99	.39	.74	.29	-.71	-.28
.92	.3632	1.37	.54	1.22	.48	-.94	-.37
2.87	1.128	2.13	.84	2.87	1.13	-1.50	-.59
5.74	2.2616	2.74	1.08	5.74	2.26	-2.13	-.84
11.48	4.5192	3.45	1.36	11.48	4.52	-2.87	-1.13
17.21	6.776	3.84	1.51	17.22	6.78	-3.25	-1.28
22.94	9.0304	3.99	1.57	22.99	9.05	-3.35	-1.32
28.66	11.284	3.91	1.54	28.73	11.31	-3.18	-1.25
34.39	13.54	3.63	1.43	34.47	13.57	-2.77	-1.09
40.16	15.81	3.15	1.24	40.21	15.83	-2.13	-.84
45.93	18.08	2.46	.97	45.90	18.07	-1.40	-.55
51.69	20.35	1.47	.58	51.61	20.32	-.66	-.26
57.40	22.60	.08	.03	57.38	22.59	-.08	-.03

(b) Coordinates 137.06 cm (53.96 in.) from center line

x_{upper}		y_{upper}		x_{lower}		y_{lower}	
cm	in.	cm	in.	cm	in.	cm	in.
0.03	0.01	0.18	0.07	0.08	0.03	-0.08	-0.03
.03	.01	.30	.12	.18	.07	-.15	-.06
.05	.02	.38	.15	.25	.10	-.20	-.08
.13	.05	.48	.19	.36	.14	-.36	-.14
.36	.14	.66	.26	.56	.22	-.43	-.17
1.17	.46	1.02	.40	1.27	.50	-.56	-.22
2.39	.94	1.27	.50	2.49	.98	-.66	-.26
4.85	1.91	1.55	.61	4.93	1.94	-.74	-.29
7.34	2.89	1.73	.68	7.32	2.88	-.84	-.33
9.80	3.86	1.75	.69	9.78	3.85	-.91	-.36
12.24	4.82	1.68	.66	12.22	4.81	-.89	-.35
14.68	5.78	1.47	.58	14.66	5.77	-.76	-.30
17.15	6.75	1.19	.47	17.09	6.73	-.56	-.22
19.58	7.71	.86	.34	19.56	7.70	-.36	-.14
22.00	8.66	.48	.19	22.00	8.66	-.15	-.06
24.46	9.63	.03	.01	24.46	9.63	-.03	-.01

TABLE III.- FLAP COORDINATES

[Coordinates are given as percent of local wing chord]

First element

x	y_{upper}	y_{lower}
0.00	1.67	1.67
1.39	4.33	.11
2.78	5.67	.00
4.17	6.44	↓
5.56	6.83	↓
6.44	6.83	↓
8.33	6.67	↓
9.72	6.28	↓
11.11	5.94	↓
12.50	5.56	↓
13.61	5.11	↓
15.28	4.61	1.50
16.67	4.06	2.39
18.06	3.61	3.00
19.17	3.22	3.17

Second element

x	y_{upper}	y_{lower}
0.00	0.94	0.94
.94	2.39	.11
1.78	2.67	.00
2.78	2.94	.17
3.72	3.06	.39
4.61	2.94	.56
5.56	2.83	.72
6.50	2.61	.94
7.06	2.39	.94
7.39	2.22	.94
8.33	1.78	.72
9.28	1.27	.56
10.17	.72	.28
11.00	.11	.00

Third element

x	y_{upper}	y_{lower}
0.00	0.72	0.72
.72	2.50	.11
1.83	3.17	.06
2.78	3.44	.00
3.72	3.50	↓
4.44	3.50	↓
5.56	3.50	↓
7.39	3.33	↓
9.28	3.06	↓
11.11	2.78	.06
12.94	2.39	.11
14.83	2.11	.17
16.67	1.83	.17
18.50	1.56	.17
20.39	1.22	.17
22.22	.83	.11
24.06	.56	.06
24.94	.28	.00

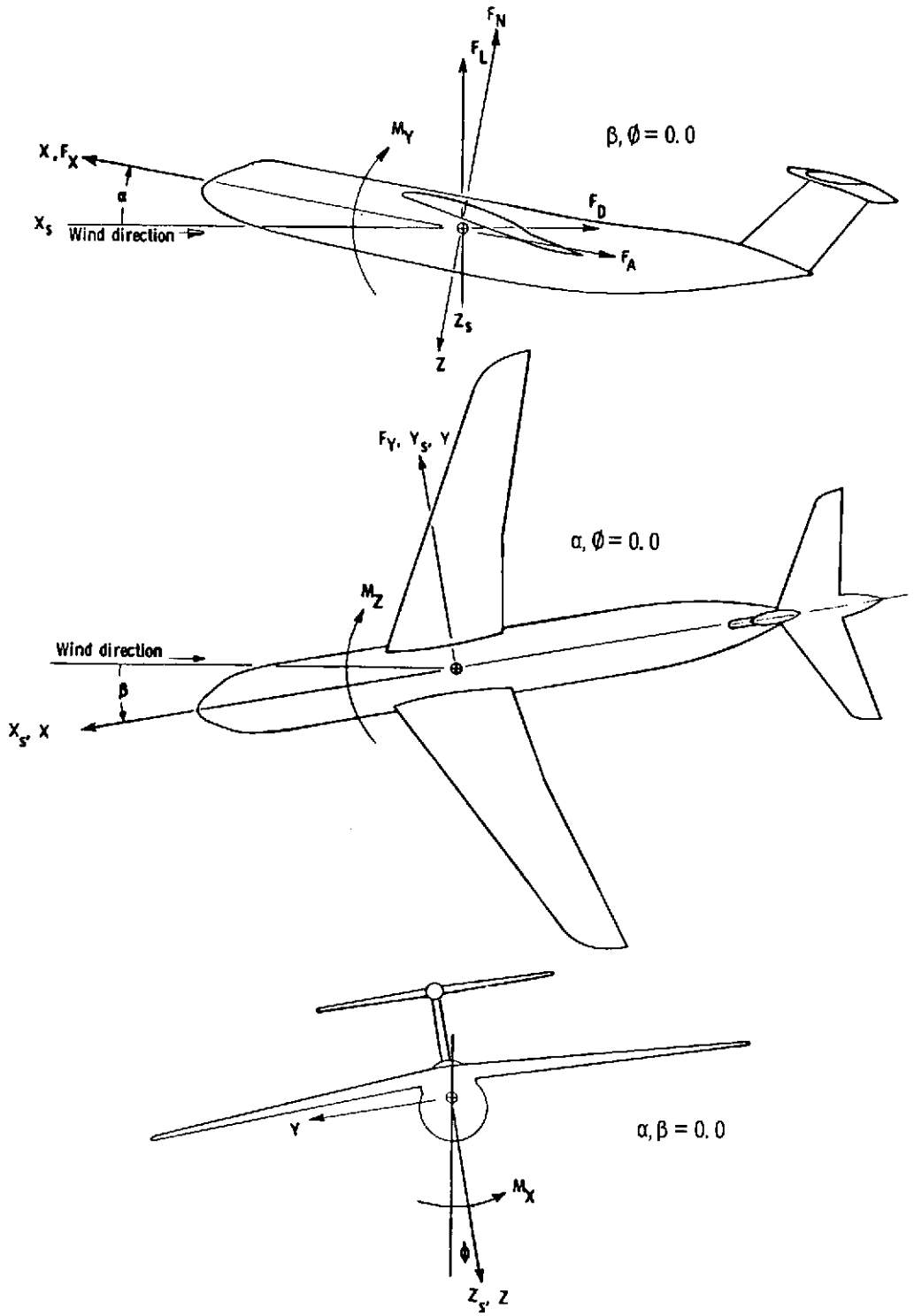

Figure 1.- Axis system used in presentation of data. Arrows indicate positive direction of forces, moments, axes directions, and angles.

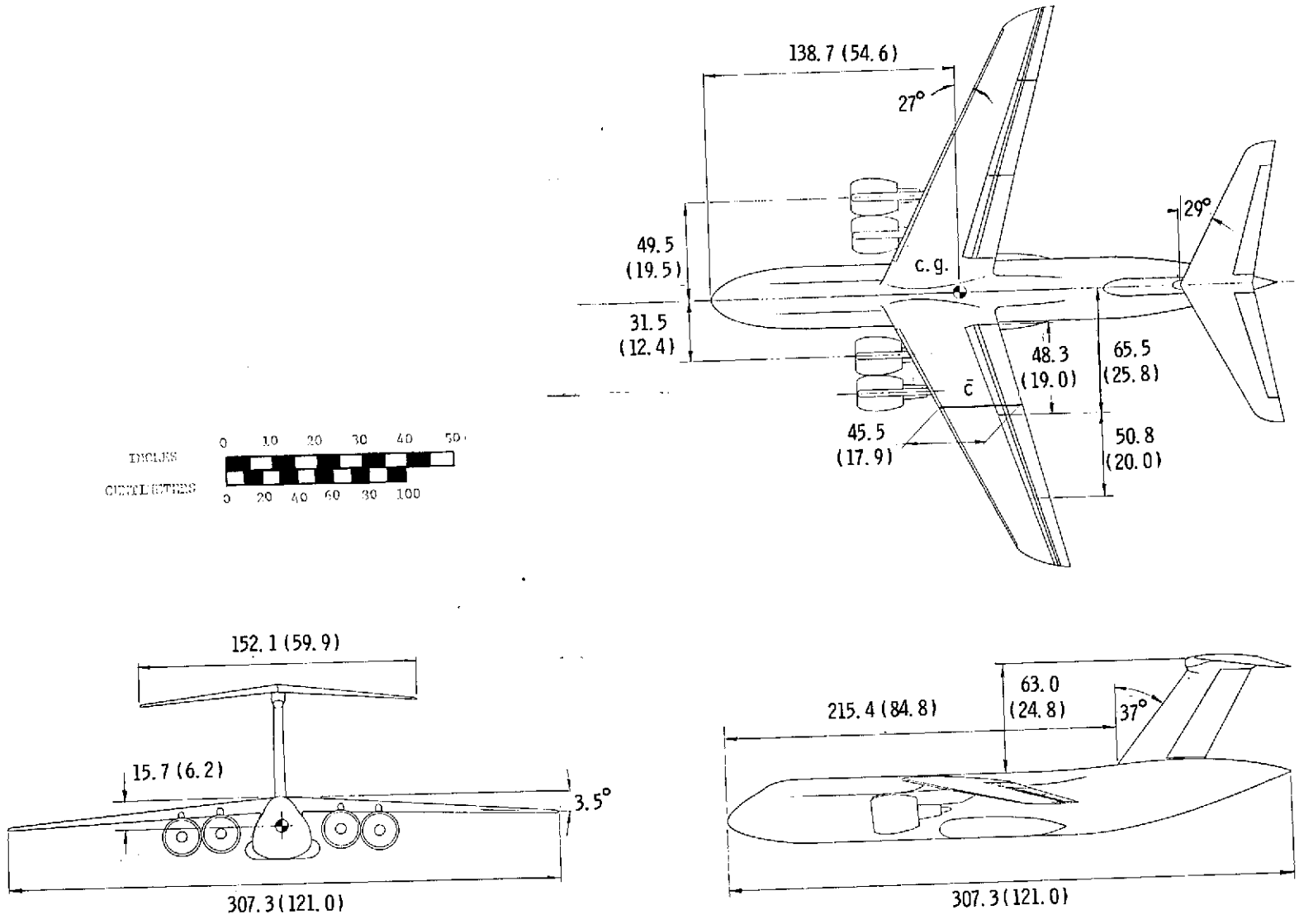

(a) Three-view drawing.

Figure 2.- Drawings of model used in tests. (All dimensions are in centimeters (inches).)

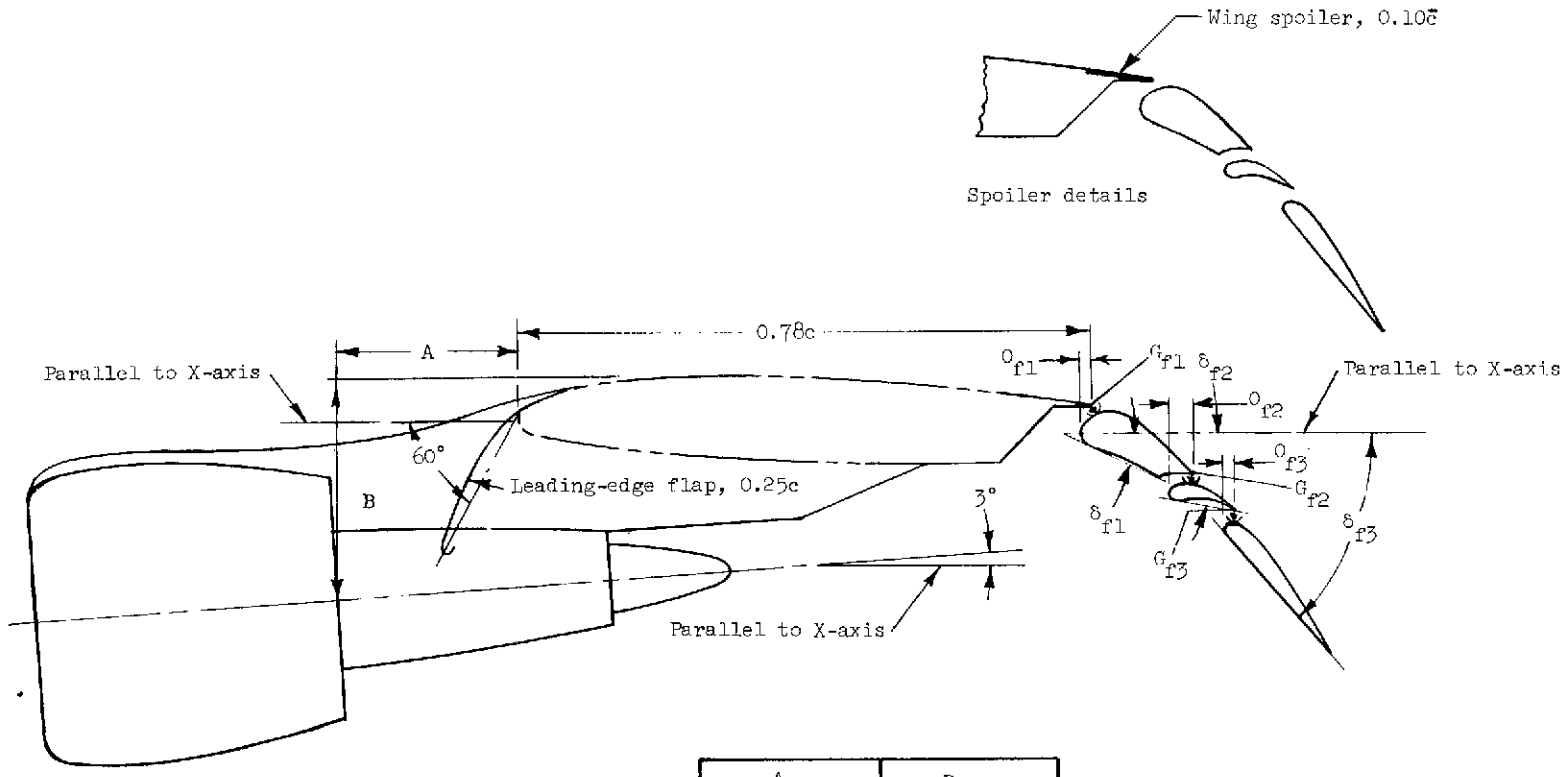

	A, cm (in.)	B, cm (in.)
Inboard	1.91 (0.75)	13.25 (5.22)
Outboard	12.20 (4.81)	14.00 (5.50)

δ_{f1}, deg	δ_{f2}, deg	δ_{f3}, deg	Overlap 1, O_{f1} percent c	Gap 1, G_{f1} percent c	Overlap 2, O_{f2} percent c	Gap 2, G_{f2} percent c	Overlap 3, O_{f3} percent c	Gap 3, G_{f3} percent c
25.0	10.0	40.0, 50.0, 70.0	1.47	1.61	3.98	1.61	1.39	1.61

(b) Flap assembly and engine-pylon details (see table III for flap coordinates in terms of local wing chord).

Figure 2.- Continued.

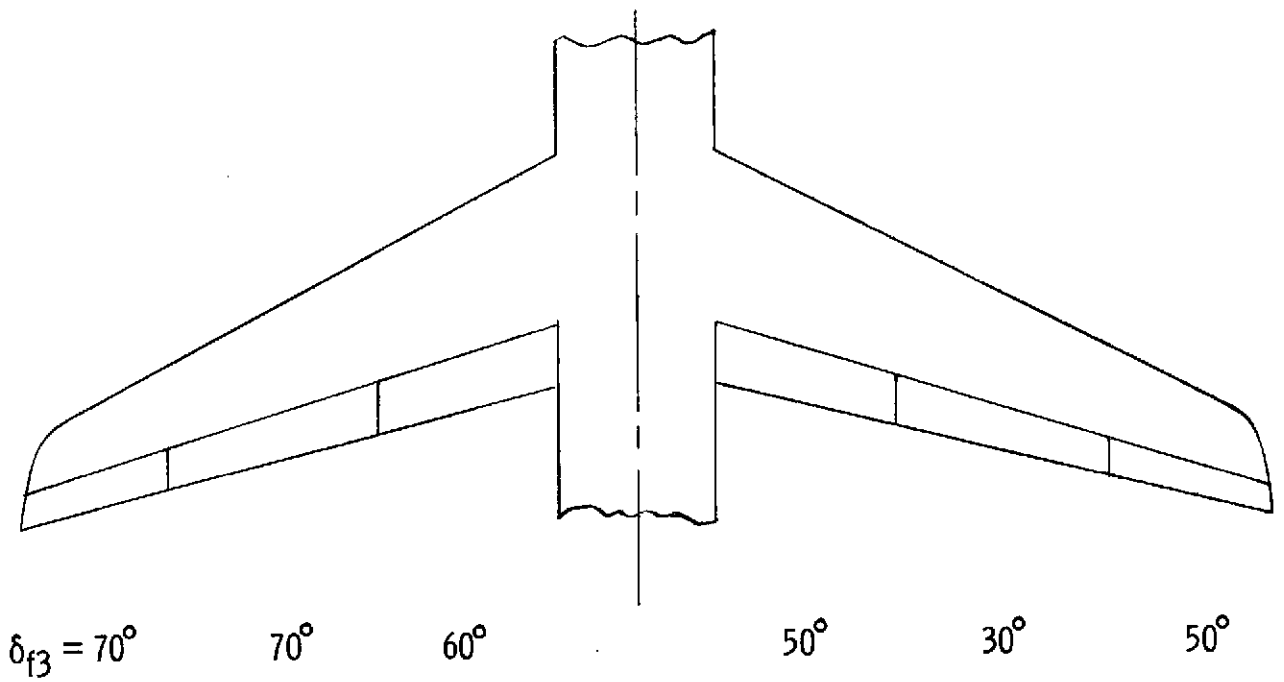

Note: Only the rear elements of the trailing-edge flaps (see fig. 2(b)) were deflected differentially. The other two elements remained fixed as shown in figure 2(b).

(c) Differential flap deflection used as source of roll trim with left outboard engine inoperative.

Figure 2.- Continued.

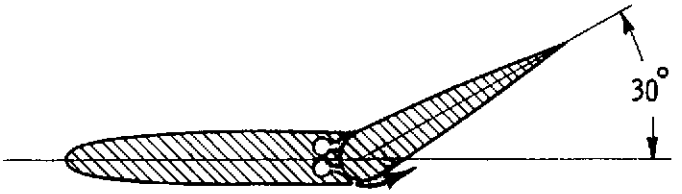

Cross section of vertical tail

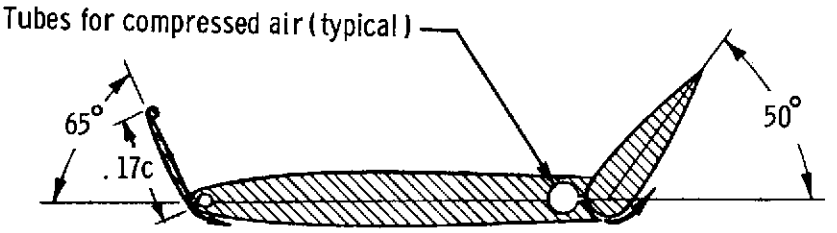

Cross section of horizontal tail

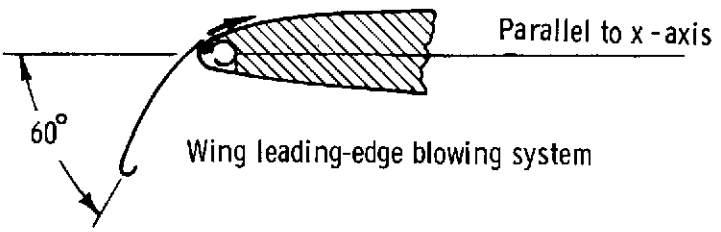

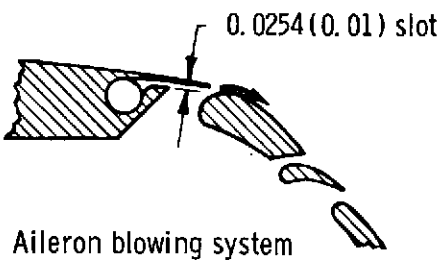

Aileron blowing system
(Outboard flap segment)

(d) Details of boundary-layer-control systems.

Figure 2.- Continued.

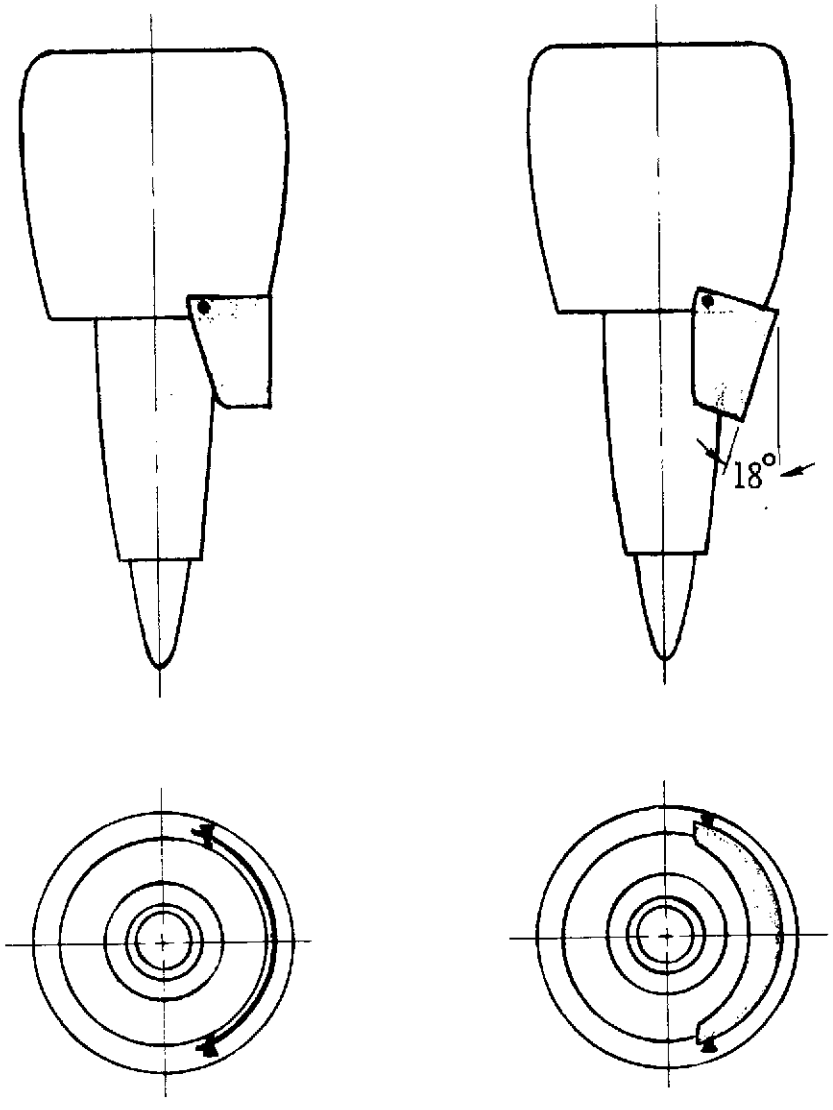

(e) Lateral thrust deflector installed on right inboard and outboard engines for some tests.

Figure 2.- Concluded.

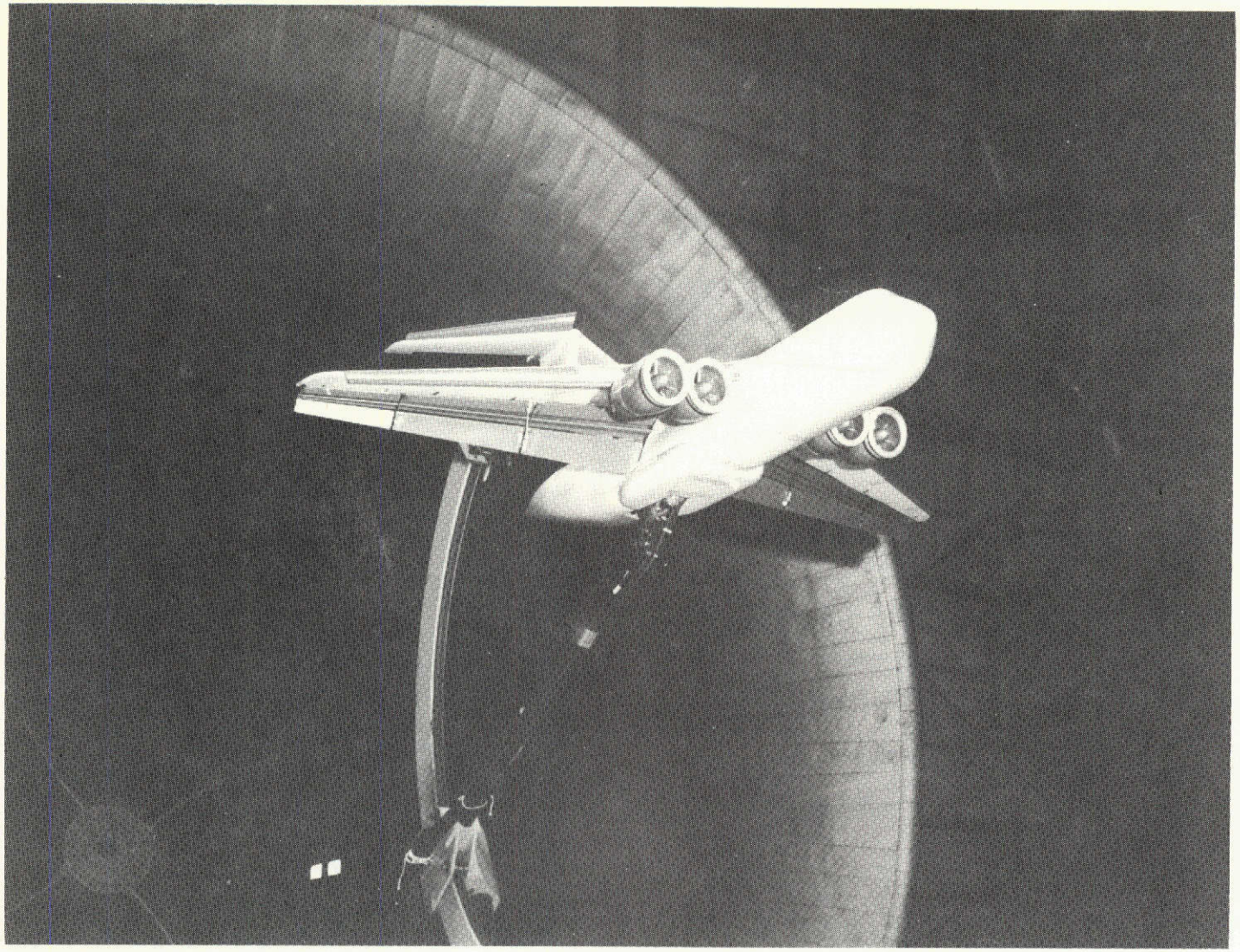

L-71-5285

(a) Model mounted for static-force tests.

Figure 3.- Photographs of model.

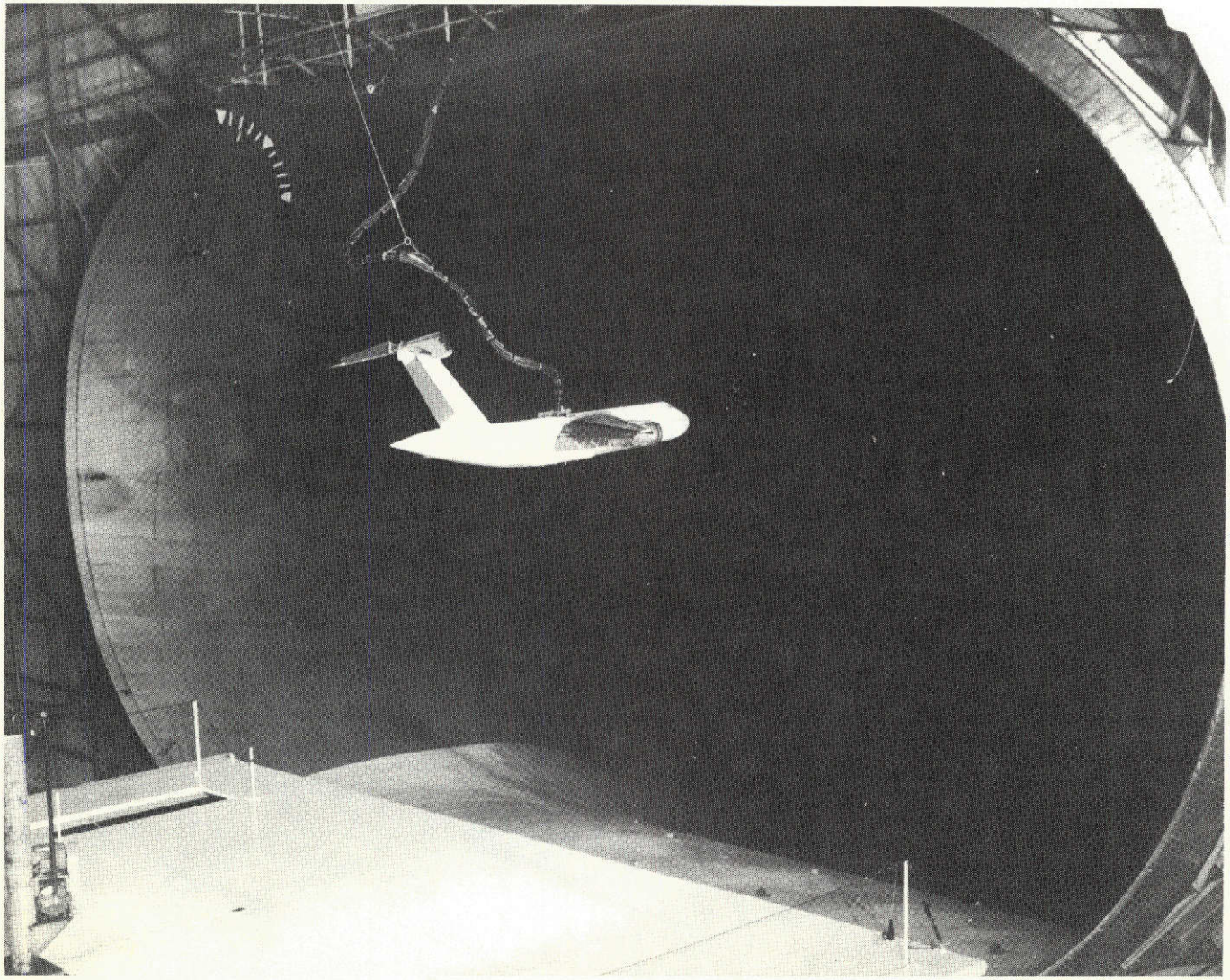

L-71-7445

(b) Model flying in tunnel.

Figure 3.- Concluded.

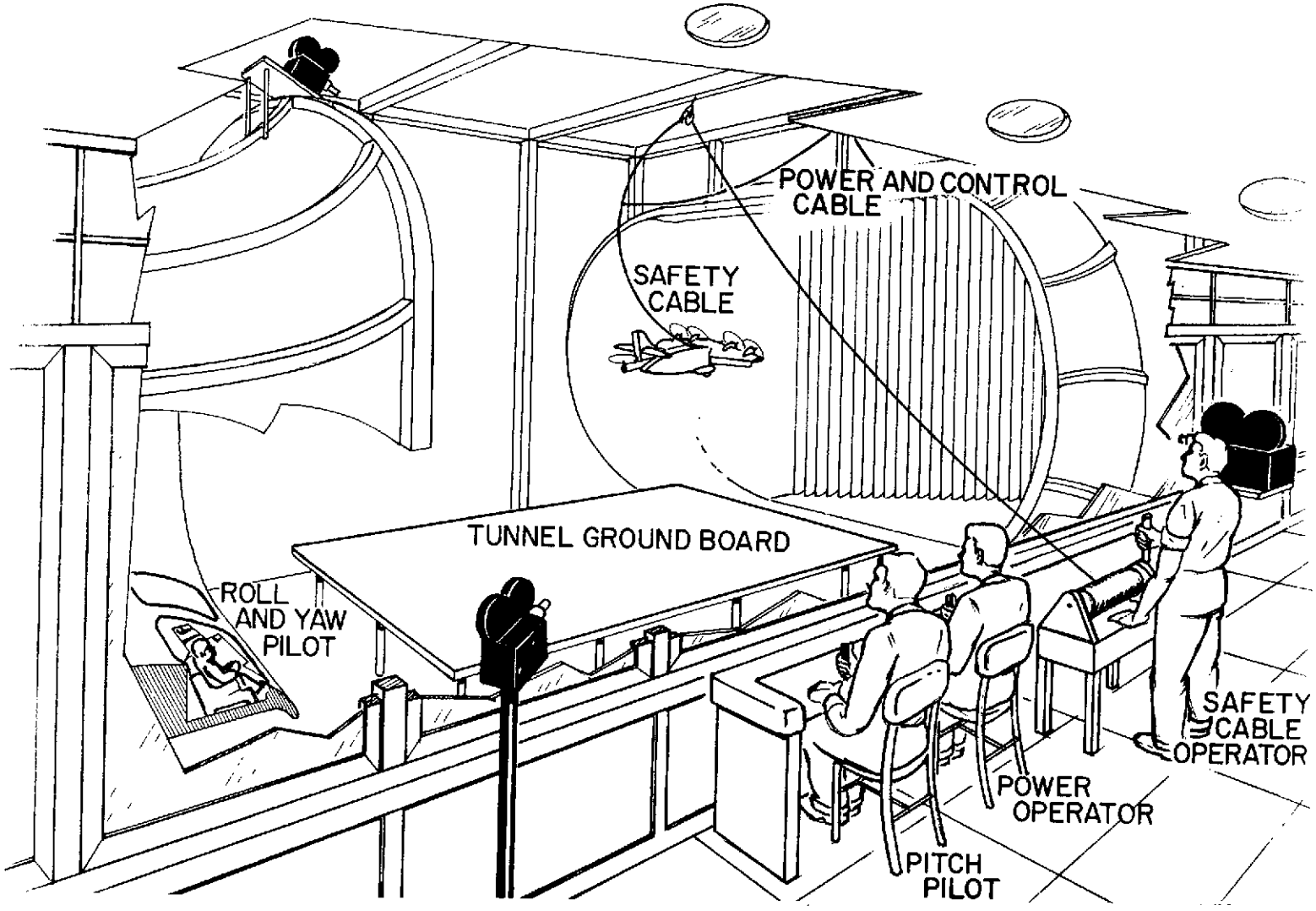

Figure 4.- Test setup for free-flight model testing in Langley full-scale tunnel

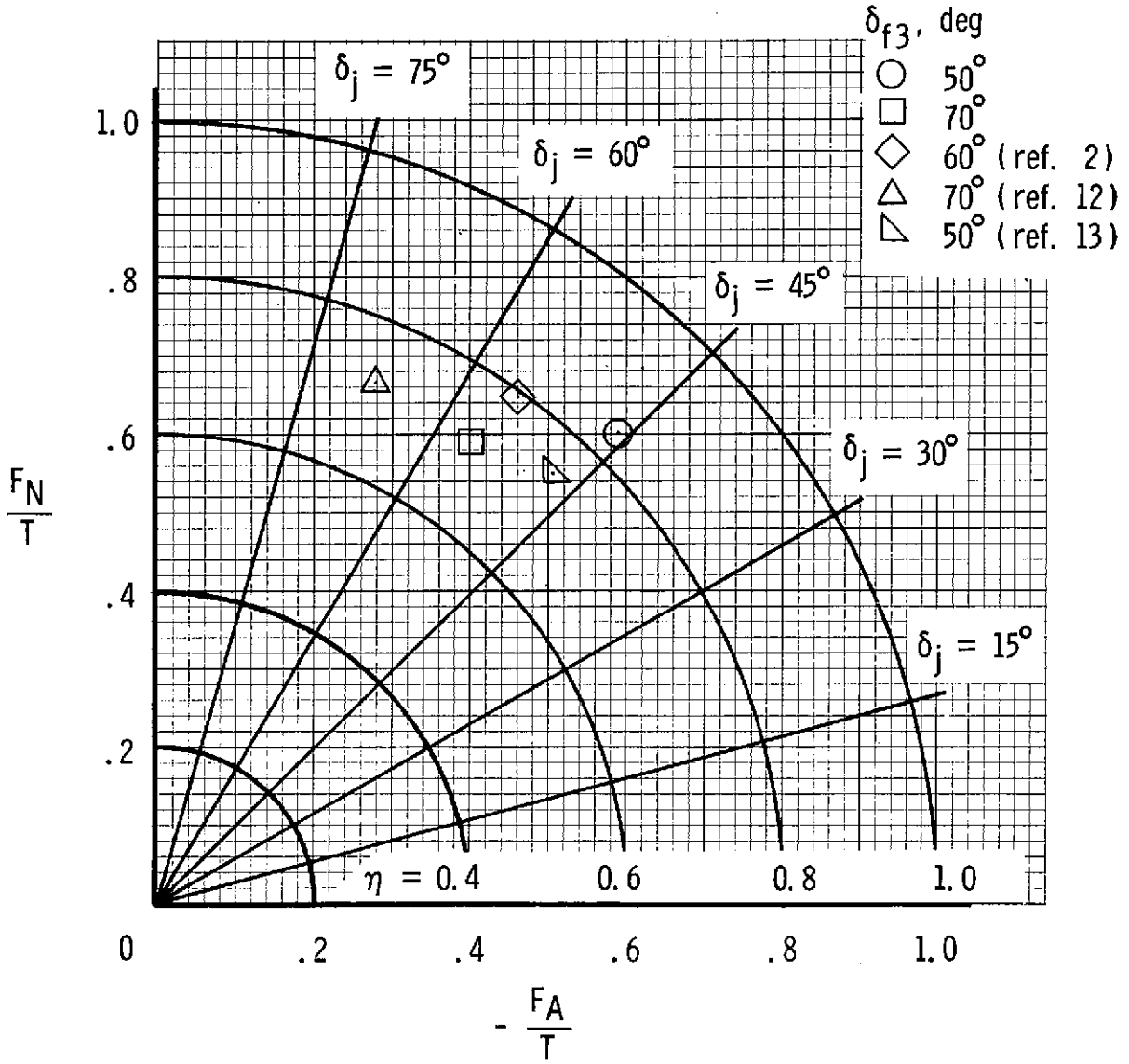

Figure 5.- Summary of static turning efficiency and jet deflection (turning angle).

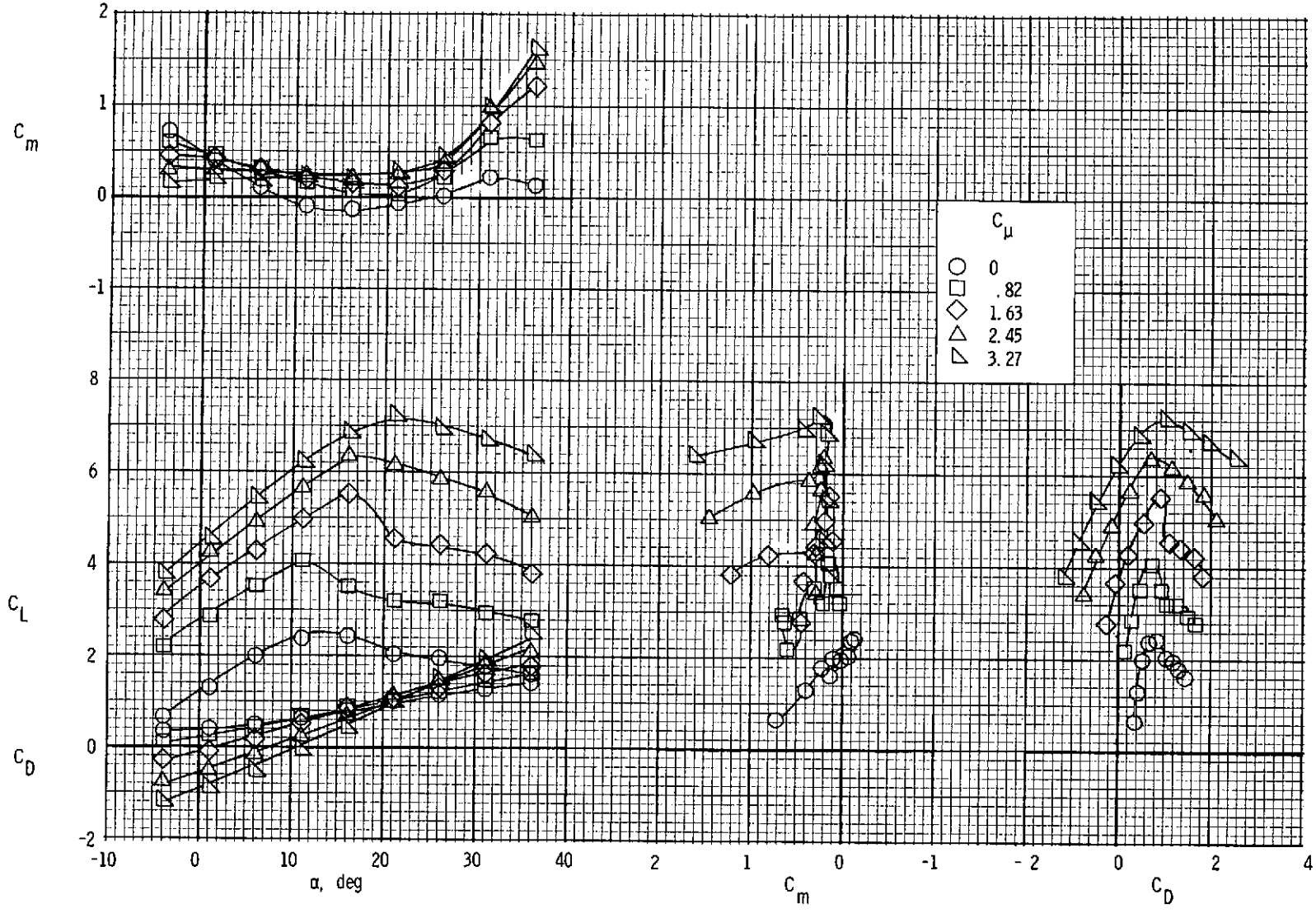

Figure 6.- Longitudinal characteristics of model. $\delta_{f3} = 40^o$; $i_t = 0^o$.

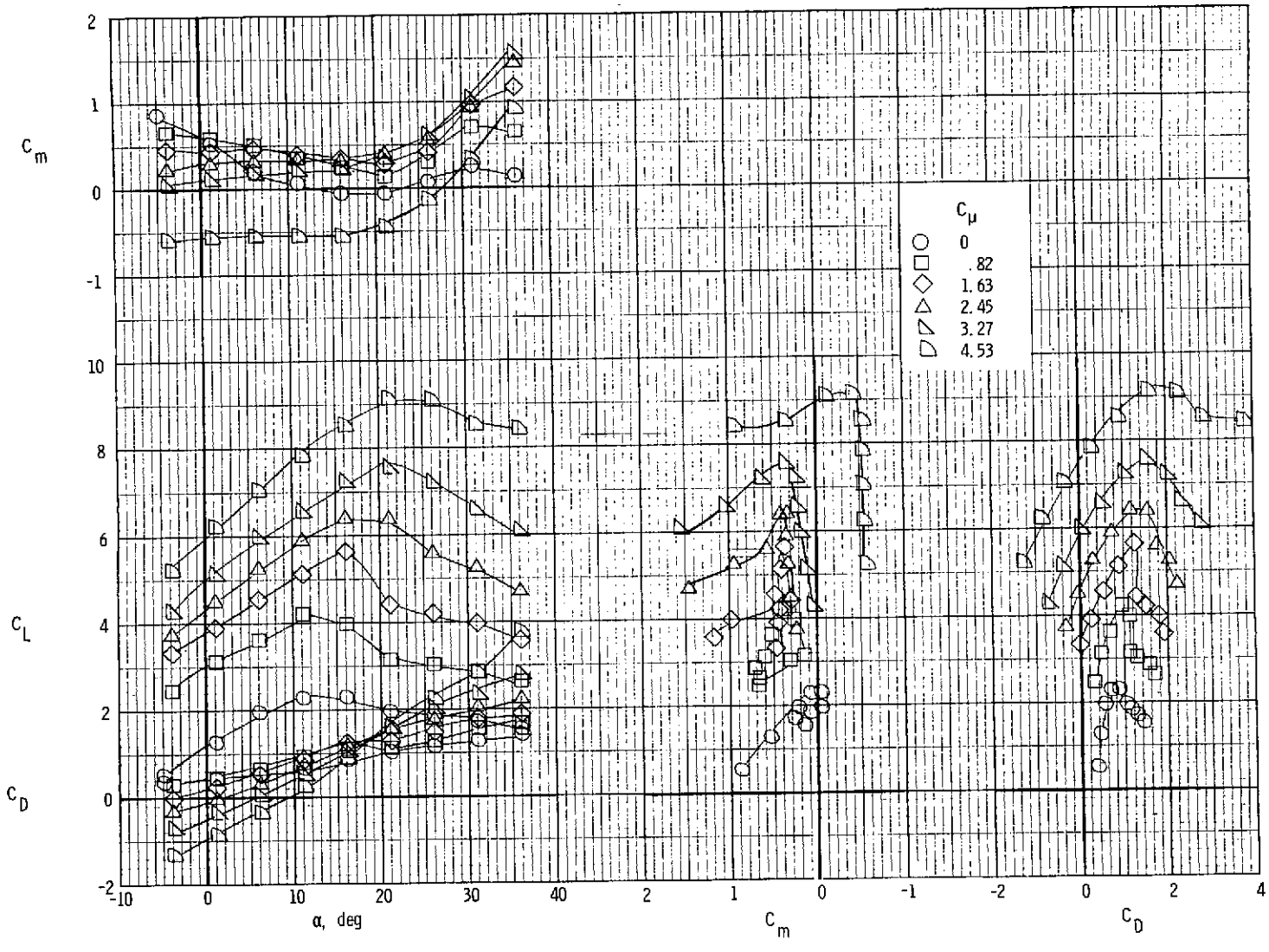

(a) $i_t = 0^o$.

Figure 7.- Longitudinal characteristics of model for three tail incidences. $\delta_{f3} = 50^o$.

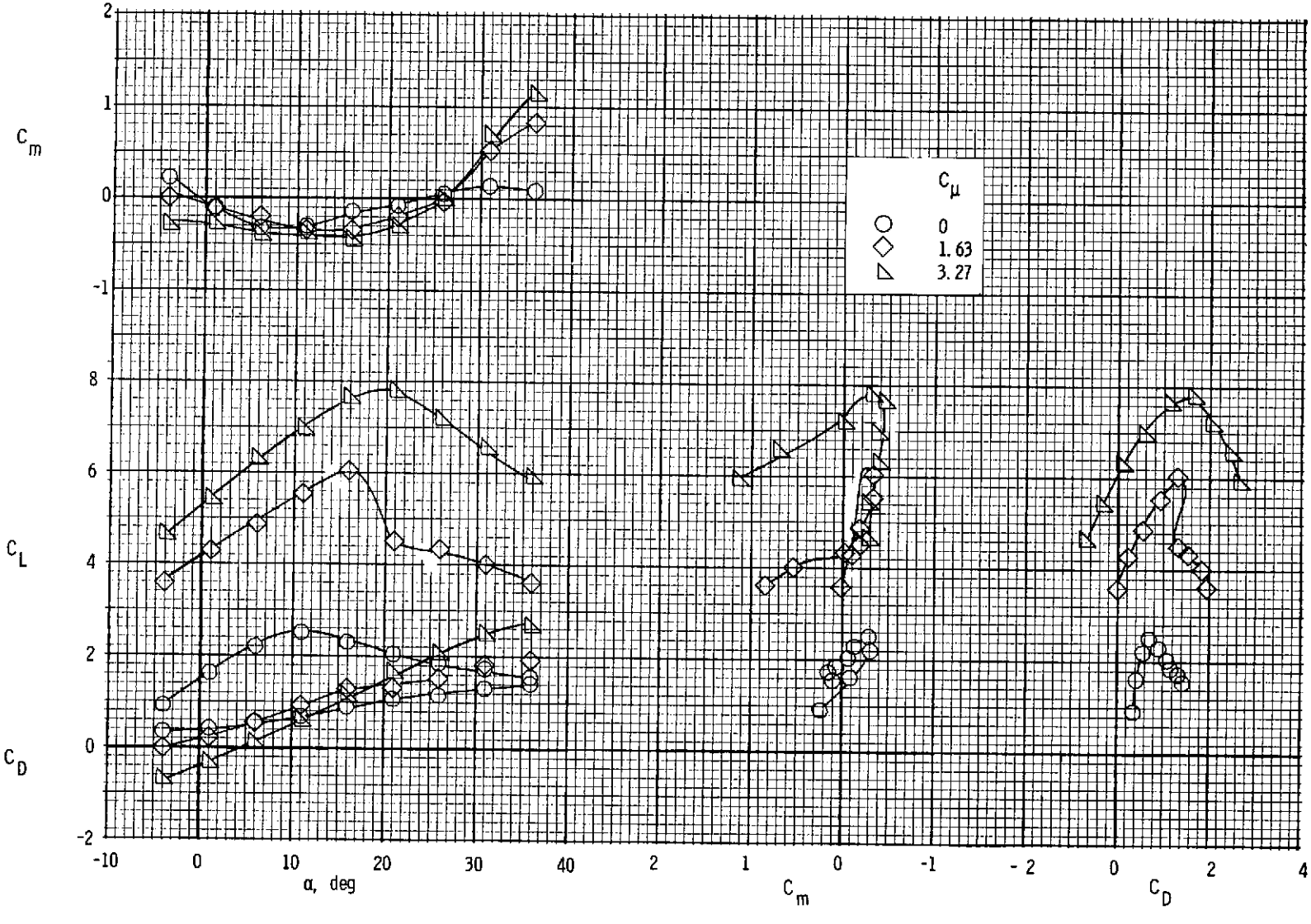

(b) $i_t = 5^o$.

Figure 7.- Continued.

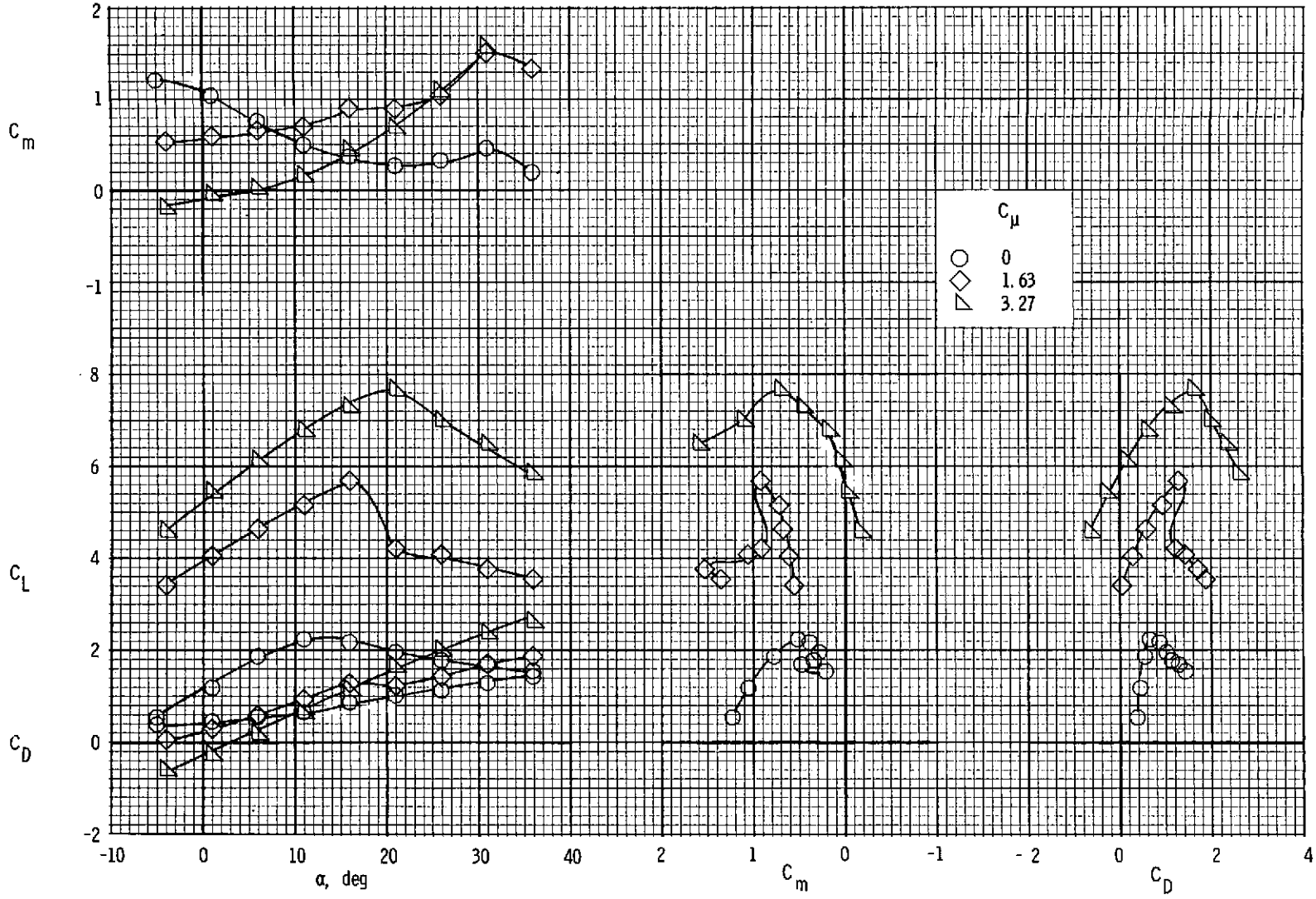

(c) $i_t = -5^o$.

Figure 7.- Concluded.

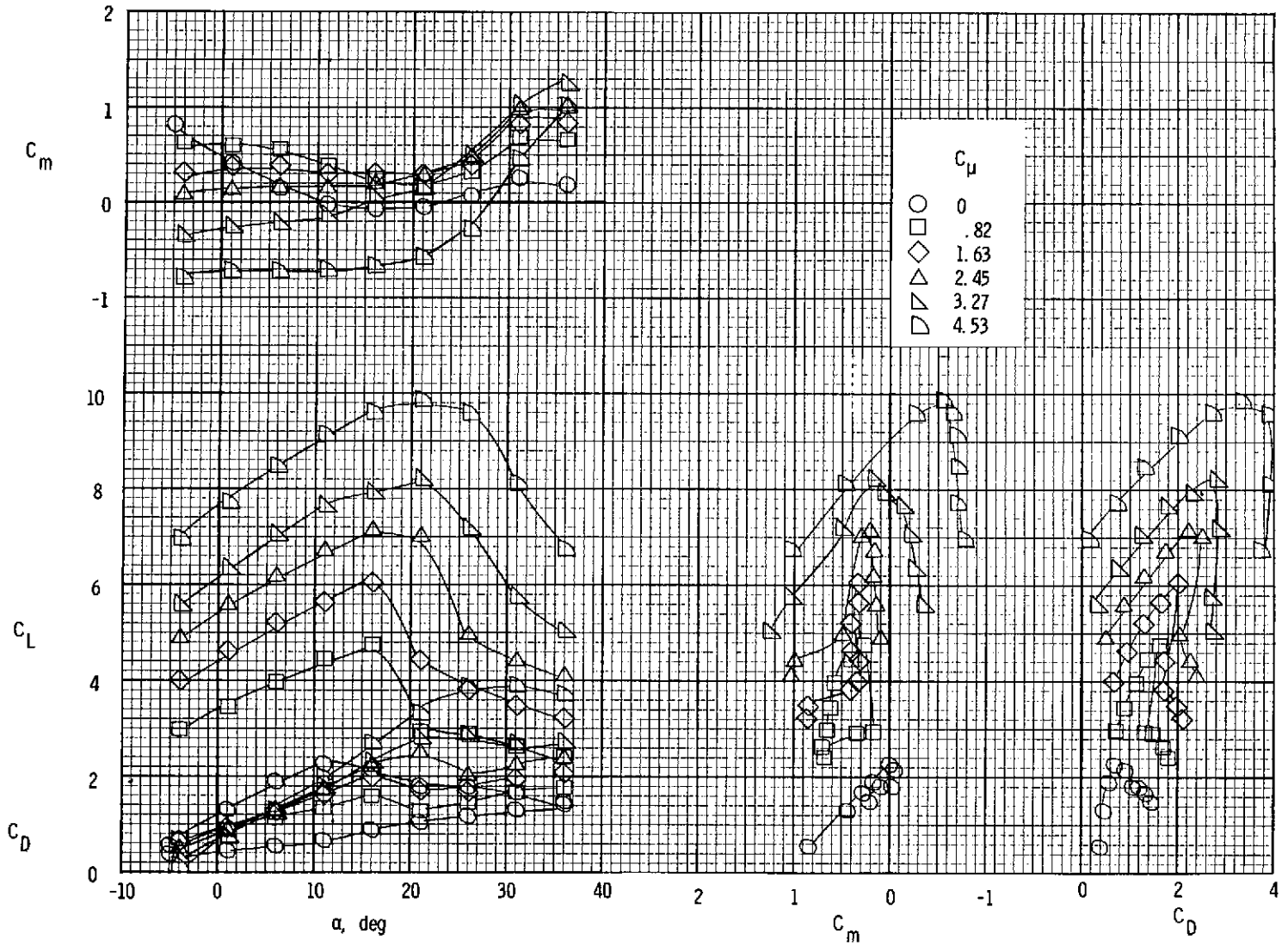

(a) $i_t = 0^o$.

Figure 8.- Longitudinal characteristics of model for three tail incidences. $\delta_{f3} = 70^o$.

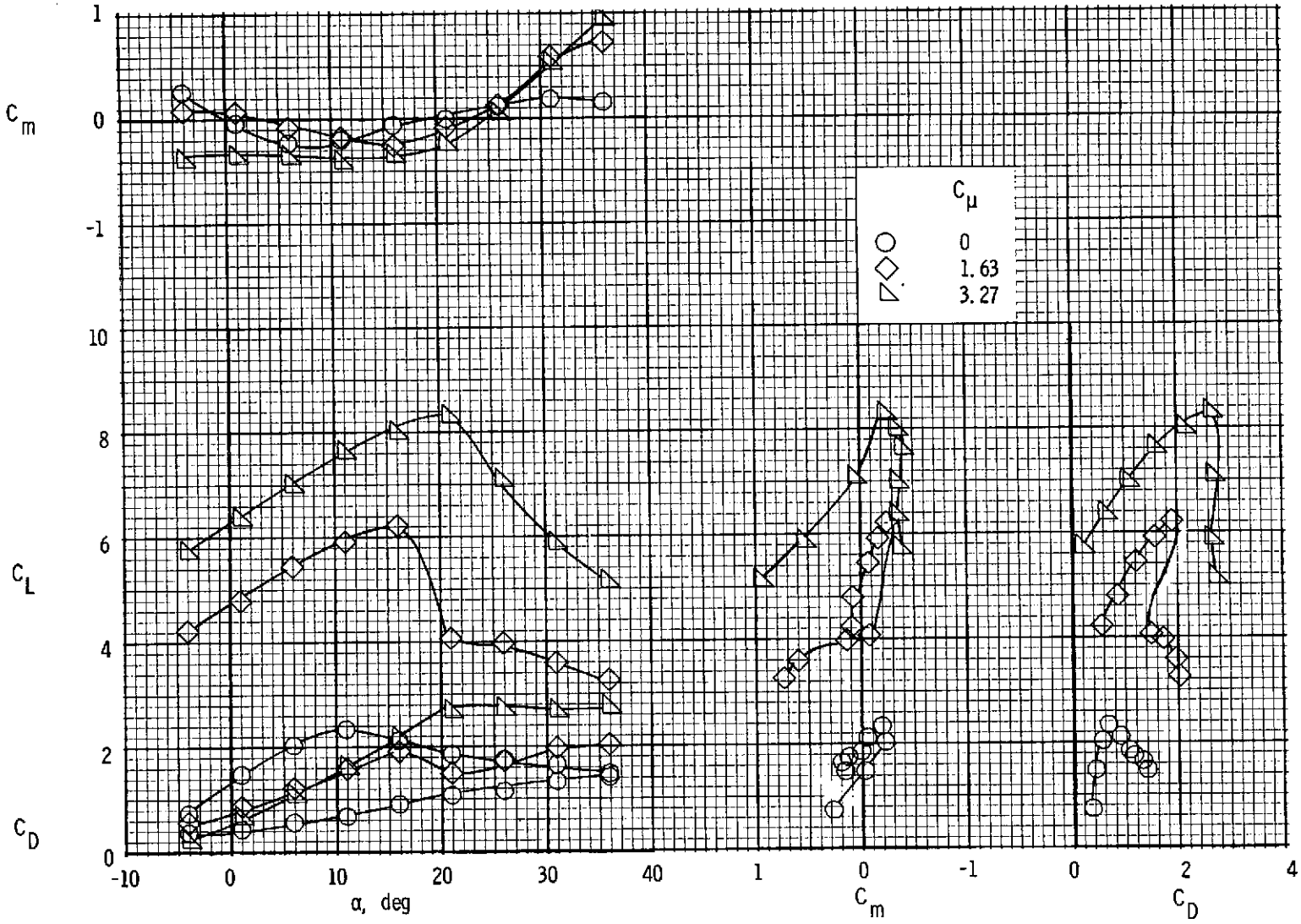

(b) $i_t = 5^o$.

Figure 8.- Continued.

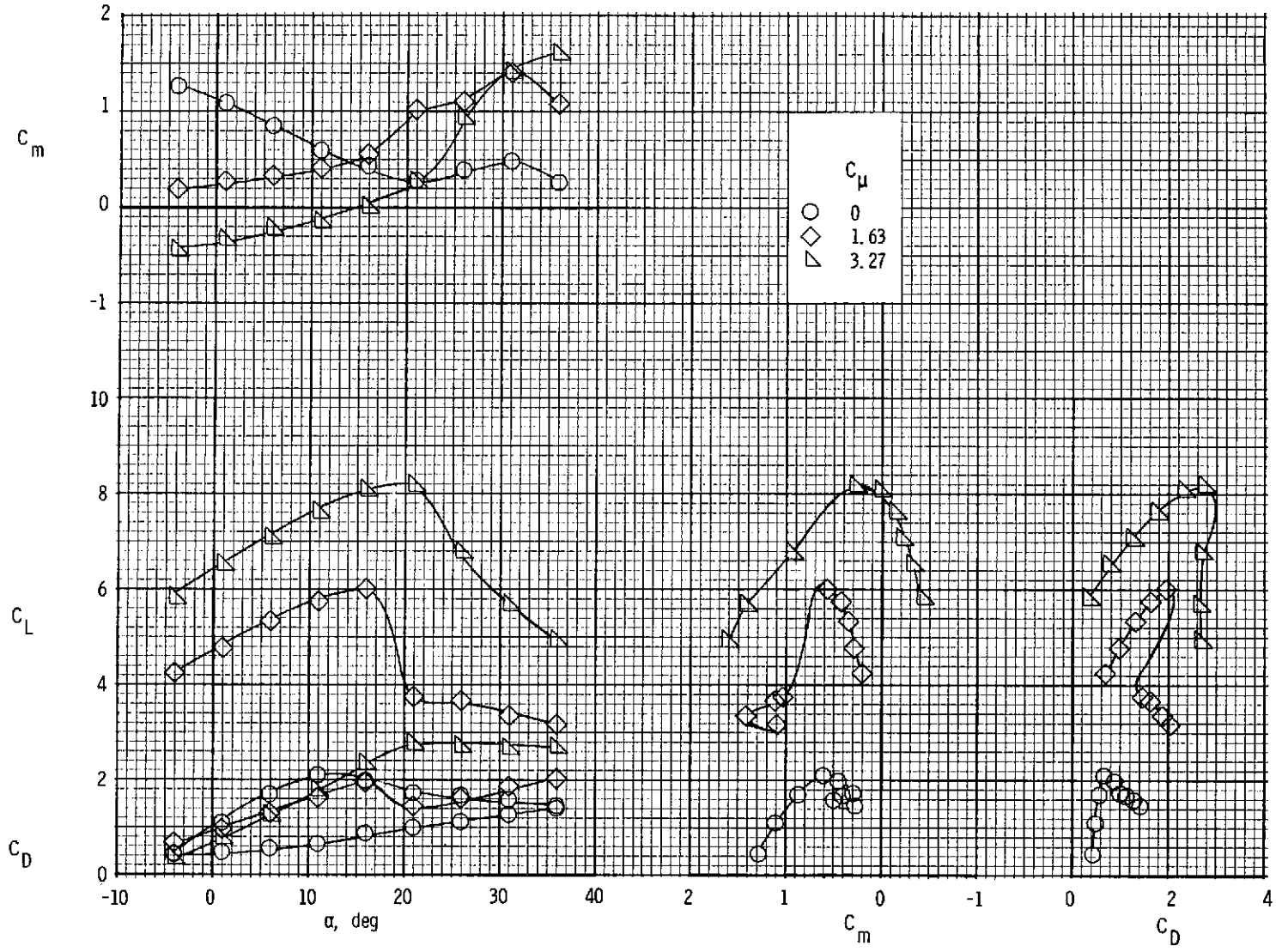

(c) $i_t = -5^o$.

Figure 8.- Concluded.

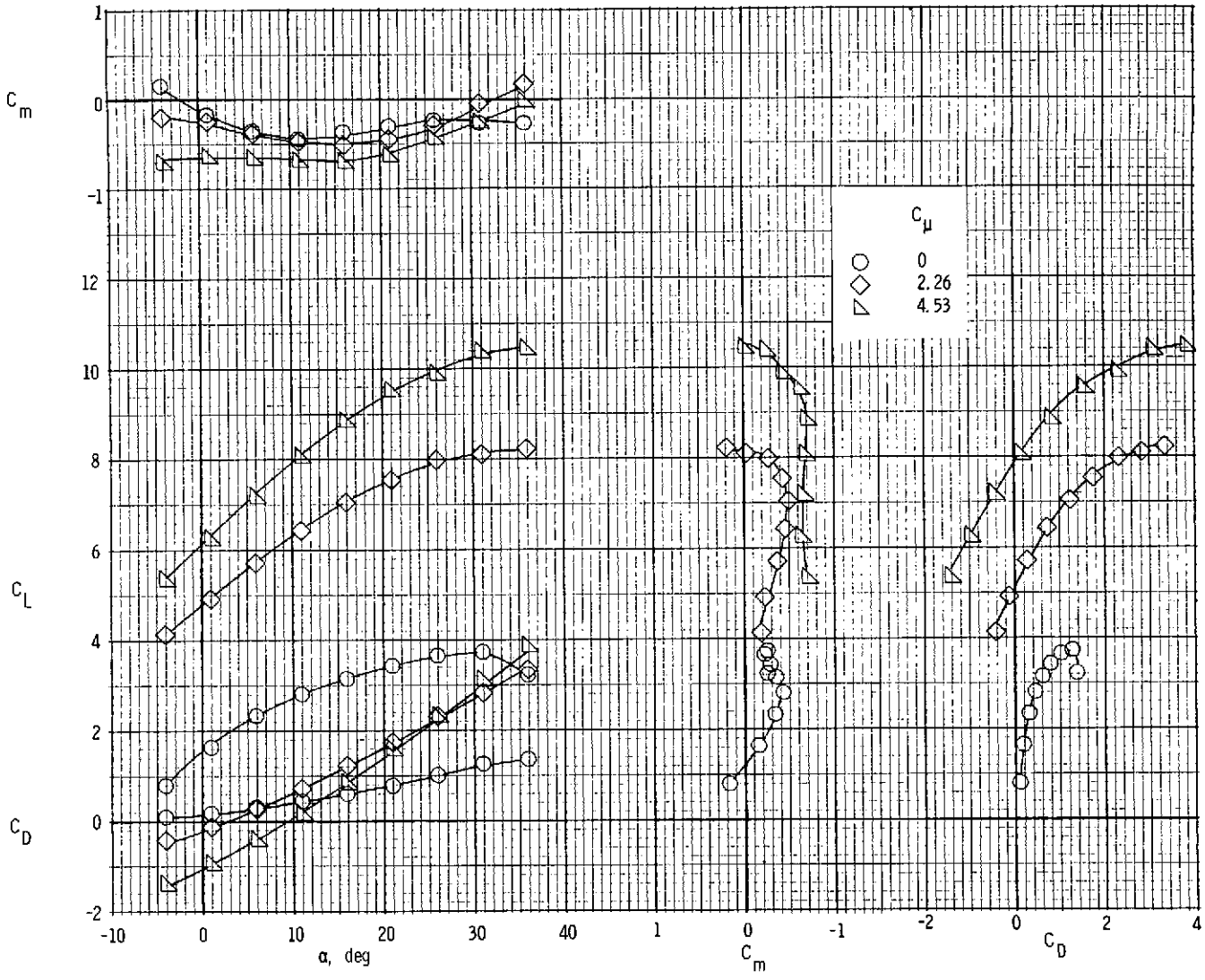

Figure 9.- Longitudinal characteristics of the model with leading-edge blowing. $\delta_{f3} = 50^o$; $i_t = 0^o$; $C_{\mu,le} = 0.23$.

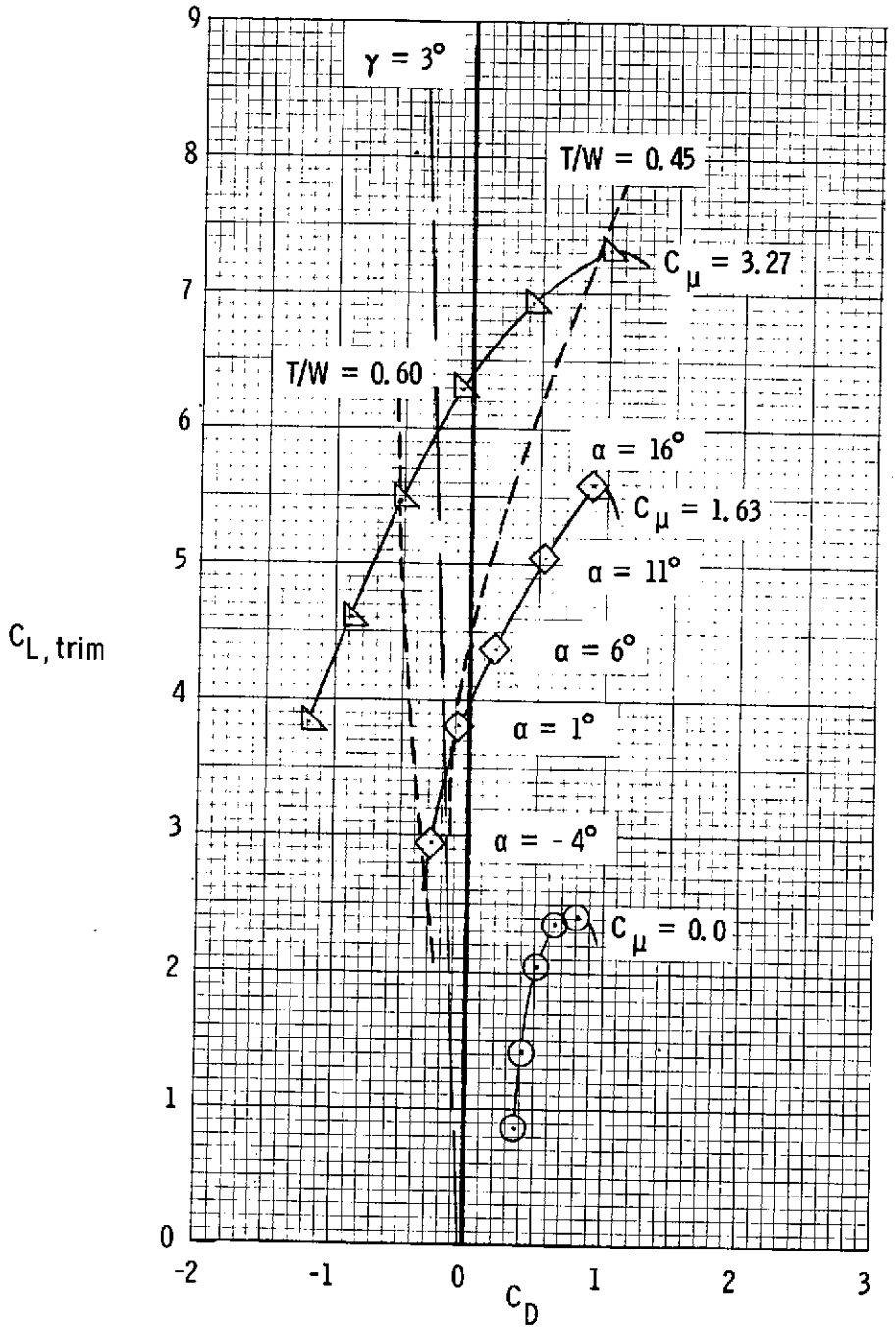

(a) $\delta_{f3} = 40^{\circ}$.

Figure 10.- Lift-drag polar for several trailing-edge flap deflections.

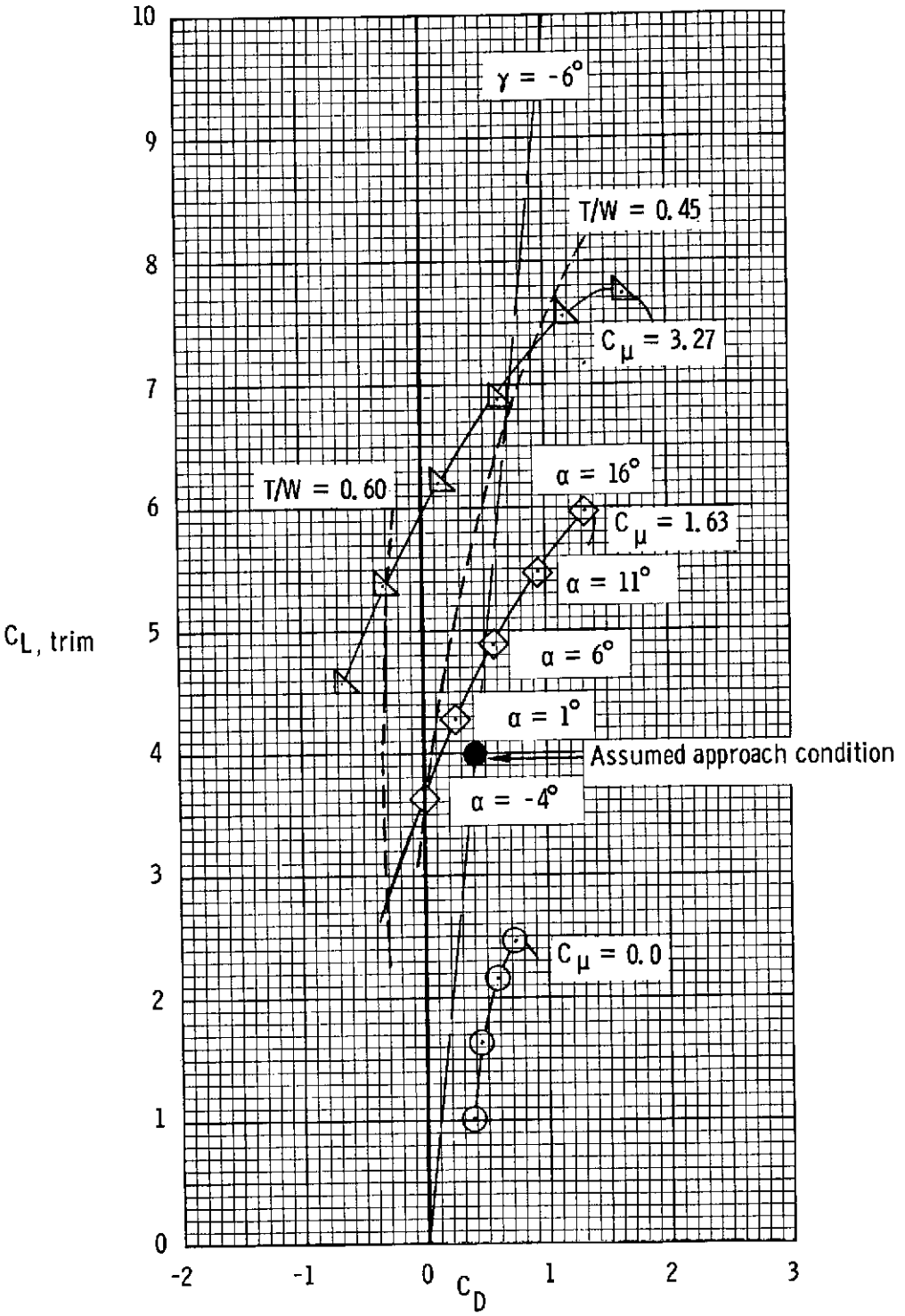

(b) $\delta_{f3} = 50^{o}$.

Figure 10.- Continued.

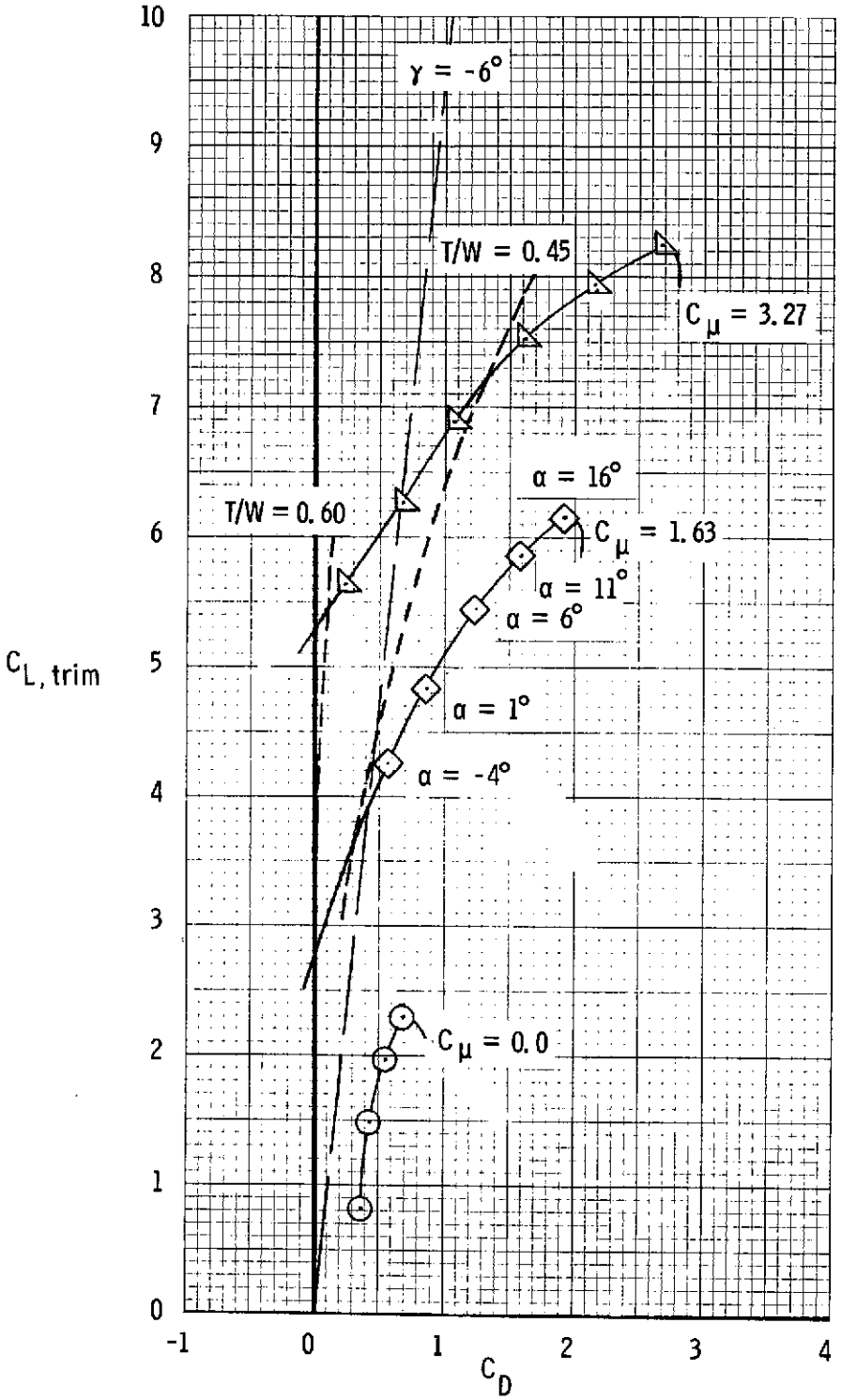

(c) $\delta_{f3} = 70^{\circ}$.

Figure 10.- Concluded.

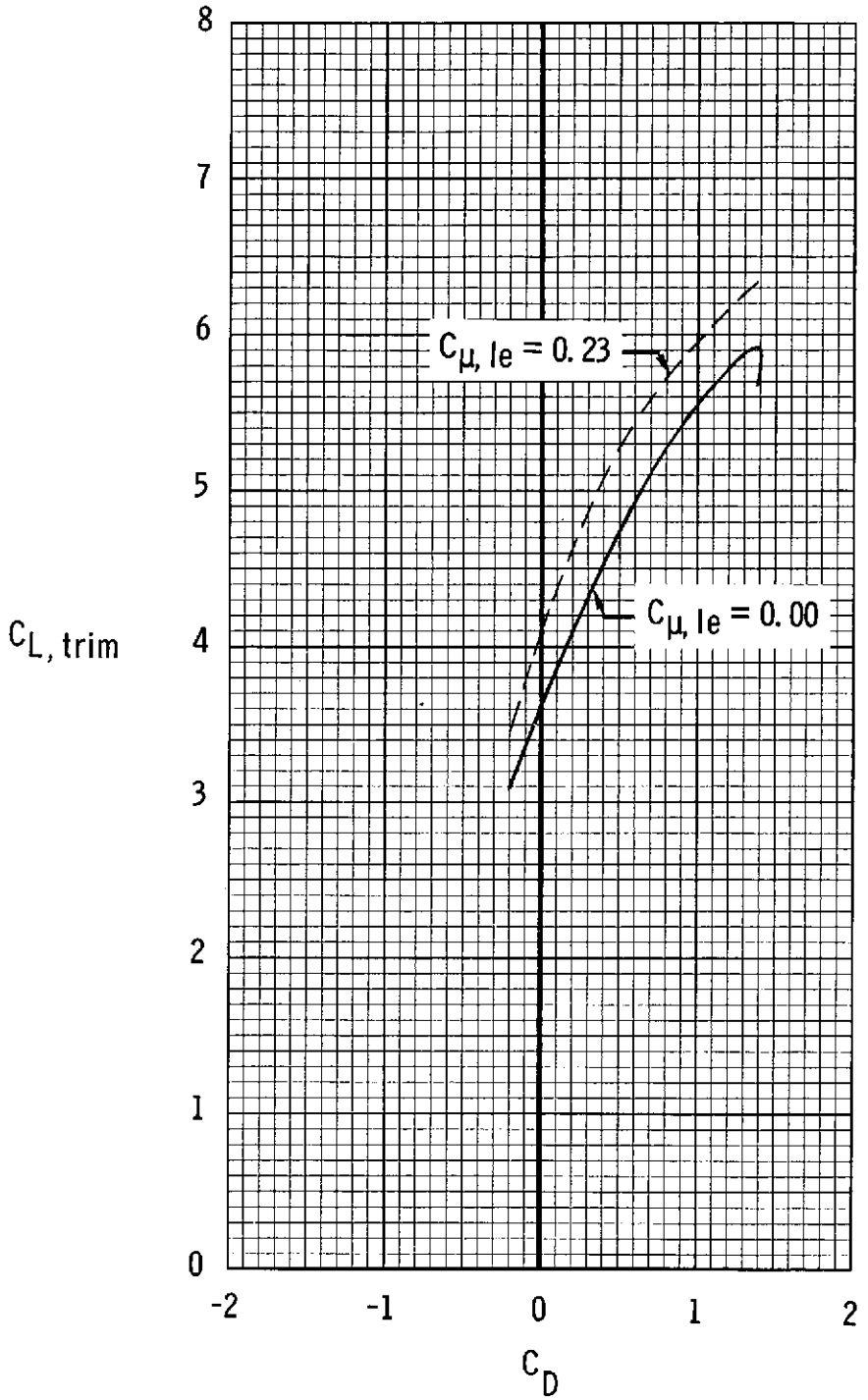

Figure 11.- Effect of leading-edge blowing on lift-drag polar. $\delta_{f3} = 50^{o}$; $C_{\mu} = 1.63$.

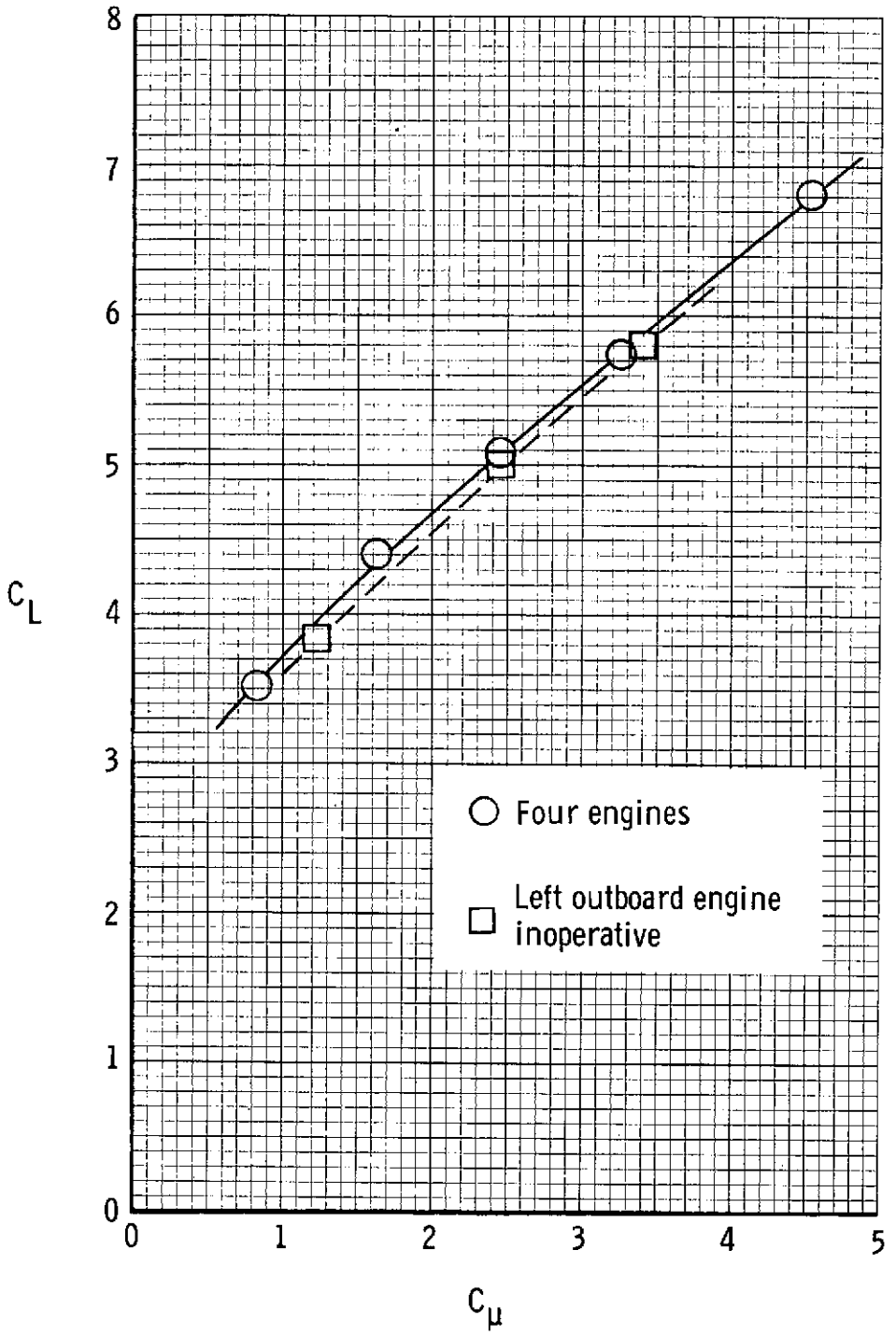

Figure 12.- Comparison of lift characteristics of the model with all engines operating and with one outboard engine inoperative. $\delta_{f3} = 50^o$; $\alpha = 5^o$; $i_t = 0^o$.

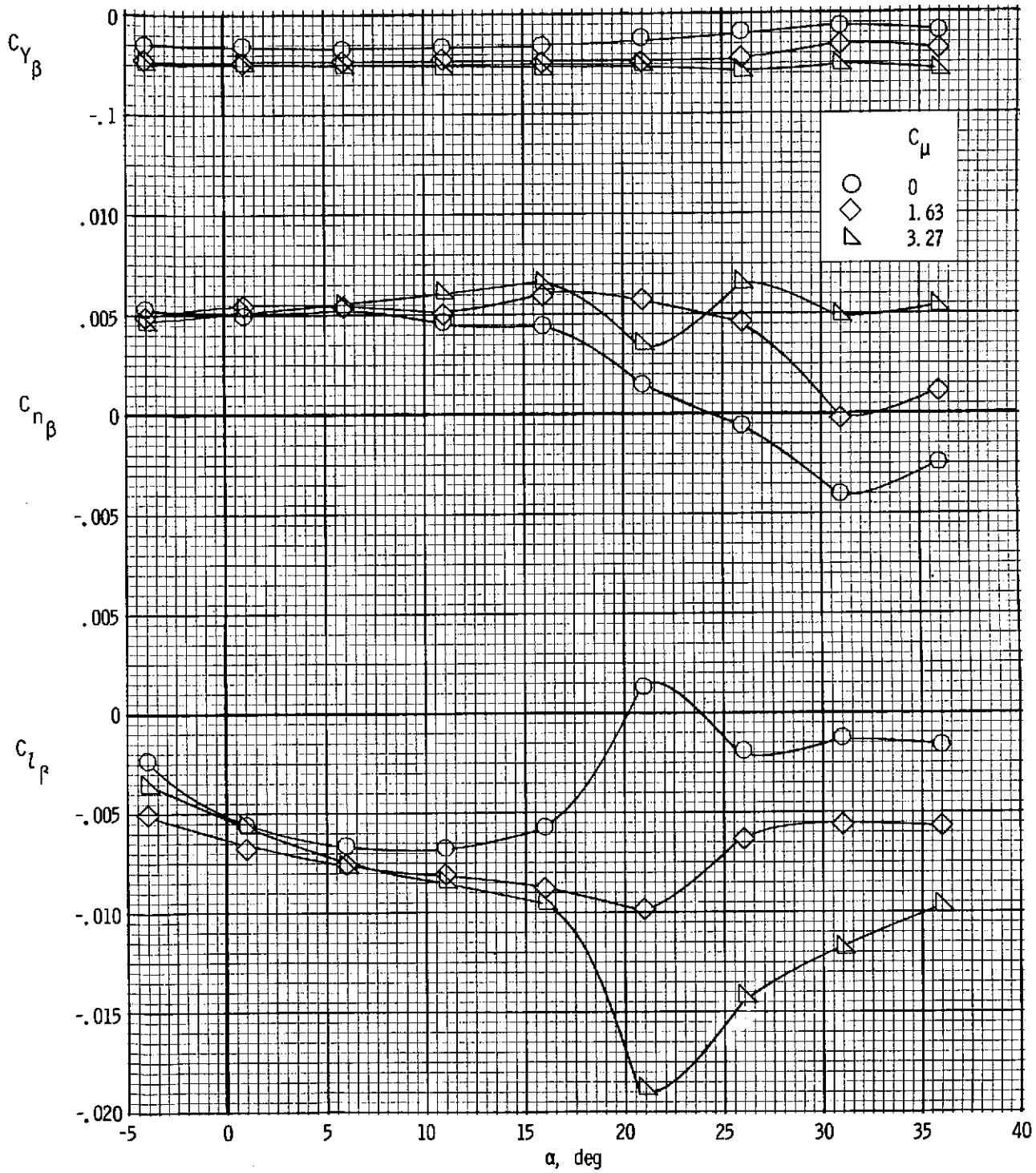

(a) $\delta_{f3} = 40^o$.

Figure 13.- Lateral stability characteristics of model for three flap deflections. $i_t = 0^o$; $\delta_e = -50^o$.

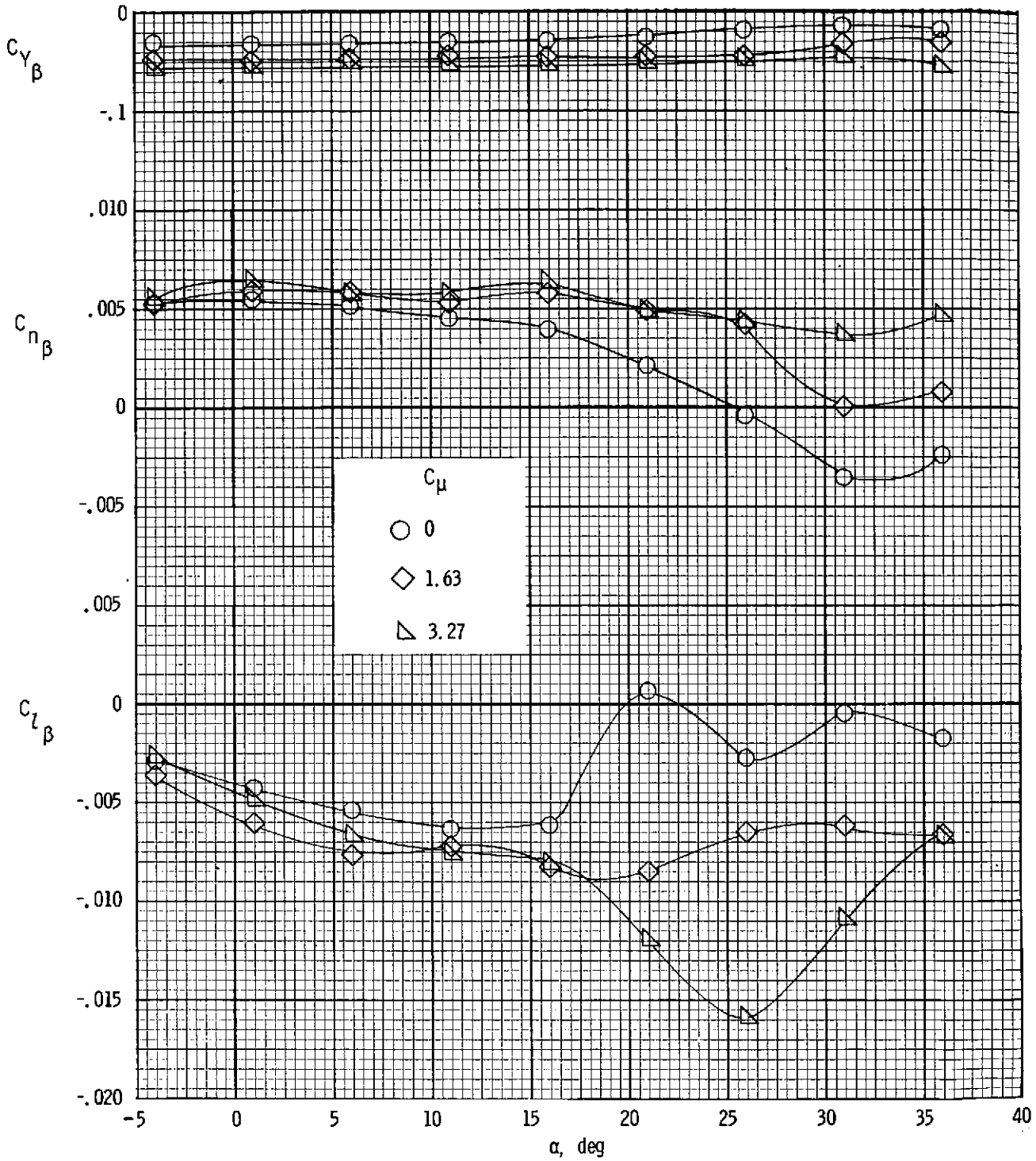

(b) $\delta_{f3} = 50^o$.

Figure 13.- Continued.

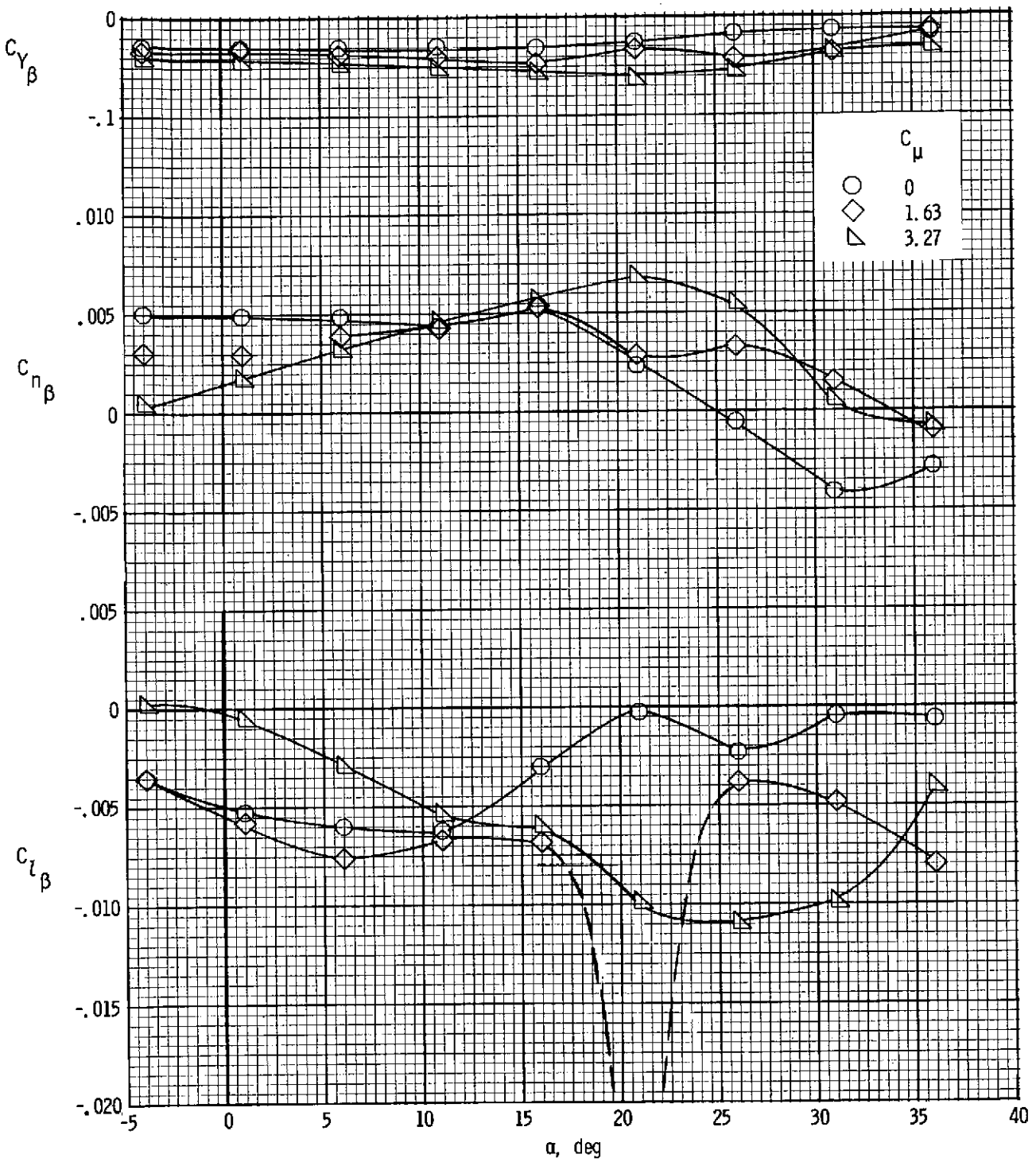

(c) $\delta_{f3} = 70^{\circ}$.

Figure 13.- Concluded.

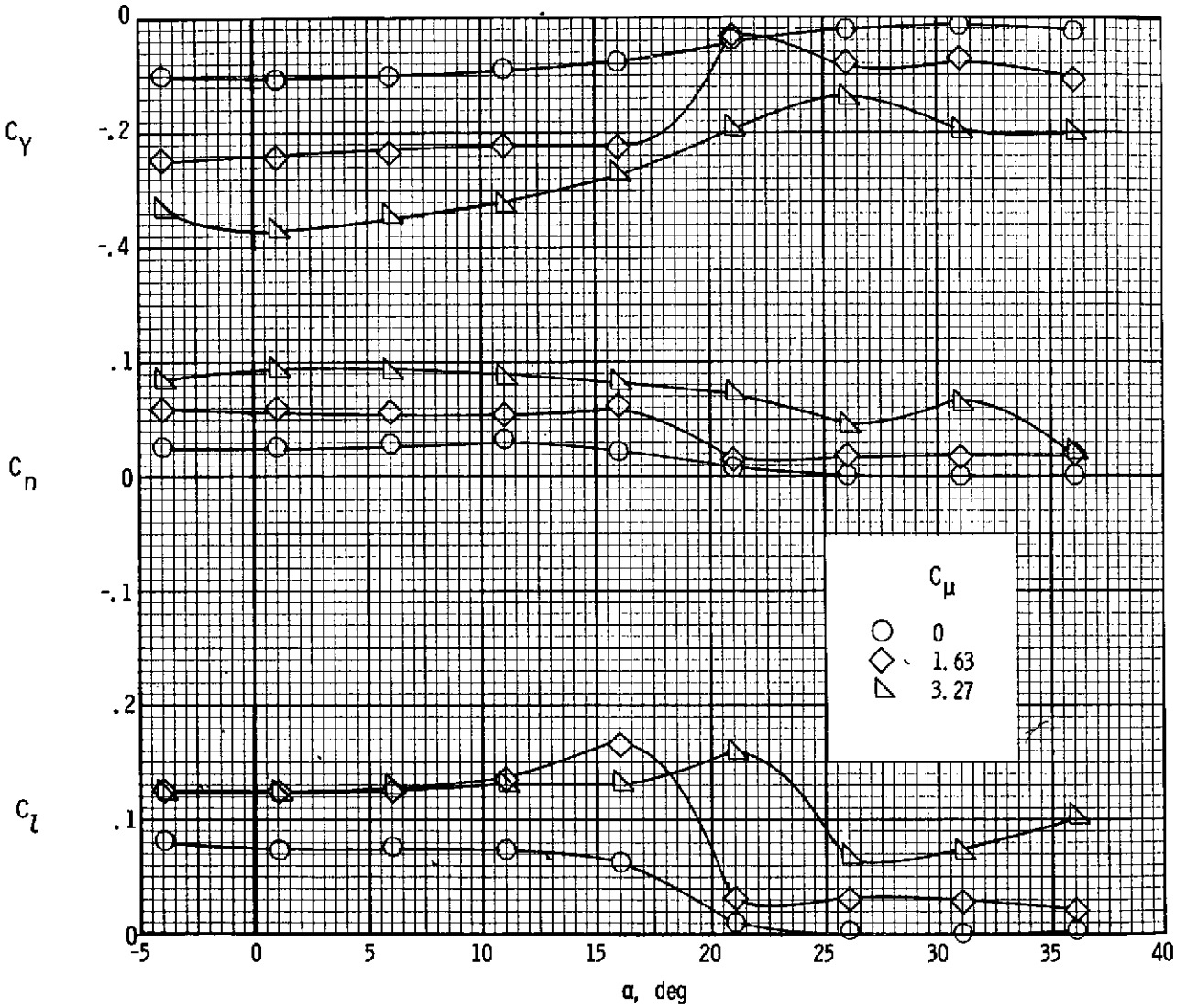

(a) Lateral characteristics.

Figure 14.- Spoiler effectiveness. Right semispan spoiler deflected 60°. $\delta_{f3} = 50°$; $i_t = 0°$; $\delta_e = -50°$.

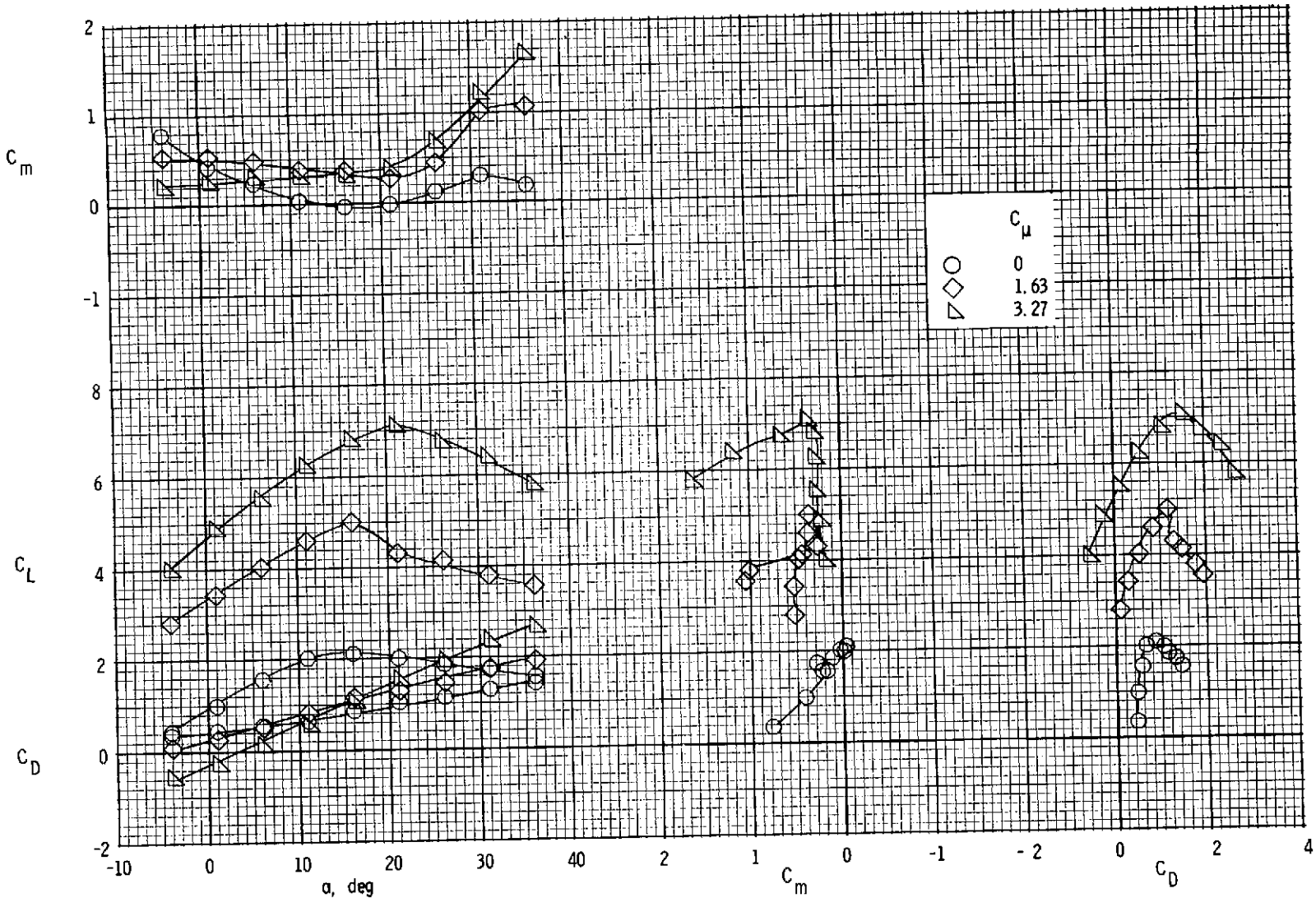

(b) Longitudinal characteristics.

Figure 14.- Concluded.

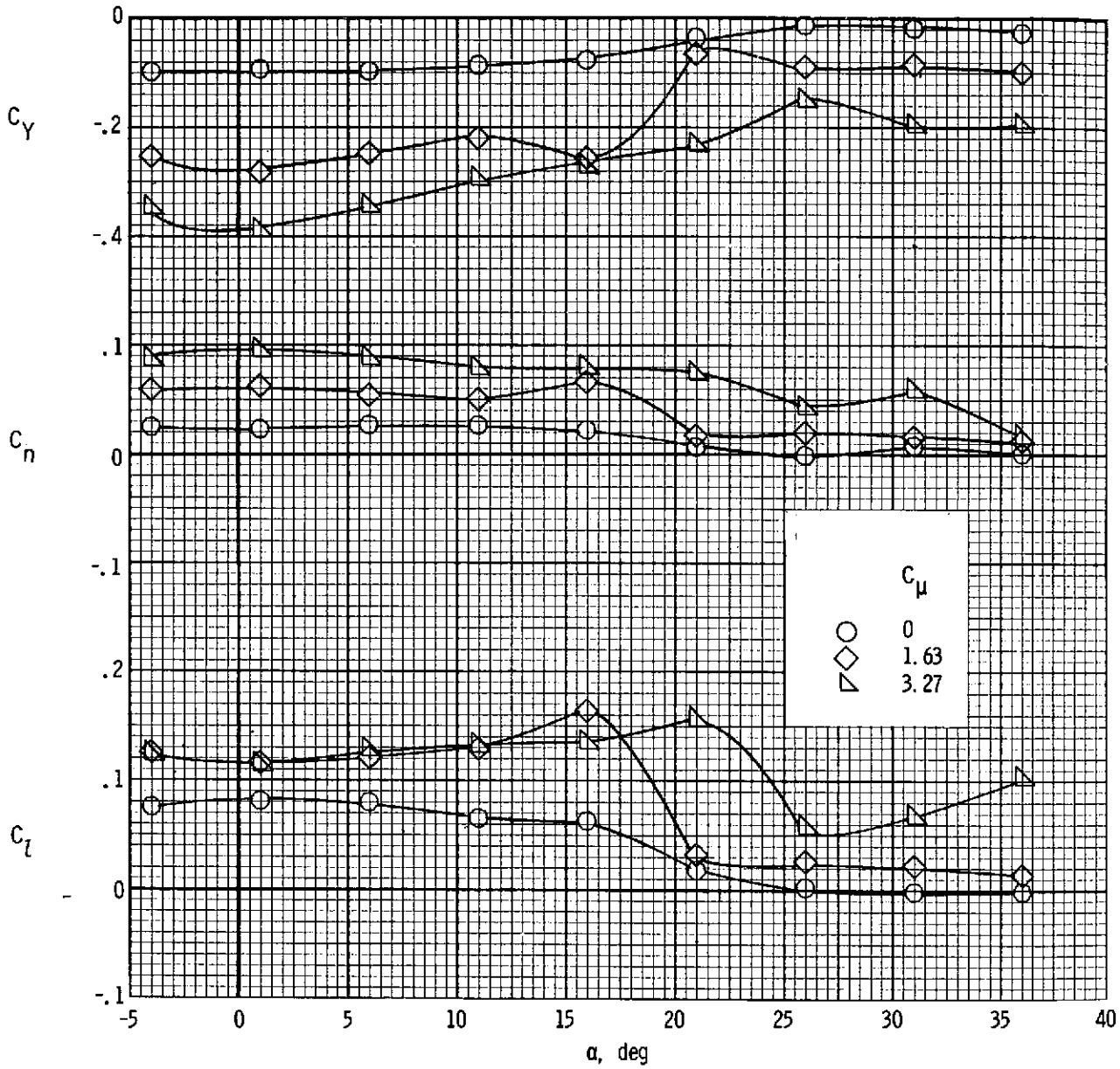

(a) Lateral characteristics.

Figure 15.- Spoiler and aileron effectiveness. Right semispan spoiler deflected 60°. Left aileron deflected 20° below initial 50° deflection. $\delta_{f3} = 50^\circ$; $i_t = 0^\circ$; $\delta_e = -50^\circ$.

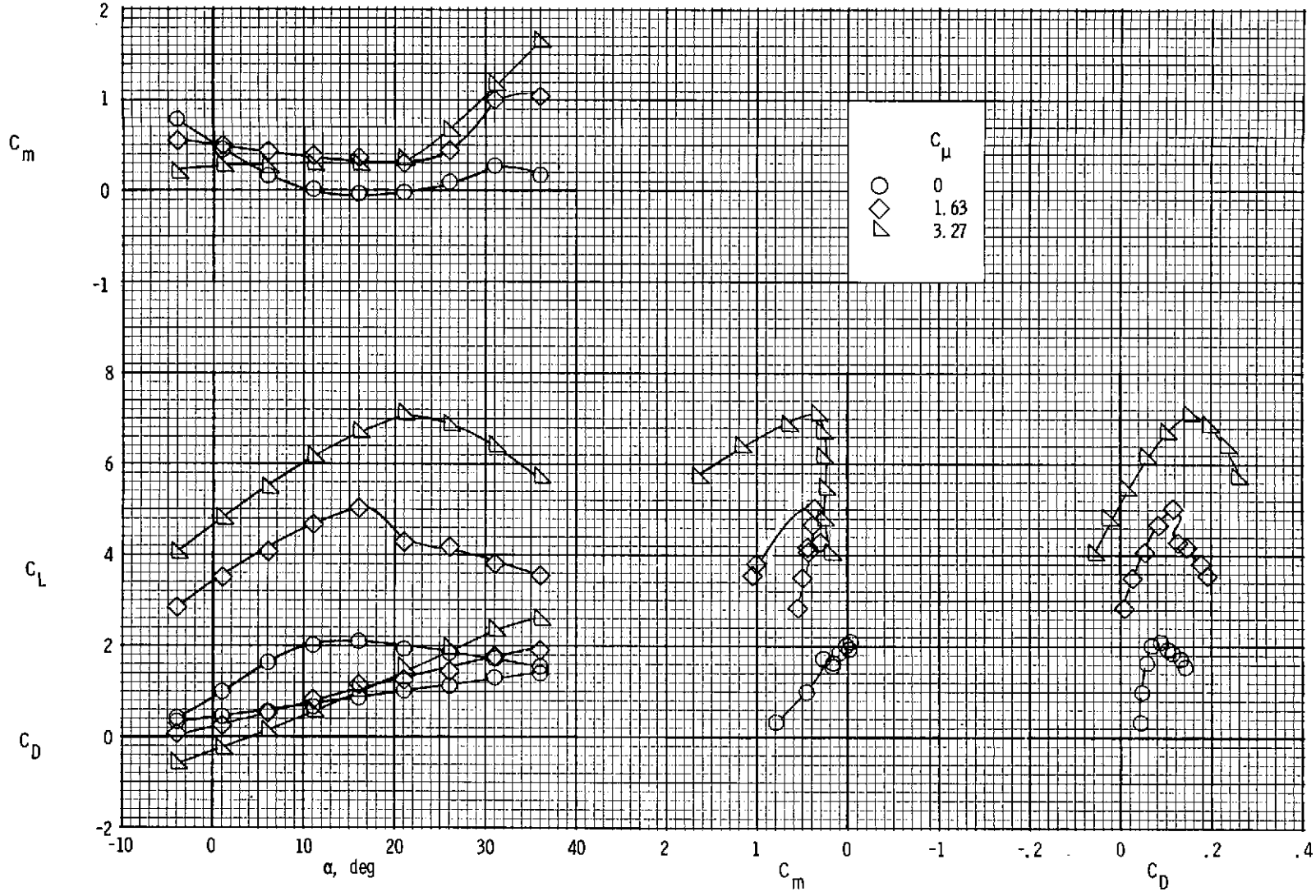

(b) Longitudinal characteristics.

Figure 15.- Concluded.

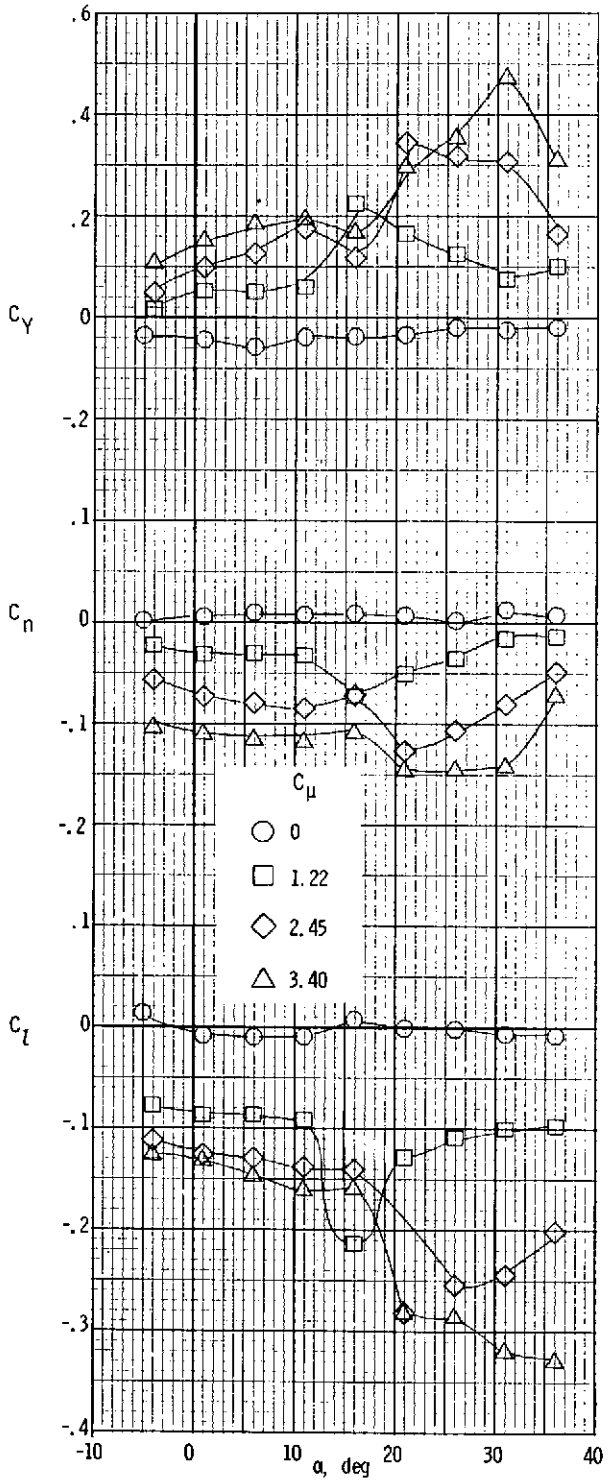

(a) Lateral; no leading edge blowing.

Figure 16.- Lateral and longitudinal characteristics, left outboard engine not operating. $\delta_{f3} = 50^{o}$; $i_t = 0^{o}$; $\delta_e = -50^{o}$.

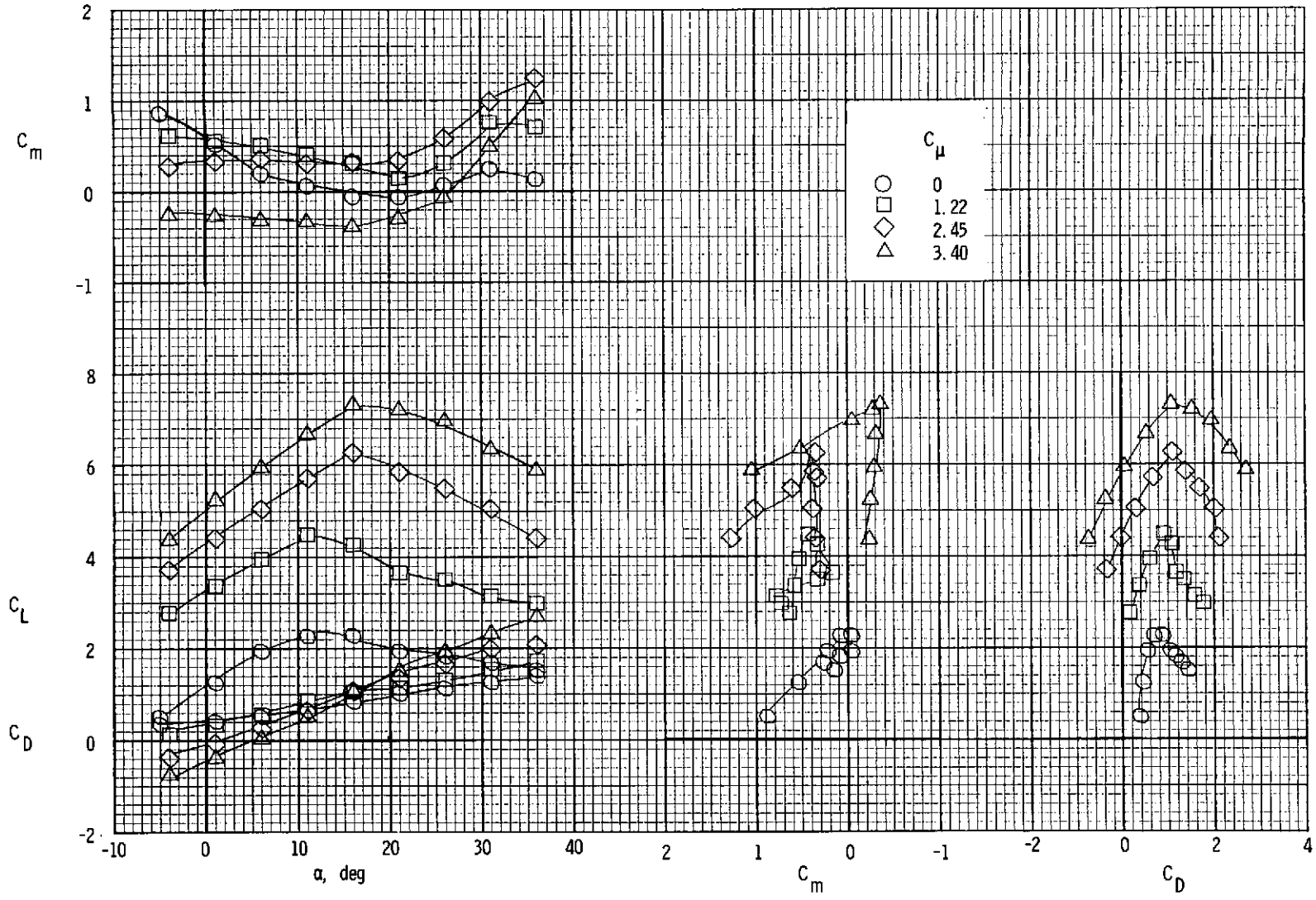

(b) Longitudinal; no leading edge blowing.

Figure 16.- Continued.

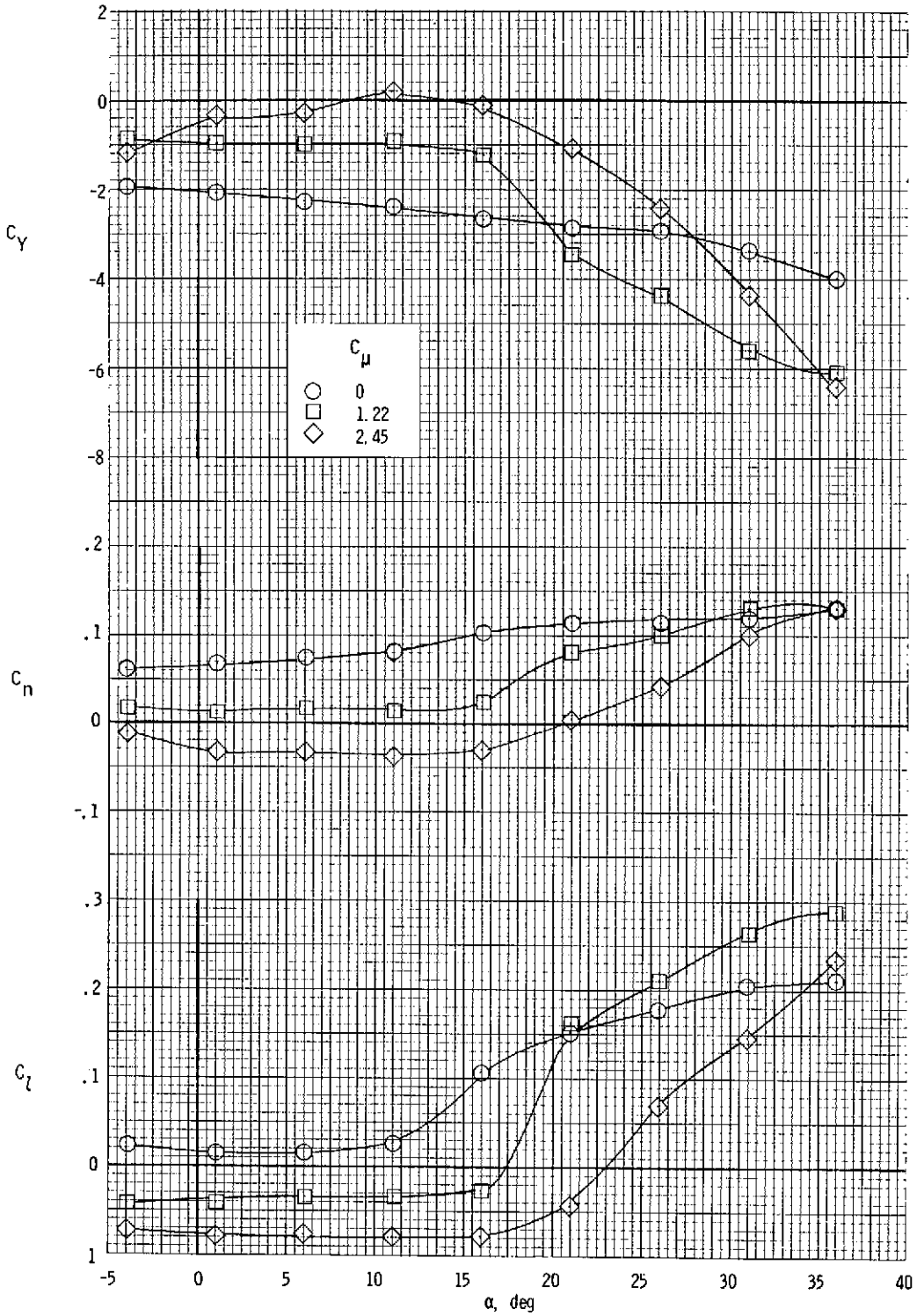

(c) Lateral; $C_{\mu,le,L} = 0.23$.

Figure 16.- Continued.

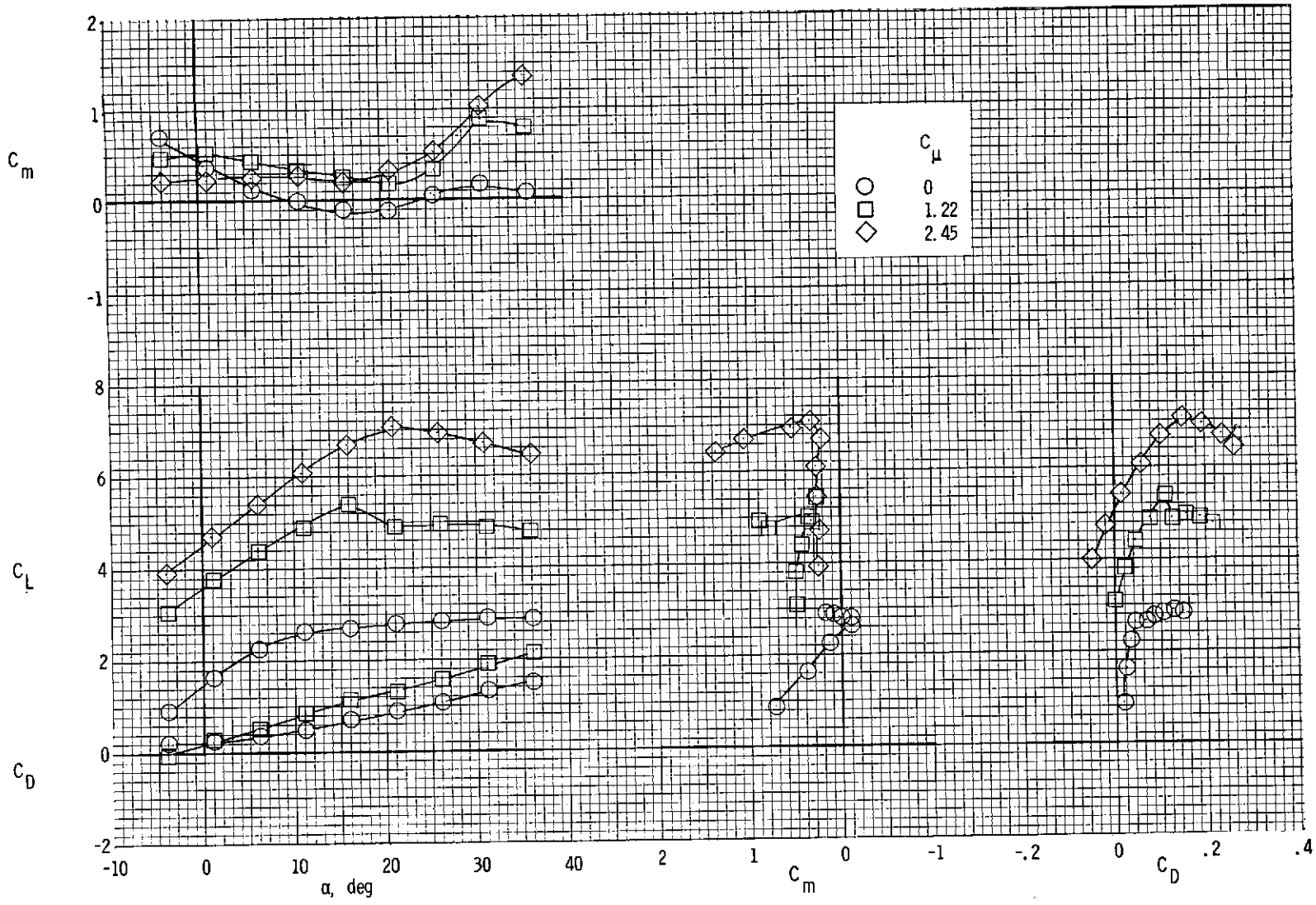

(d) Longitudinal; $C_{\mu,le,L} = 0.23$.

Figure 16.- Concluded.

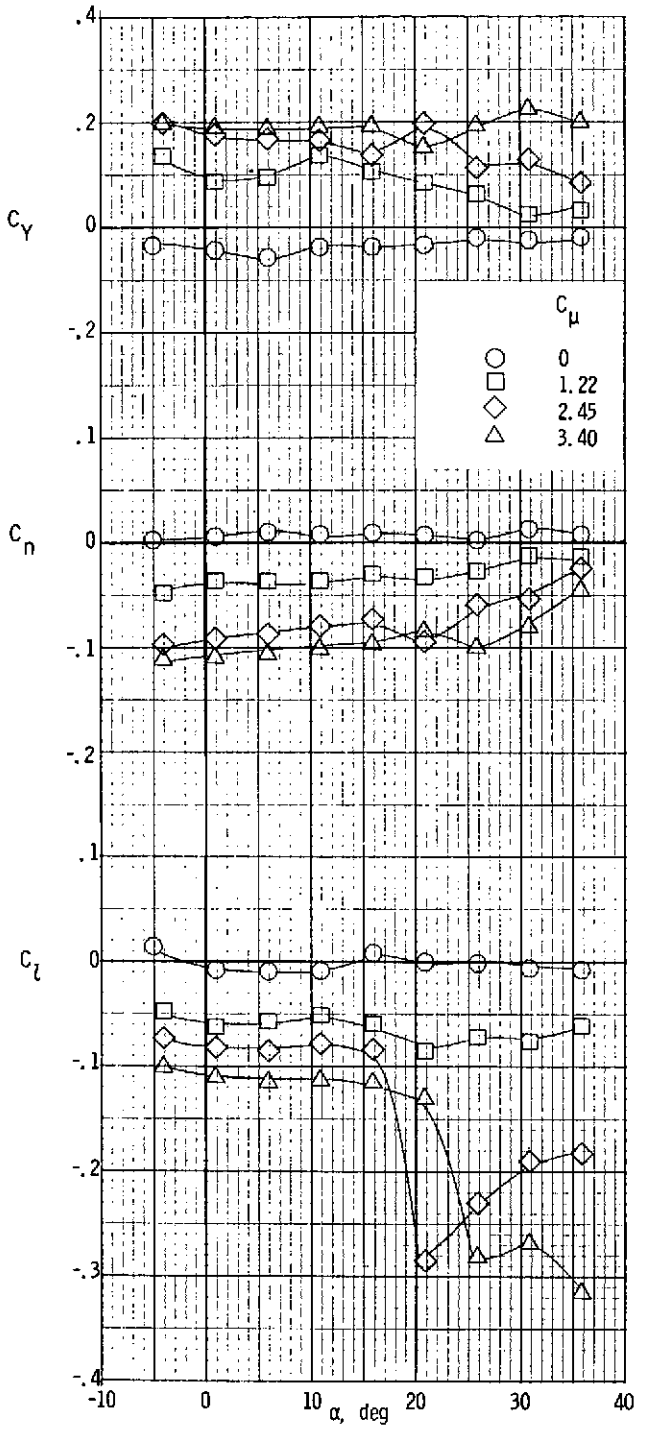

(a) Lateral characteristics.

Figure 17.- Lateral and longitudinal characteristics, left inboard engine not operating. $\delta_{f3} = 50^o$; $i_t = 0^o$; $\delta_e = -50^o$.

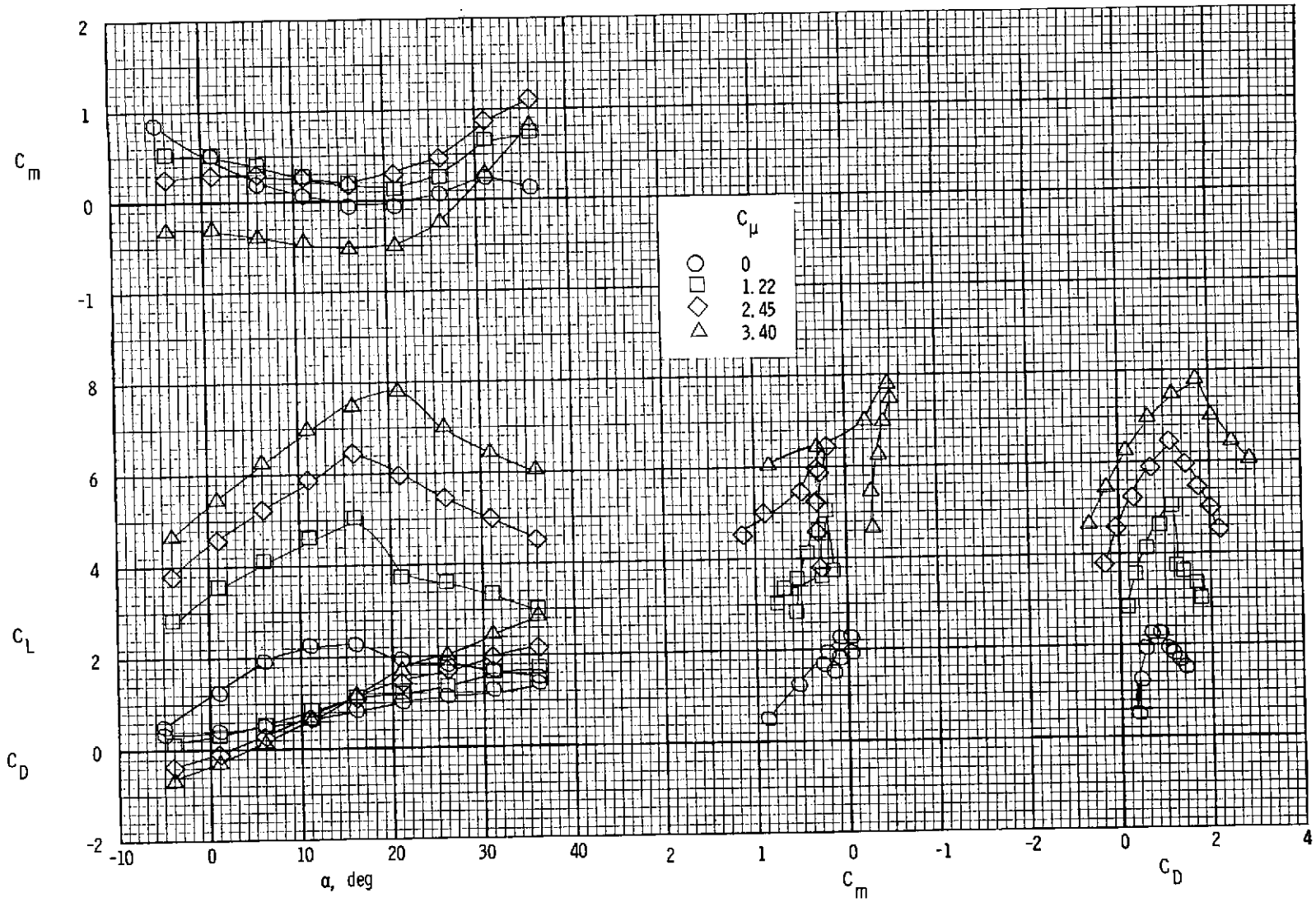

(b) Longitudinal characteristics.

Figure 17.- Concluded.

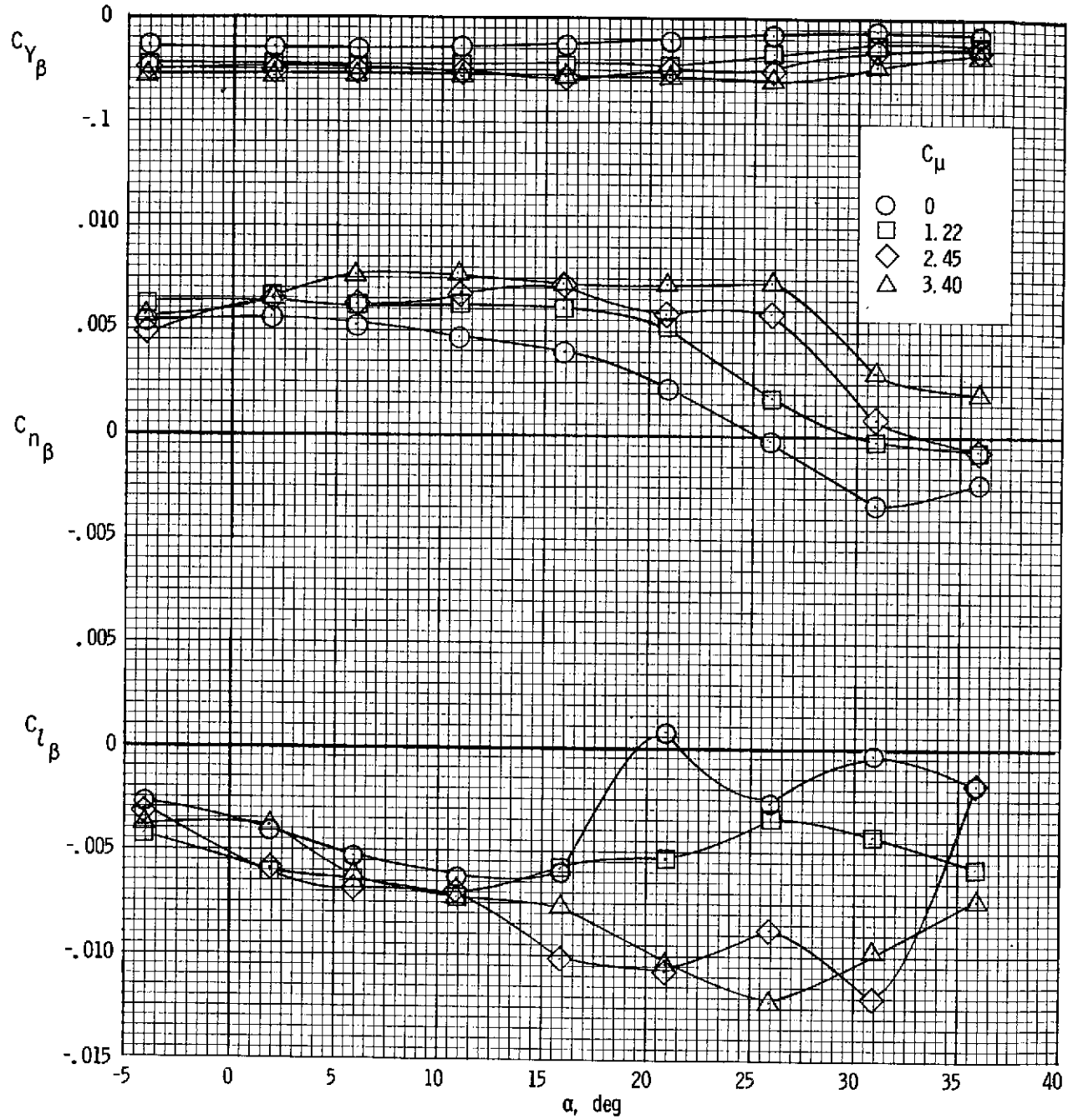

Figure 18.- Lateral stability characteristics, left outboard engine not operating.
$\delta_{f3} = 50^o$; $i_t = 0^o$; $\delta_e = -50^o$.

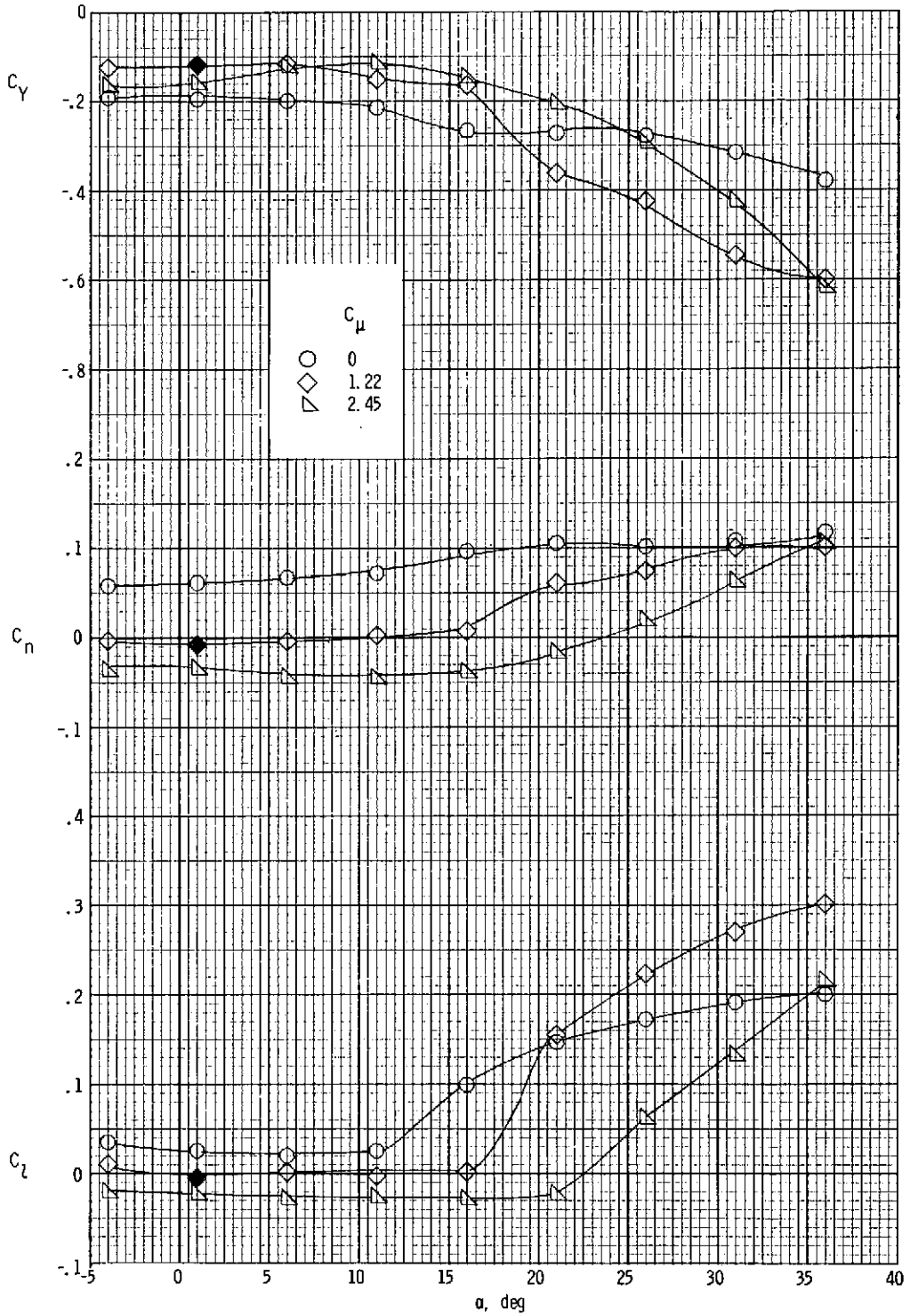

(a) Lateral characteristics.

Figure 19.- Lateral and longitudinal characteristics, left outboard engine not operating. Solid symbol represents approach condition in figure 10(b). Differential flap deflection (see fig. 2(c)); $C_{\mu,le,L} = 0.23$; $i_t = 0^o$; $\delta_e = -50^o$.

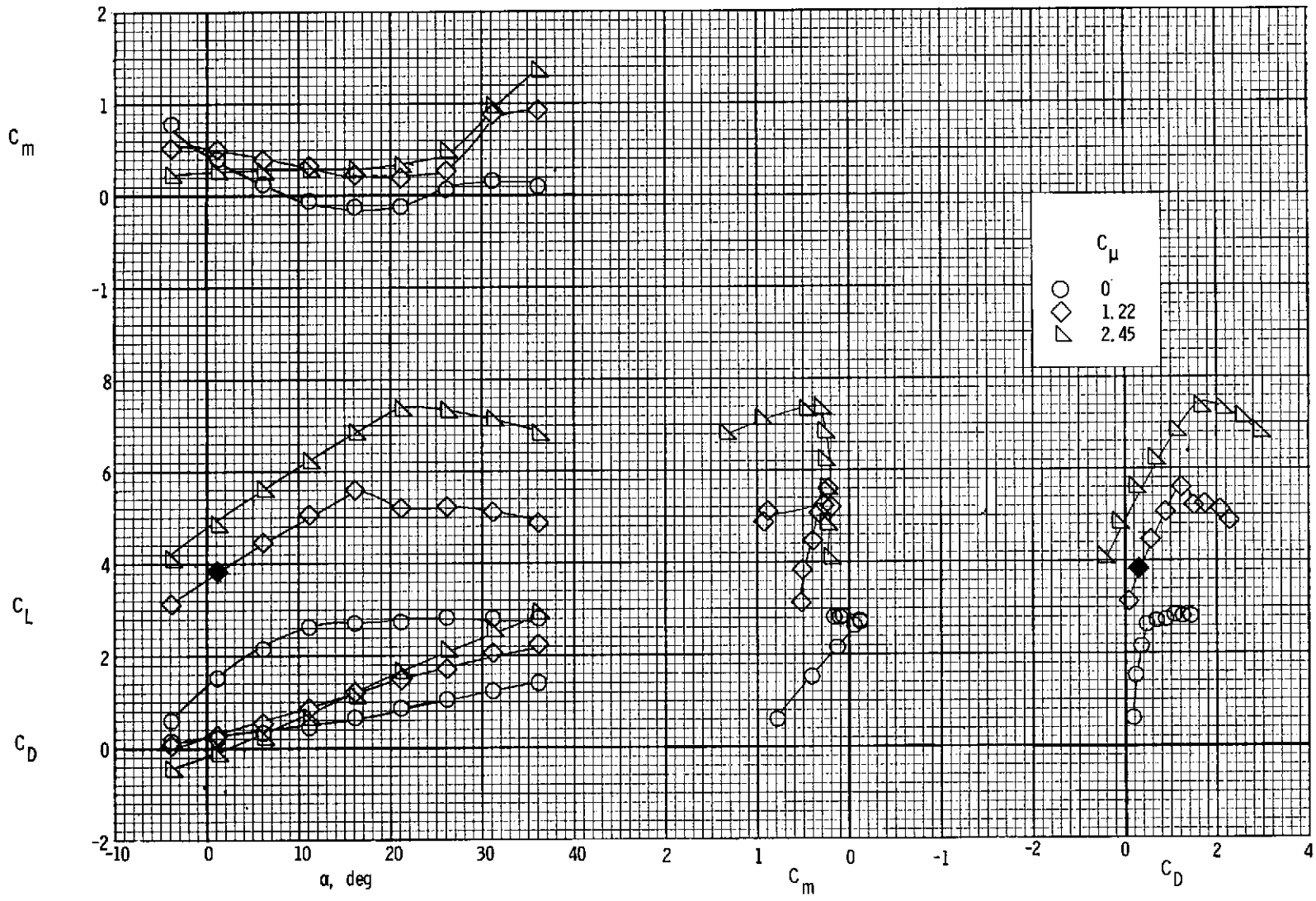

(b) Longitudinal characteristics.

Figure 19.- Concluded.

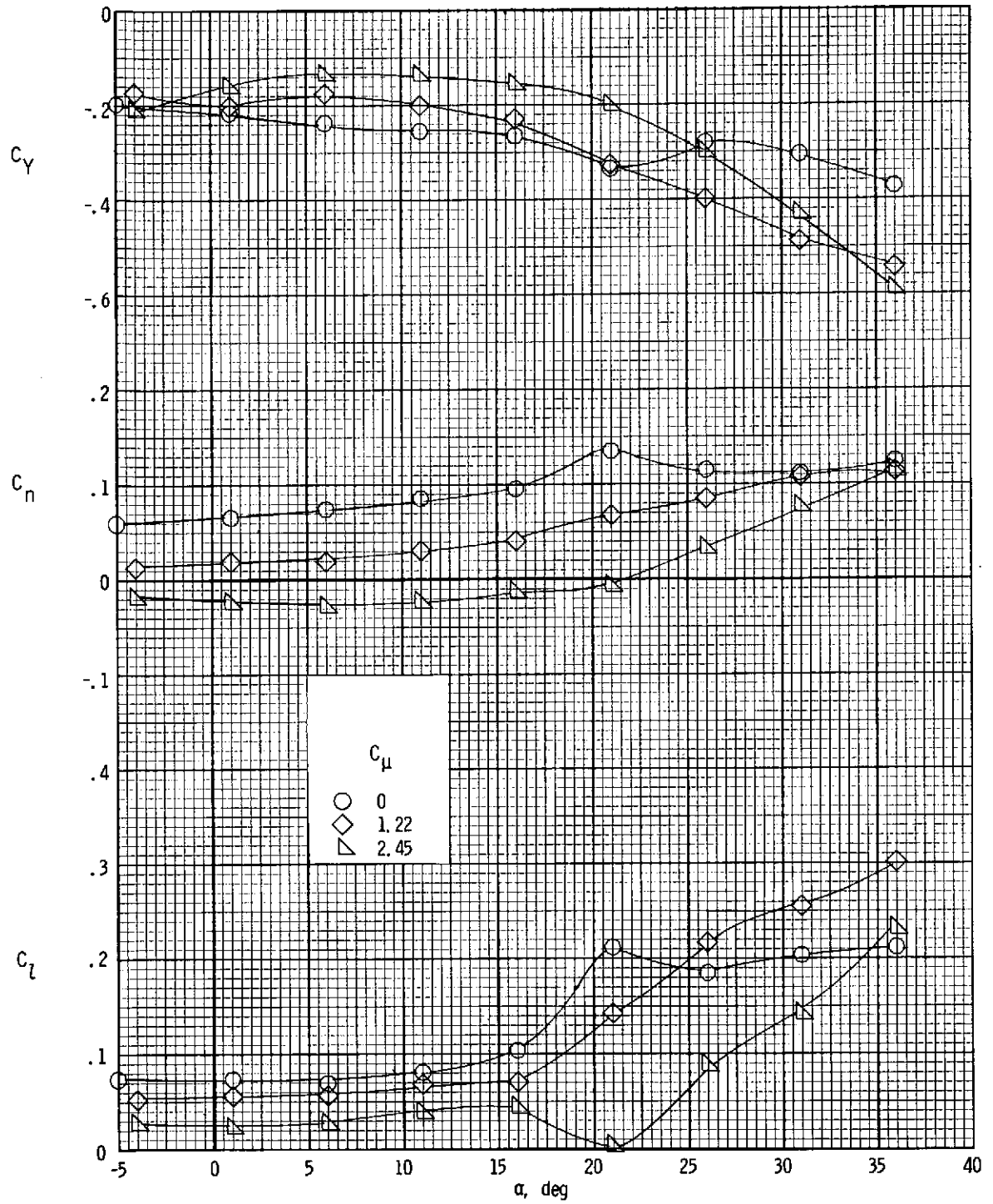

(a) Lateral characteristics.

Figure 20.- Lateral and longitudinal characteristics, left outboard engine not operating. Differential flap deflection (see fig. 2(c)); $C_{\mu,le,L} = 0.23$; $C_{\mu,ail,L} = 0.032$; $i_t = 0^o$; $\delta_e = -50^o$.

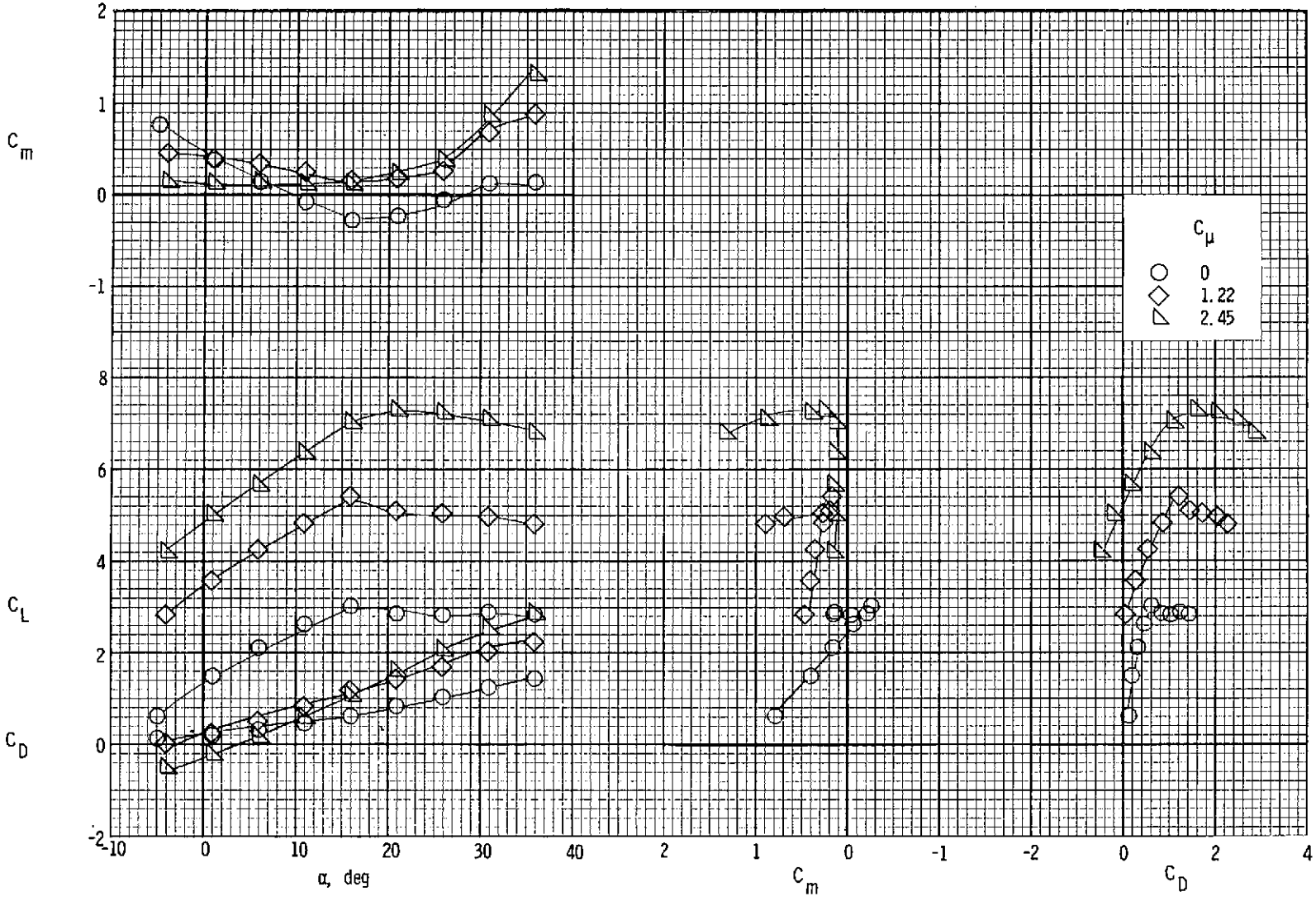

(b) Longitudinal characteristics.

Figure 20.- Concluded.

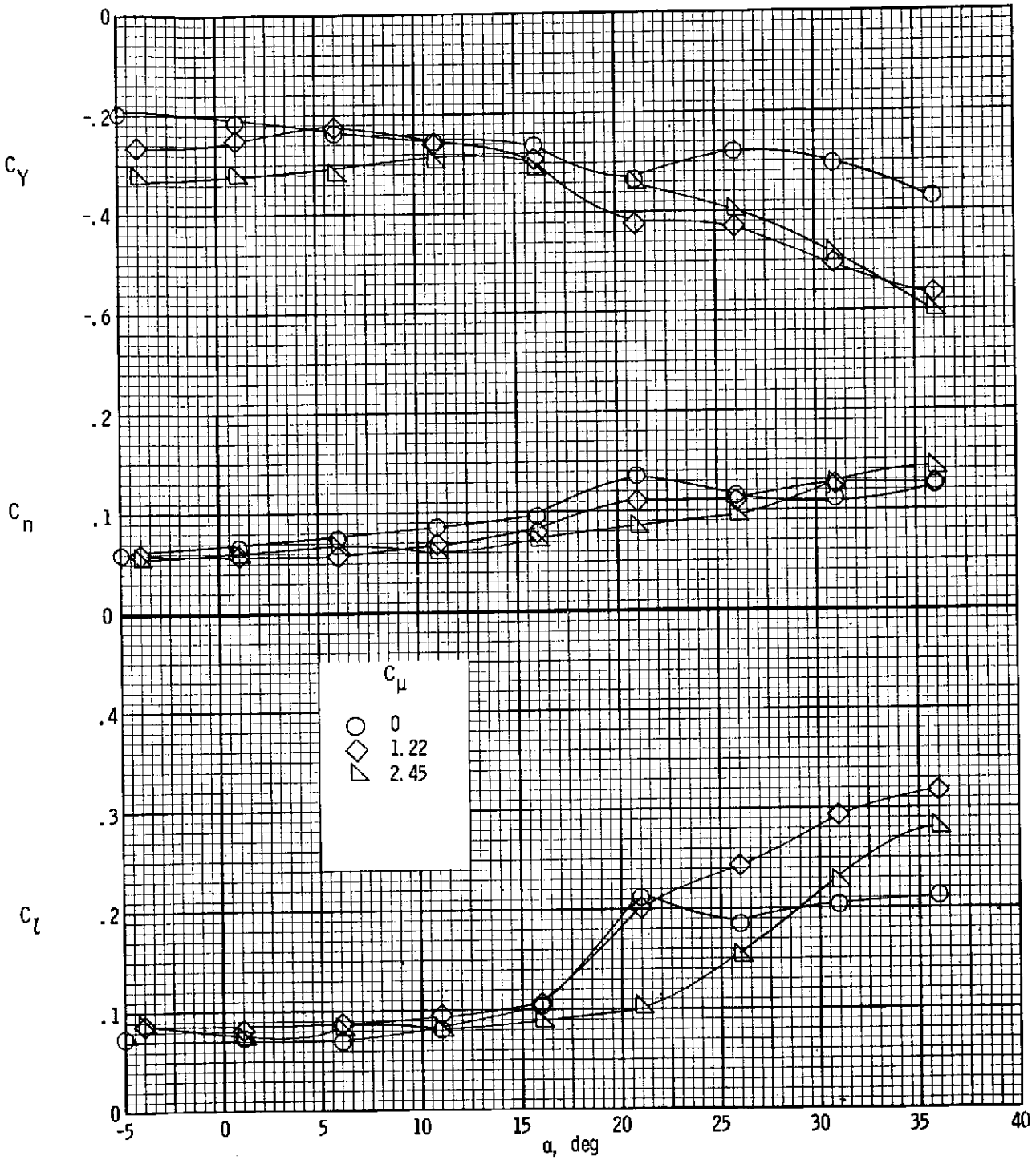

(a) Lateral characteristics.

Figure 21.- Lateral and longitudinal characteristics, left outboard engine not operating. Differential flap deflection (see fig. 2(c)); $C_{\mu,le,L} = 0.23$; $C_{\mu,ail,L} = 0.032$; lateral deflectors deflected 18^o; $i_t = 0^o$; $\delta_e = -50^o$.

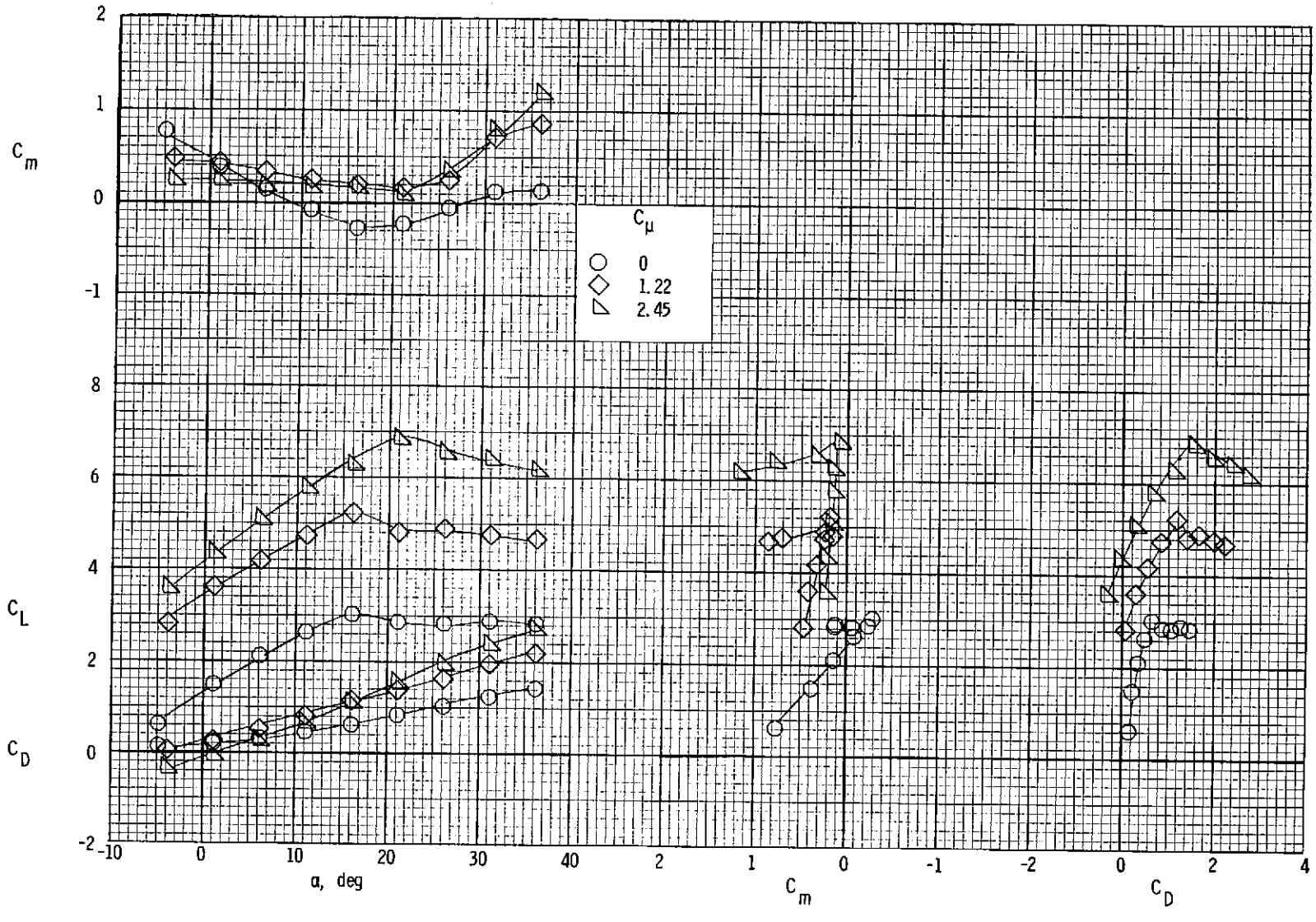

(b) Longitudinal characteristics.

Figure 21.- Concluded.

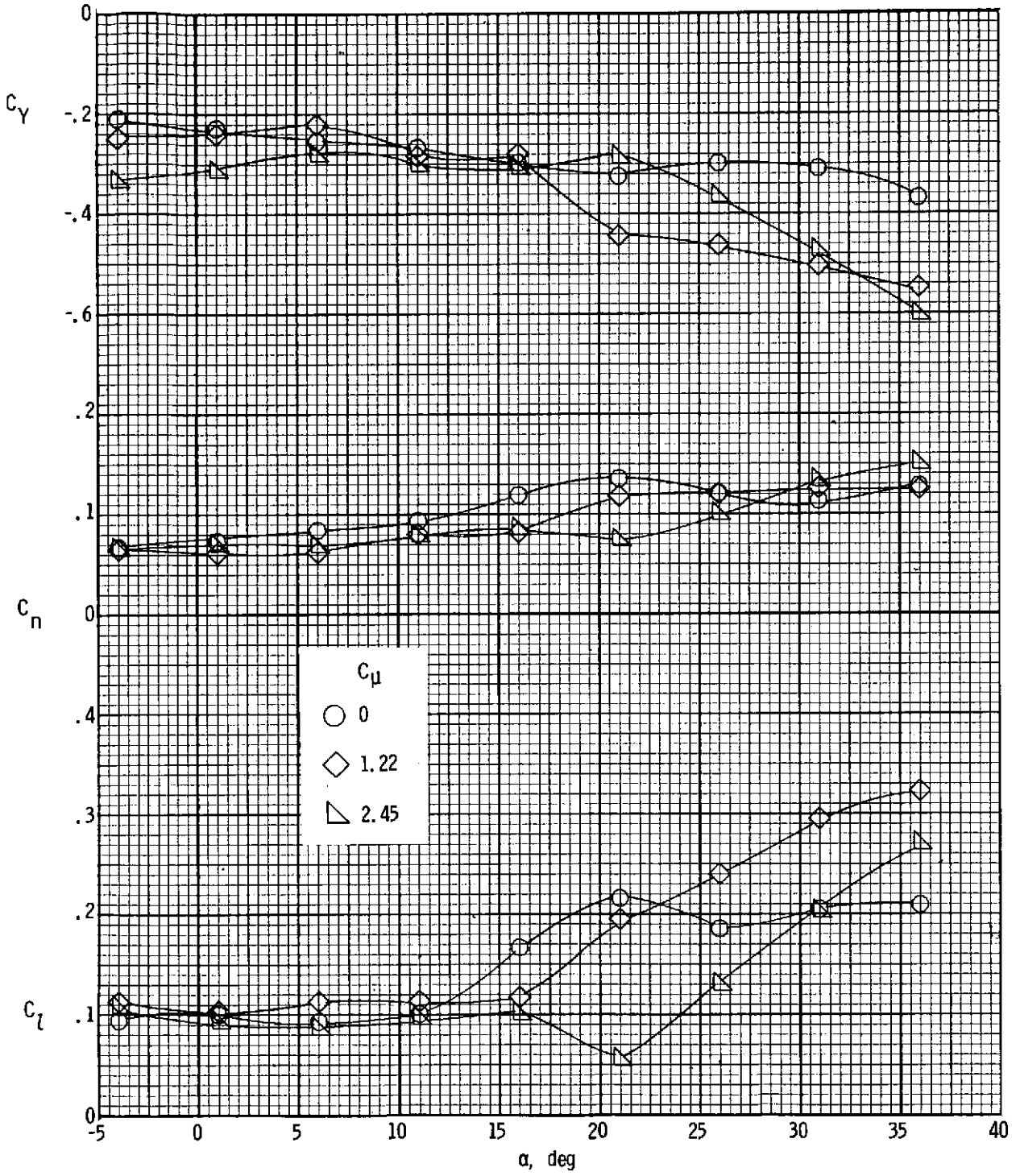

(a) Lateral characteristics.

Figure 22.- Lateral and longitudinal characteristics, left outboard engine not operating. Differential flap deflection (see fig. 2(c)); $C_{\mu,le,L} = 0.23$; $C_{\mu,ail,L} = 0.032$; lateral deflectors deflected 18°; right semispan spoiler deflected 60°; $i_t = 0°$; $\delta_e = -50°$.

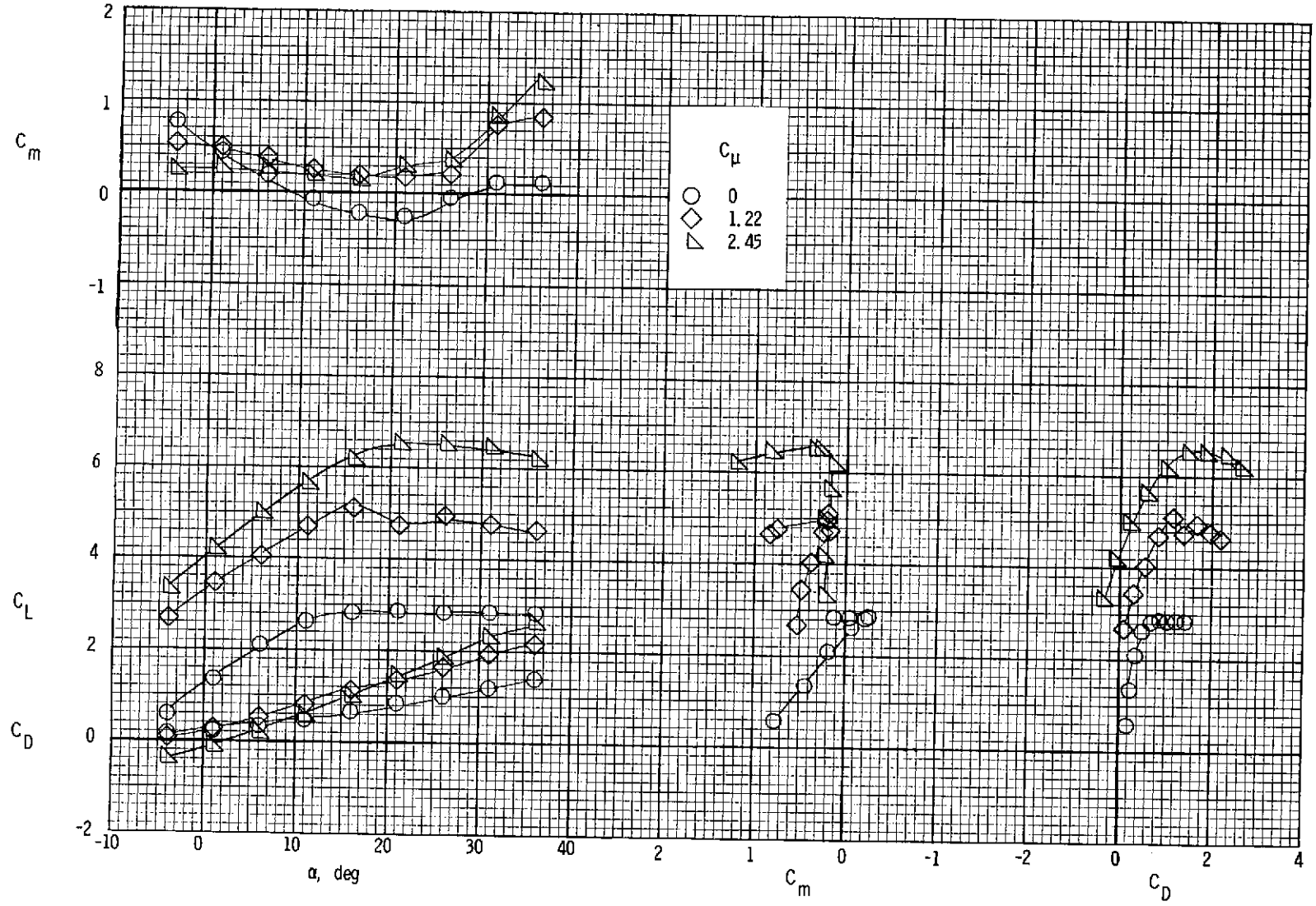

(b) Longitudinal characteristics.

Figure 22.- Concluded.

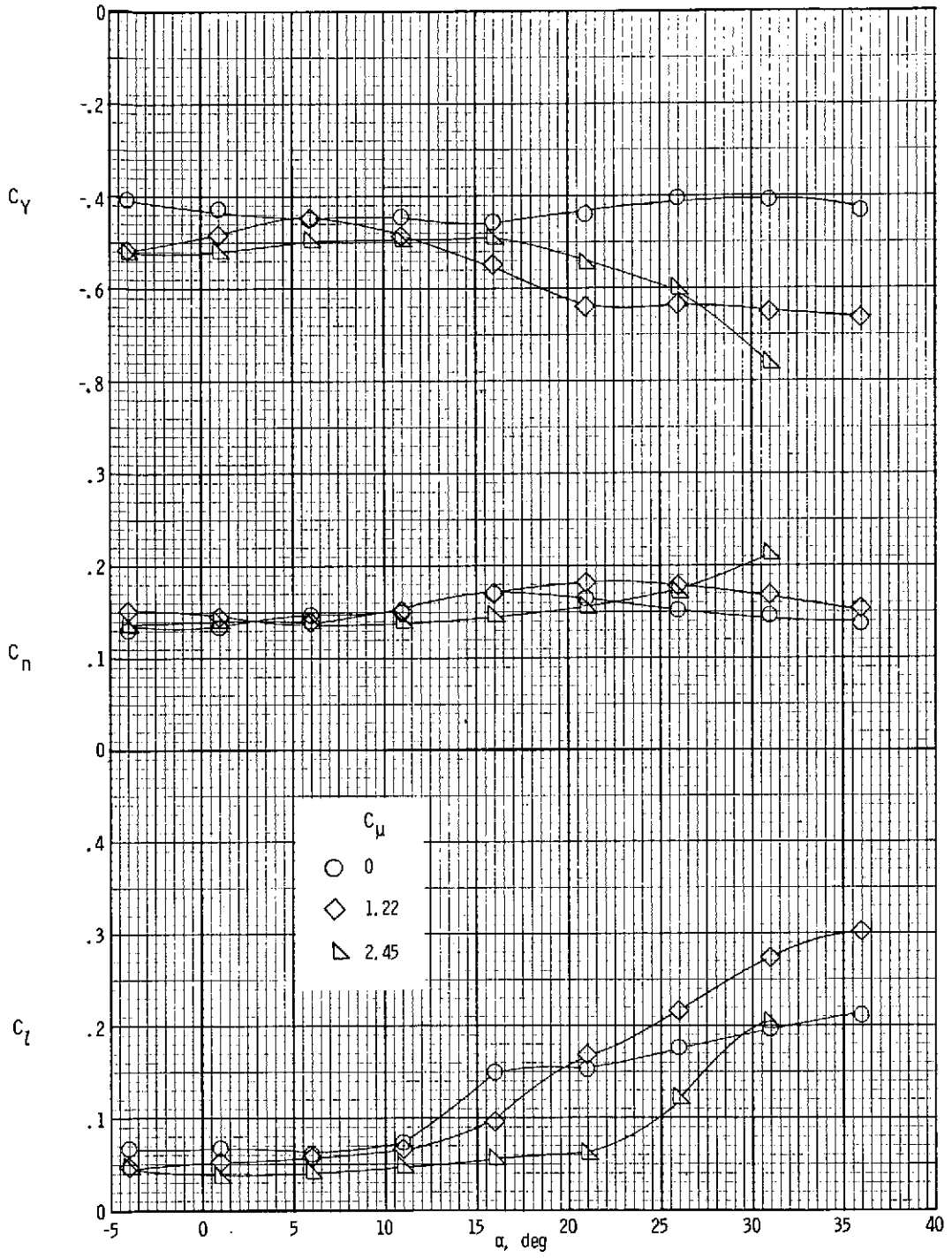

(a) Lateral characteristics.

Figure 23.- Lateral and longitudinal characteristics, left outboard engine not operating. Differential flap deflection (see fig. 2(c)); $C_{\mu,le,L} = 0.23$; $C_{\mu,ail,L} = 0.032$; lateral deflectors deflected 18°; right semispan spoiler deflected 60°; rudder deflected -30°; $i_t = 0°$; $\delta_e = -50°$.

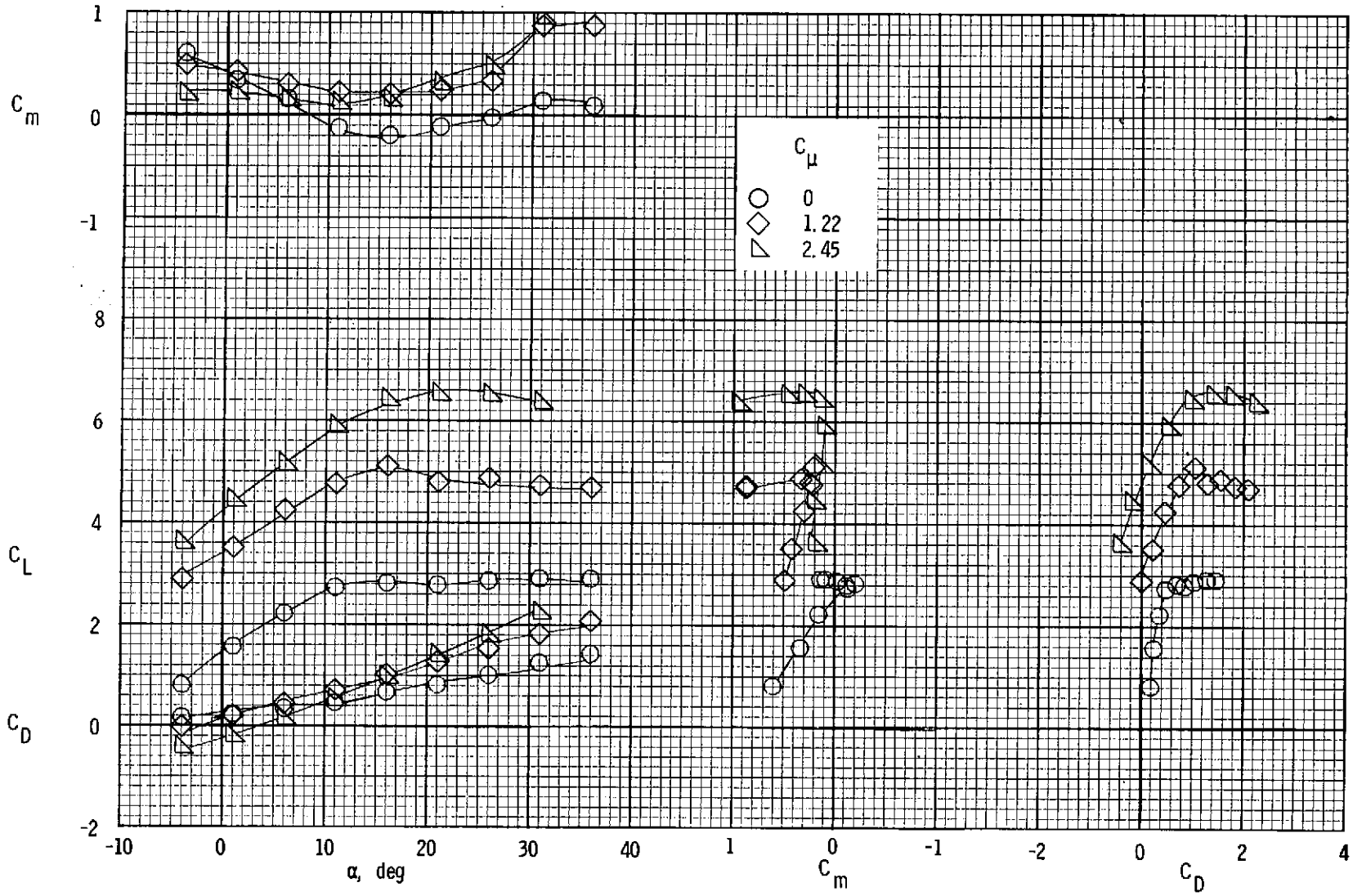

(b) Longitudinal characteristics.

Figure 23.- Concluded.

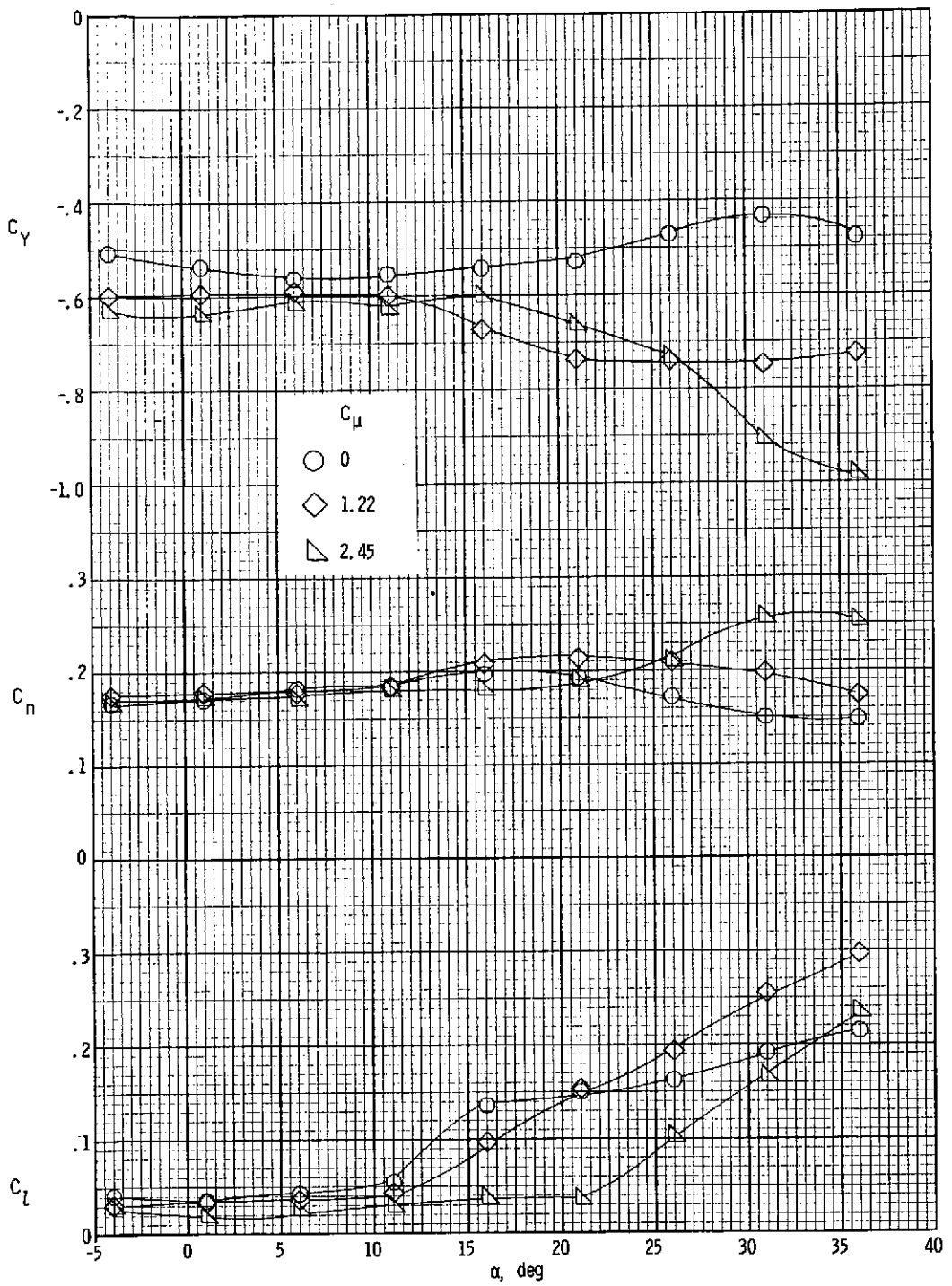

(a) Lateral characteristics.

Figure 24.- Lateral and longitudinal characteristics, left outboard engine not operating. Differential flap deflection (see fig. 2(c)); $C_{\mu,le,L} = 0.23$; $C_{\mu,ail,L} = 0.032$; lateral deflectors deflected 18°; right semispan spoiler deflected 60°; rudder deflected -30°; $C_{\mu,rud} = 0.019$; $i_t = 0°$; $\delta_e = -50°$.

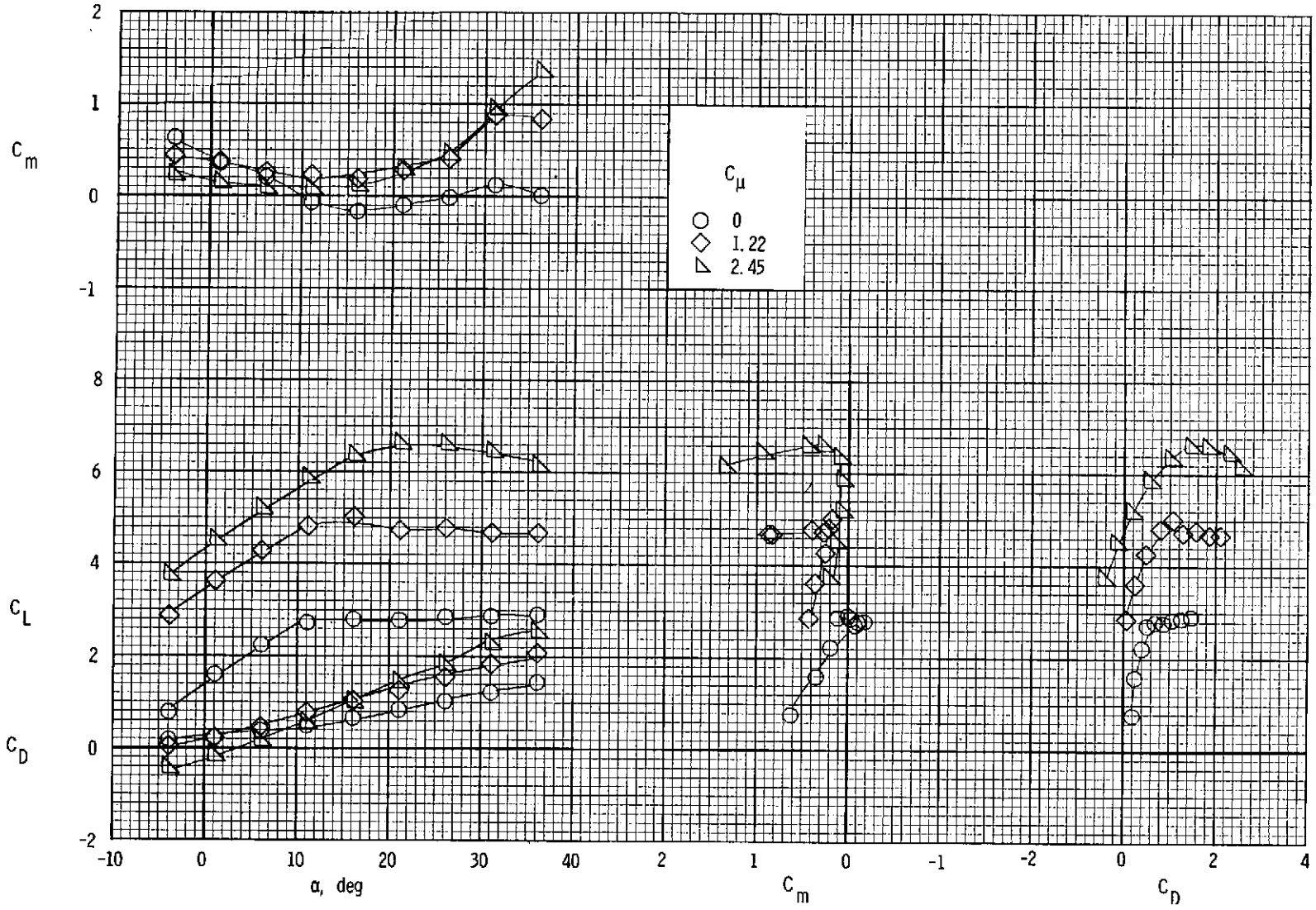

(b) Longitudinal characteristics.

Figure 24.- Concluded.

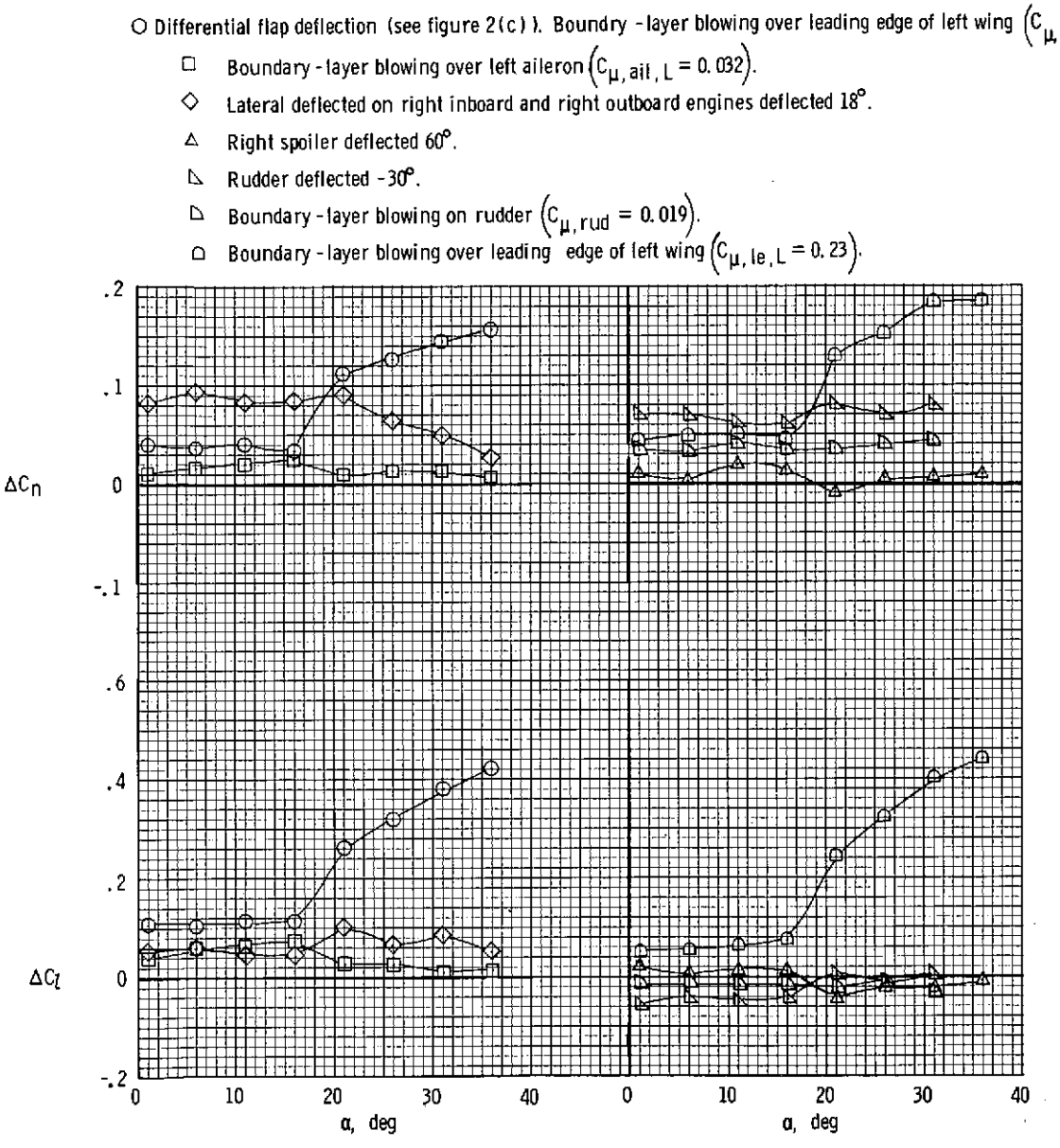

Figure 25.- Individual contributions of each of several lateral trim devices. Left outboard engine not operating. $C_\mu = 2.45$; $i_t = 0^o$; $\delta_{f3} = 50^o$; $\gamma = 0^o$; $\delta_e = -50^o$.

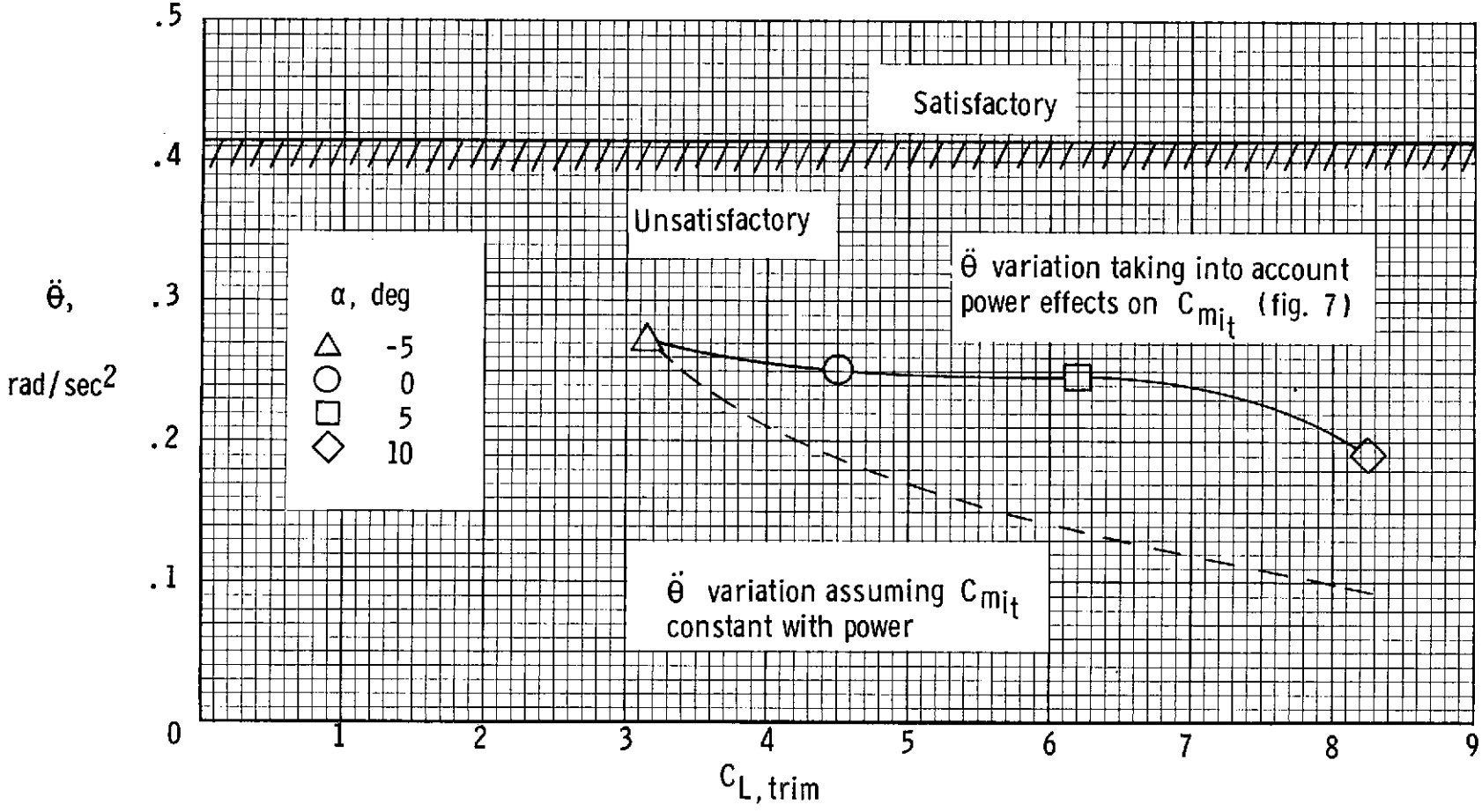

Figure 26.- Initial pitch acceleration (produced by 10° deflection of the horizontal tail) scaled up to a 24.4-m (80-ft) span airplane and compared to the requirements for satisfactory pitch response for STOL aircraft from reference 15. δ_{f3} = 50°; 341 kN (76 700 lb); γ = 0°.

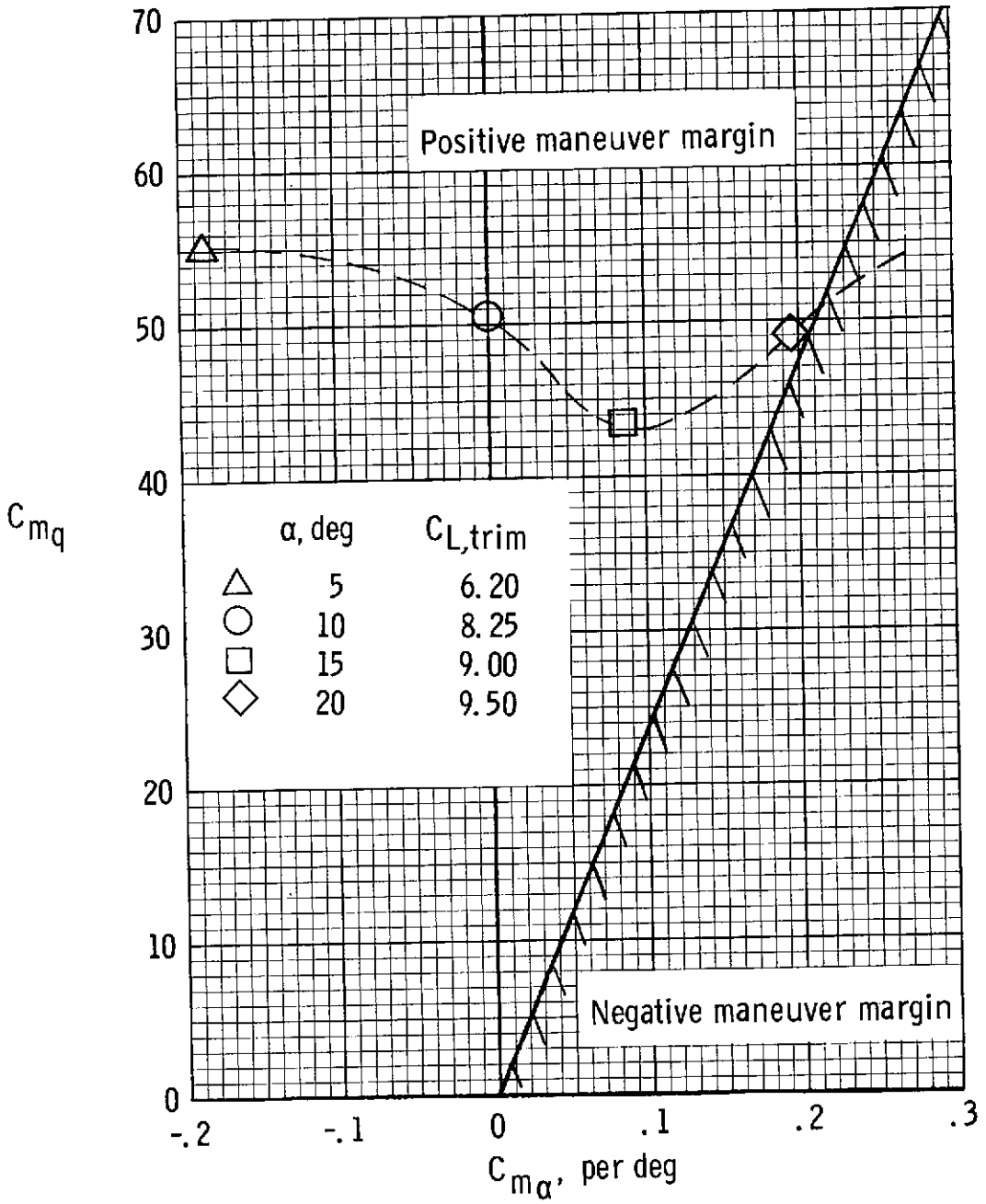

Figure 27.- Effect of damping in pitch and static longitudinal stability on the longitudinal flight characteristics of the model. $\delta_{f3} = 50^{o}$.

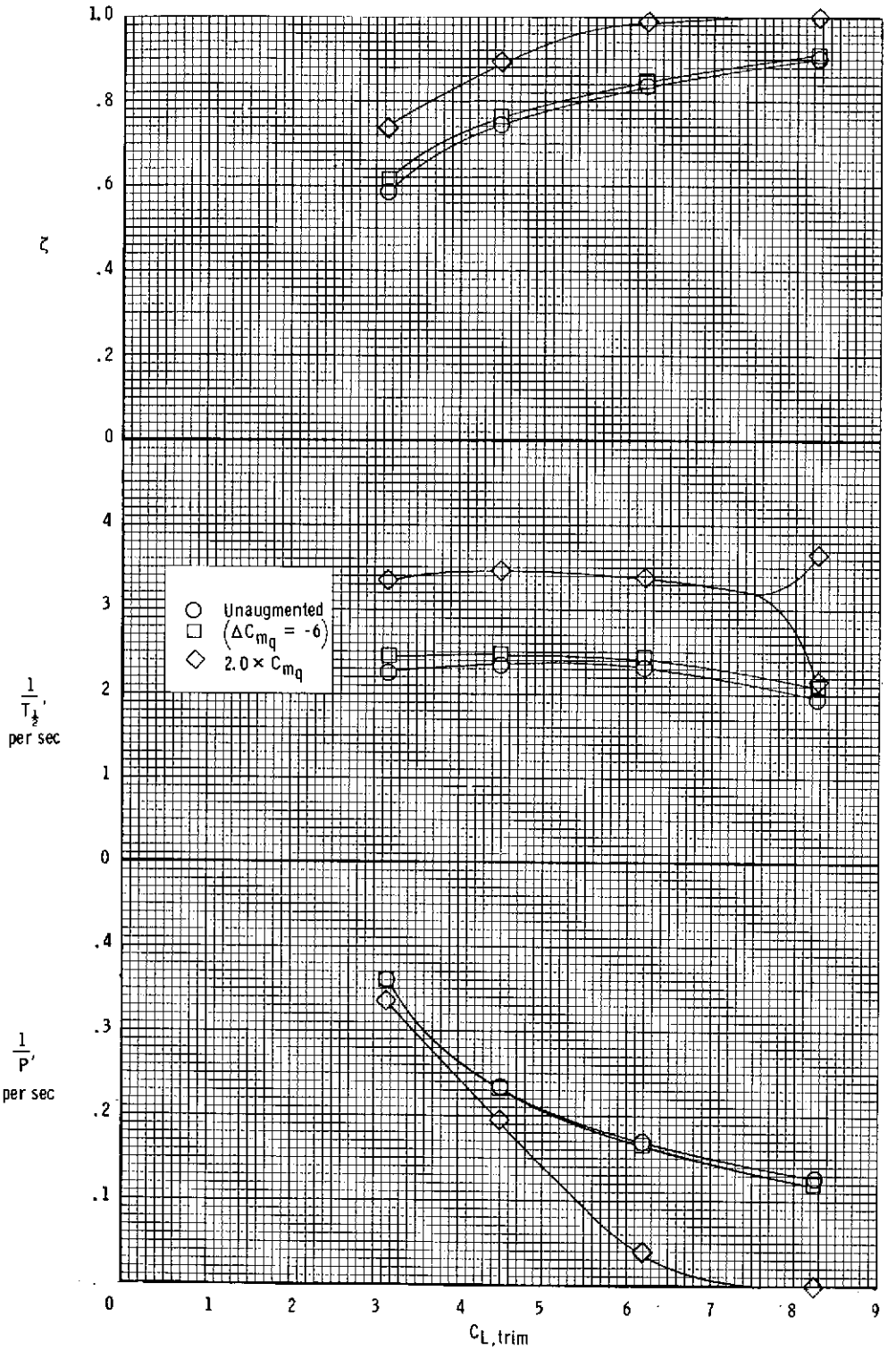

Figure 28.- Calculated short-period longitudinal dynamic stability characteristics of the model. $\delta_{f3} = 50^{o}$; $\gamma = 0^{o}$.

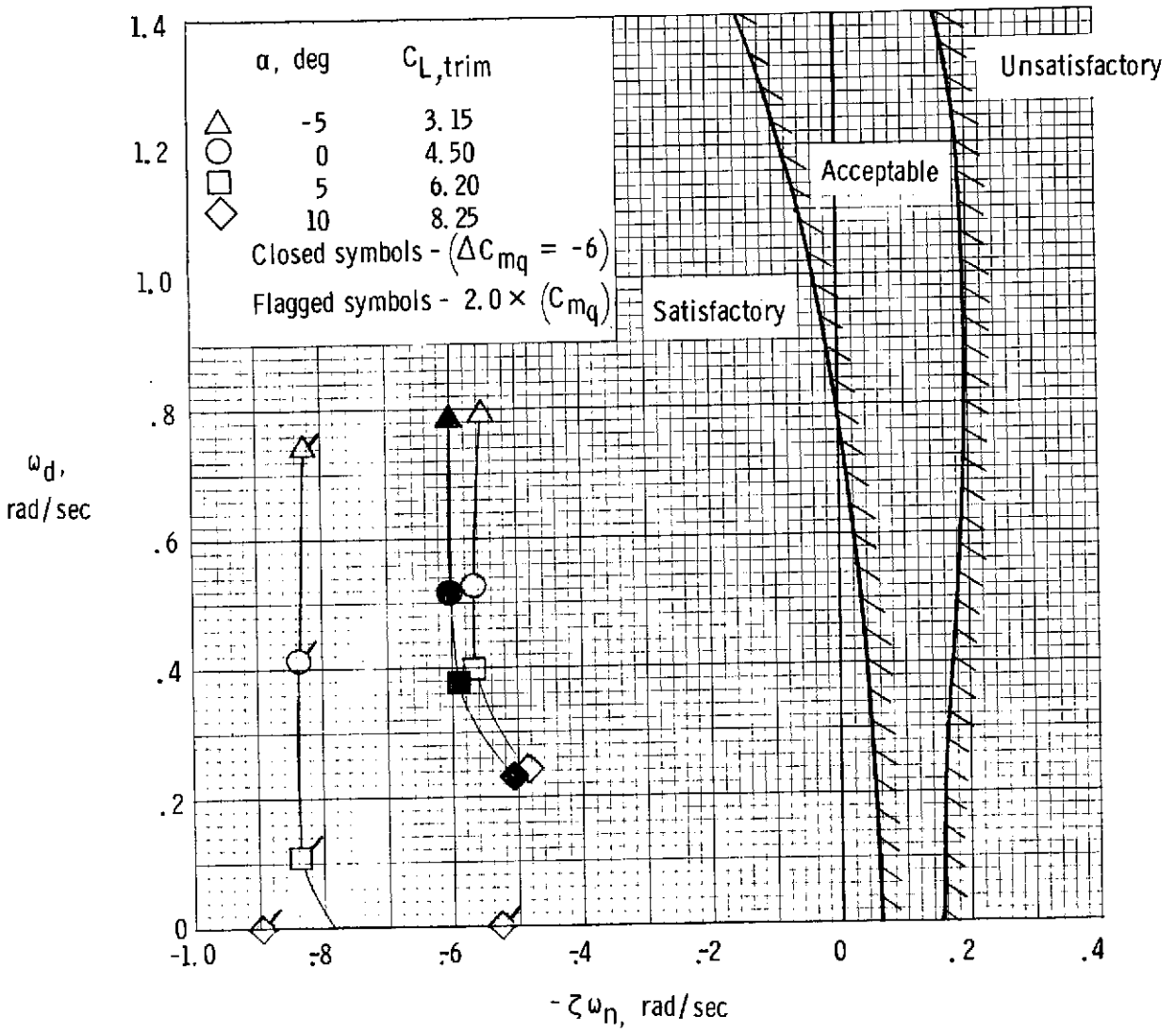

Figure 29.- Calculated short-period longitudinal characteristics scaled up to a 24.4-m (80-ft) span airplane and compared to requirements for STOL aircraft from reference 17. $\delta_{f3} = 50^{o}$; $\gamma = 0^{o}$.

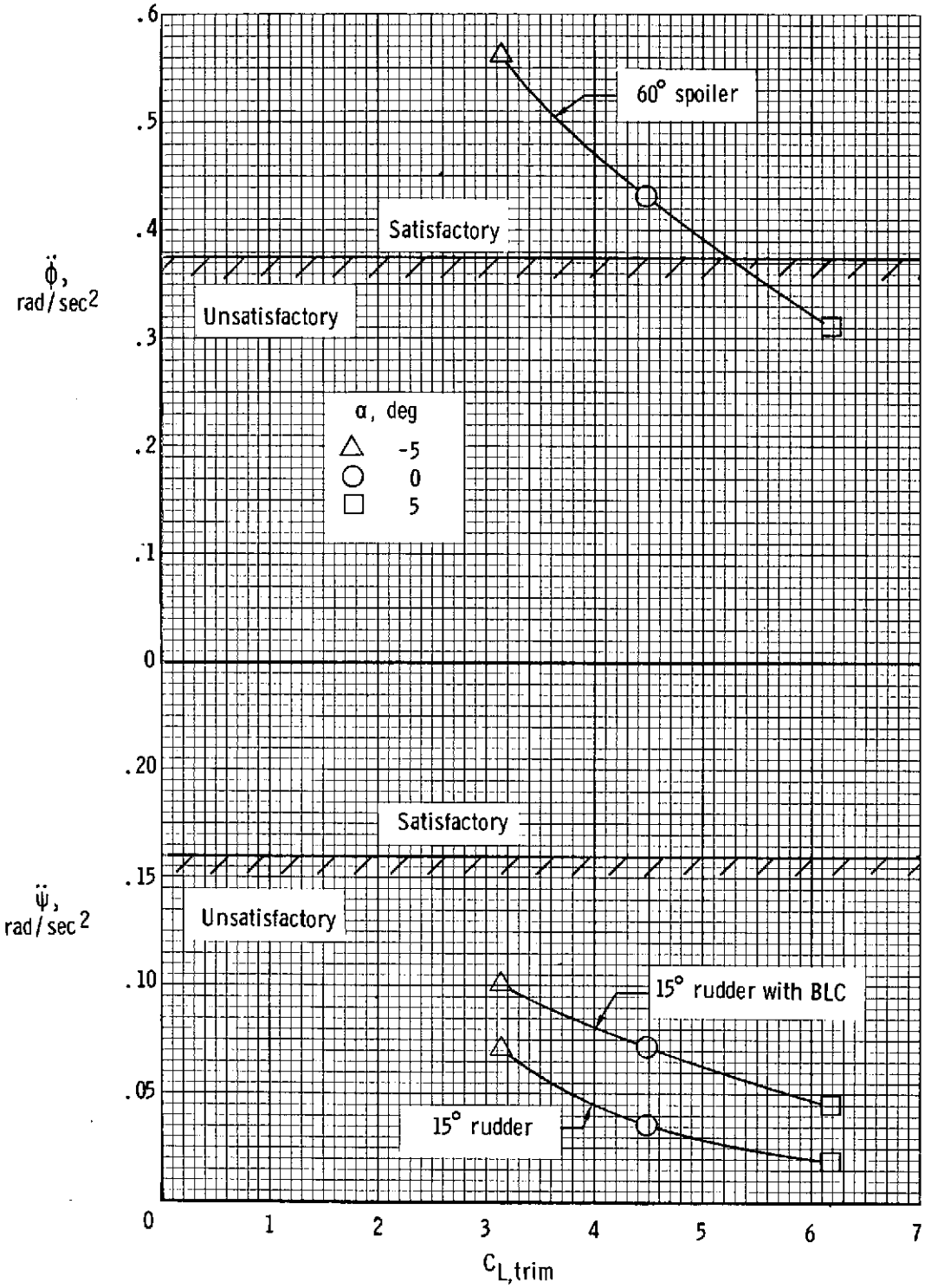

Figure 30.- Initial roll and yaw accelerations scaled up to a 24.4-m (80-ft) span airplane compared to lateral response requirements for STOL aircraft from reference 15. $\delta_{f3} = 50^{o}$; 341 kN (76 700 lb); $\gamma = 0^{o}$.

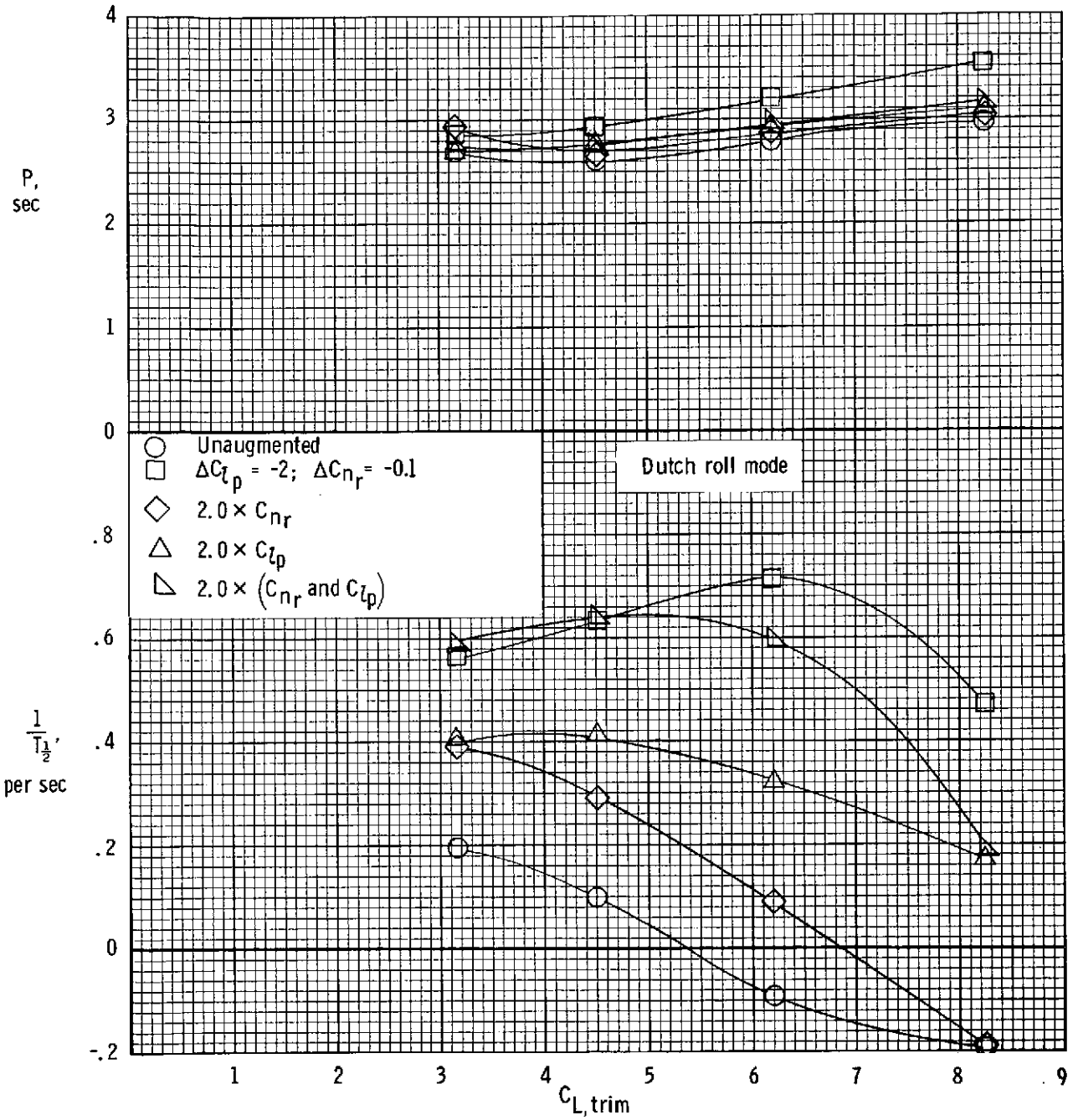

(a) Dutch roll mode.

Figure 31.- Calculated lateral dynamic stability characteristics of the model. $\delta_{f3} = 50^{o}$; $\gamma = 0^{o}$.

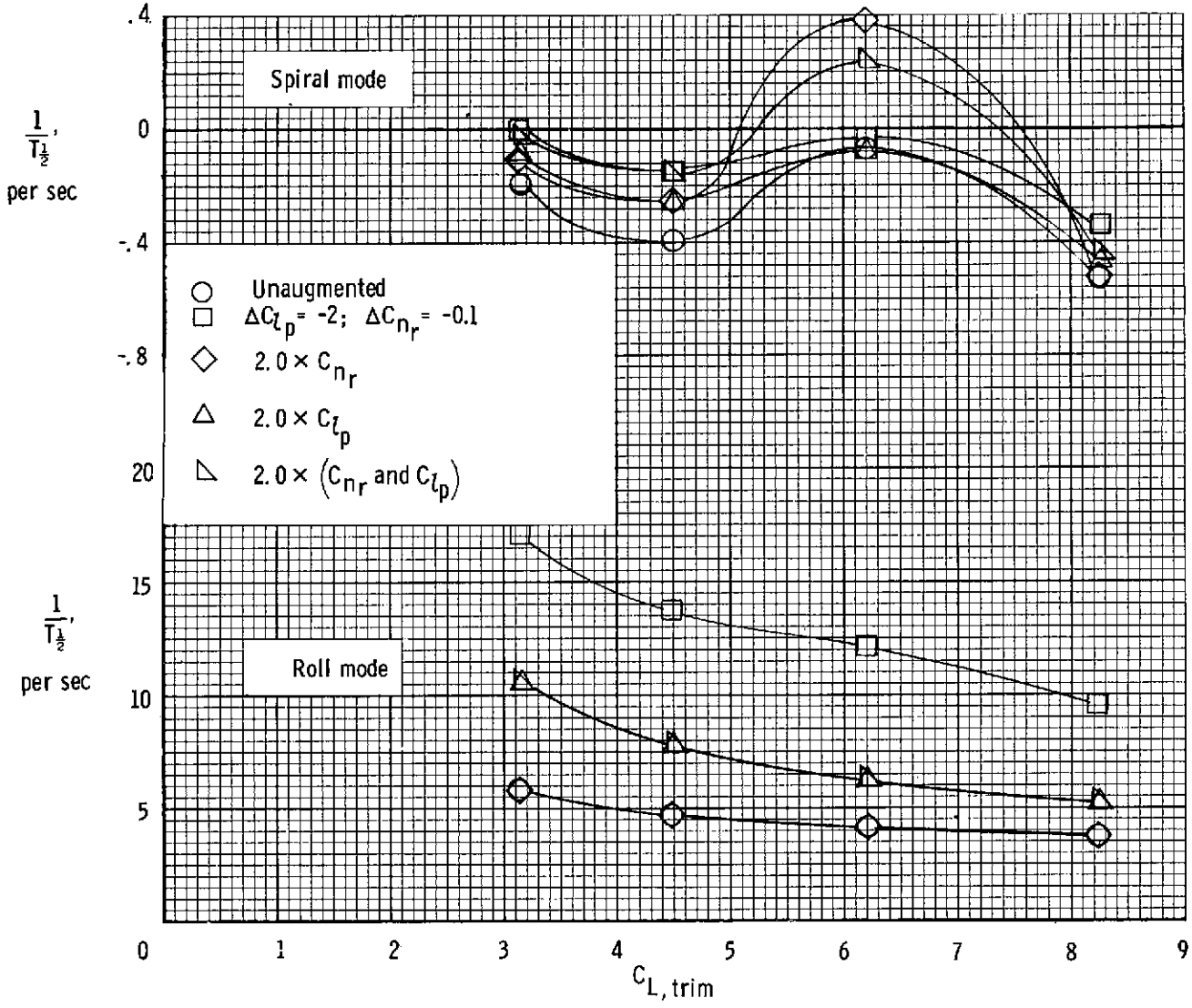

(b) Spiral and roll modes.

Figure 31.- Concluded.

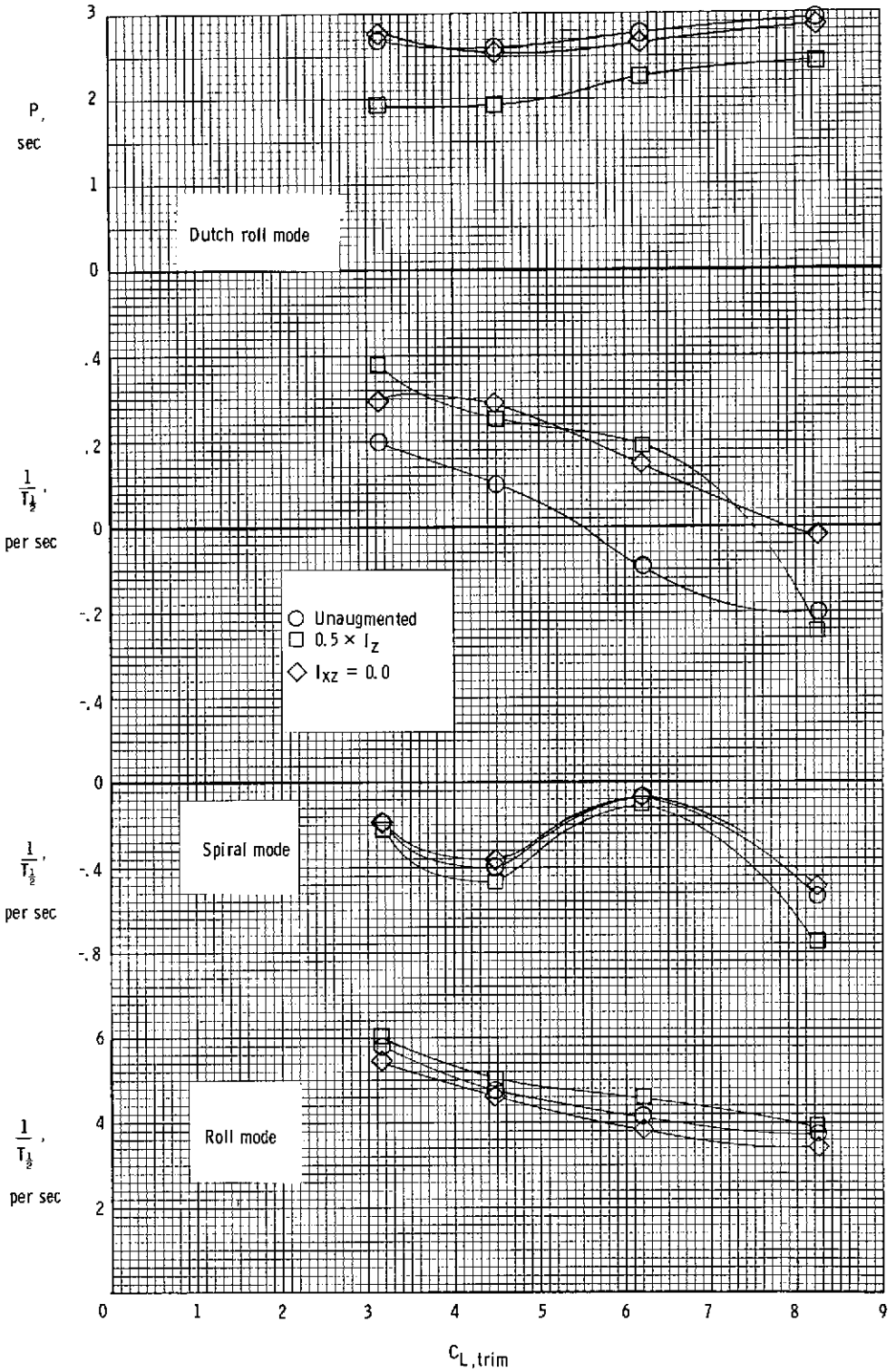

Figure 32.- Calculated inertia effects on lateral dynamic stability characteristics of the model. $\delta_{f3} = 50^{o}$; $\gamma = 0^{o}$.

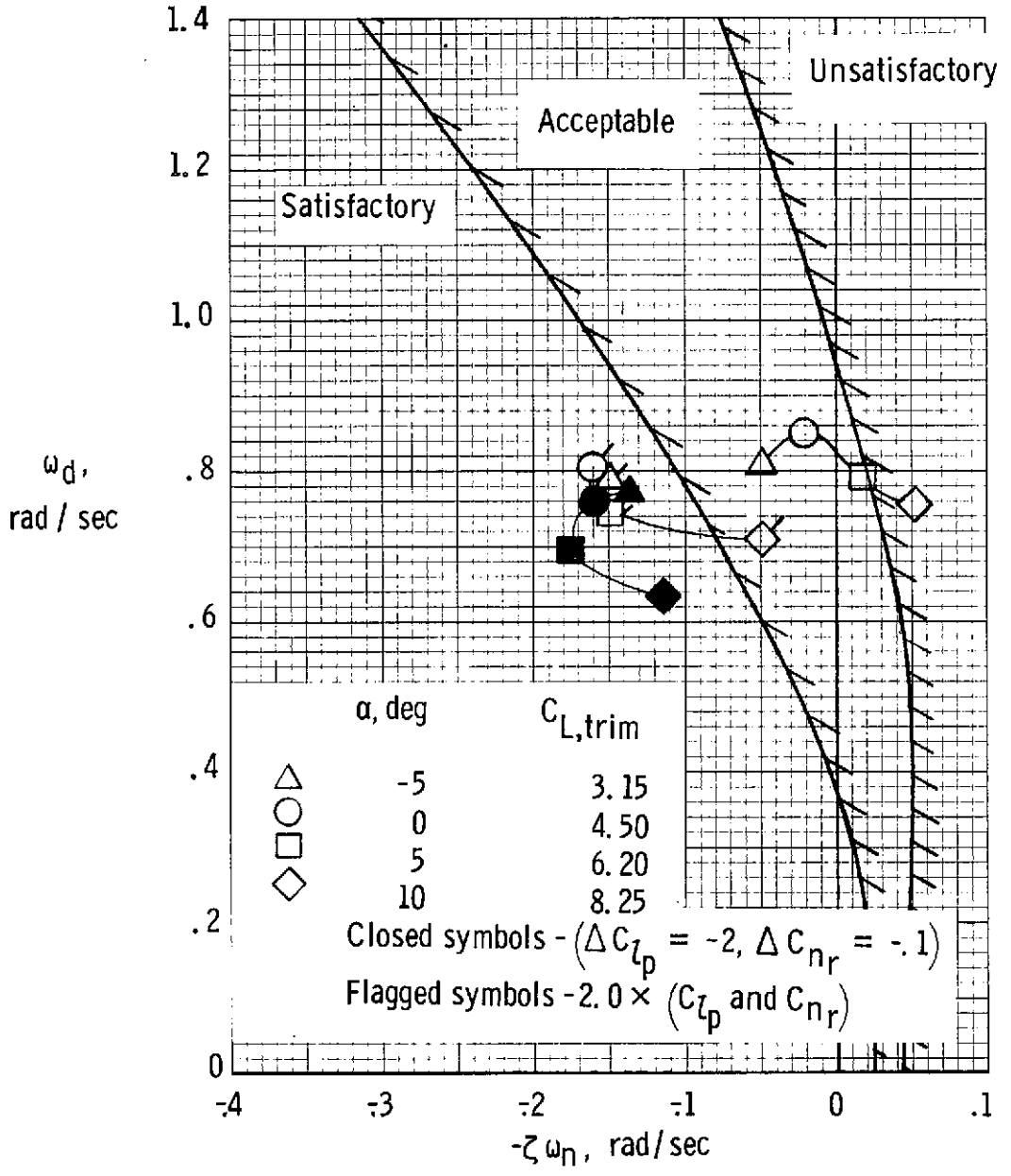

Figure 33.- Calculated lateral oscillatory characteristics scaled up to a 24.4-m (80-ft) span airplane and compared to requirements for STOL aircraft from reference 17. $\delta_{f3} = 50^{o}$; $\gamma = 0^{o}$.